Lawrence Berkeley Laboratory
UNIVERSITY OF CALIFORNIA

CHEMICAL BIODYNAMICS DIVISION

STUDIES OF CHROMATIN *in situ* BY FLUORESCENCE CORRELATION SPECTROSCOPY

Stanley M. Sorscher
(Ph.D. thesis)

November 1979

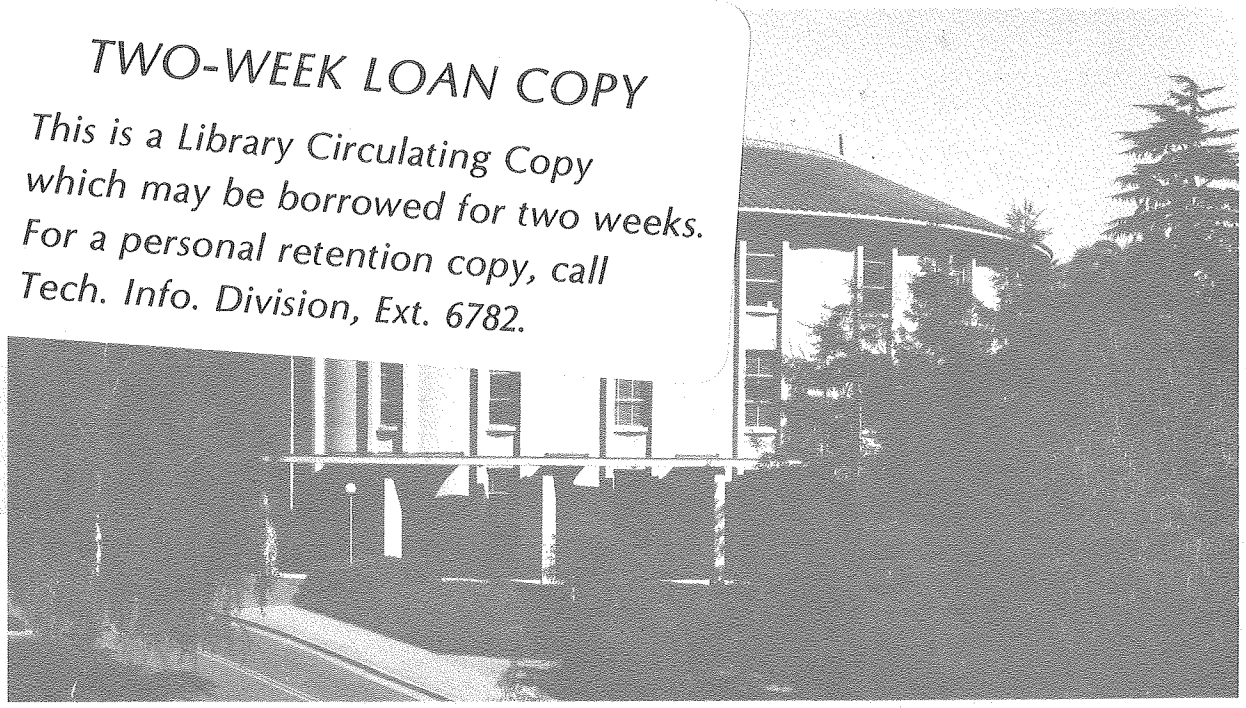

Prepared for the U.S. Department of Energy under Contract W-7405-ENG-48

DISCLAIMER

STUDIES OF CHROMATIN *in situ* BY FLUORESCENCE CORRELATION SPECTROSCOPY

Stanley Mark Sorscher

Lawrence Berkeley Laboratory
University of California
Berkeley, California

This work was prepared with the support of the U. S. Department of Energy under Contract W-7405-ENG-48.

ABSTRACT

STUDIES OF CHROMATIN *in situ* BY
FLUORESCENCE CORRELATION SPECTROSCOPY

STANLEY MARK SORSCHER

All systems in thermodynamic equilibrium are subject to spontaneous fluctuations from equilibrium. For very small systems, the fluctuations become apparent, and can be used to study the behavior of the system without introducing any external perturbations. The mean squared fluctuation amplitude contains information about the absolute size of the system. The characteristic time of the fluctuation autocorrelation function contains kinetic information.

The fluorescent dye Ethidium Bromide is especially useful as a probe of DNA because the changes in the fluorescence properties of the dye upon binding to DNA greatly enhance the effect of spontaneous fluctuations in the binding equilibrium. An autocorrelation function is obtained from as few as 5000 dye molecules. This sensistivity makes small regions of individual cell nuclei appropriate objects for study.

All the measurements described employ a laser beam focussed to dimensions of the order of one micron. Knowledge of the beam radius is critical, and a new method for its determination *in situ* is reported.

Experiments are described employing well characterized DNA preparations, including calf thymus DNA, SV-40 DNA, and calf thymus

nucleohistone particles. Measurements made in small regions of isolated cell nuclei and on nuclei *in vivo* are described. These data indicate that the strength of dye binding increases in nuclei isolated from green monkey kidney cells when the cells have been stimulated to enter the cell growth cycle. Data are used to infer that the viscosity of nuclear material is between one and two orders of magnitude greater than that of water. It is shown that the viscosity decreases as the cells leave the resting state, and enter the cell growth cycle. Washing the nuclei also lowers the viscosity.

These experiments demonstrate that fluorescence correlation spectroscopy can provide information at the subnuclear level that is otherwise unavailable.

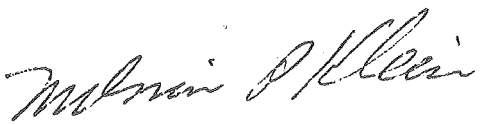

INTRODUCTION

The goal of the research described here is to establish fluorescence correlation spectroscopy as a suitable technique for measurements in the cell nucleus. Quantitative measurements in the cell nucleus are generally very difficult because of low signal levels and very small sample volumes. Fluorescence correlation spectroscopy requires small sample sizes for successful data collection, and relies on spontaneous fluctuations from equilibrium to generate the signal. Thus, the technique should be applicable to small delicate biological systems.

The theory of fluctuation correlation spectroscopy has been reviewed.[1,2,3] Only a brief discussion will be given here. Fluctuation spectroscopy can be applied to systems in thermodynamic equilibrium. If such a system were subjected to an external perturbation, it might be displaced from equilibrium. After small perturbations, the system will relax back to equilibrium in a manner characteristic of the kinetics of the original thermodynamic eqiulibrium. For instance, if the system is intrinsically fast, then the relaxation is rapid. The time course of the relaxation after a small perturbation i s usually exponential. The time constant can be measured and interpreted in terms of the kinetic parameters of the system near eqiulibrium.

Fluctuation spectroscopy takes advantage of spontaneous fluctuations from eqiulibrium undergone by any system in thermodynamic eqiulibrium. If the state of such a system could be recorded with arbitrarily high precision as a function of time, then the record might have the appearance of figure 1. The state of the system should evolve according to the same kinetic parameters observed with the

Figure 1. A signal may fluctuate over time from its average value. Some fluctuations persist, and are said to have a correlation time, indicated by τ_c.

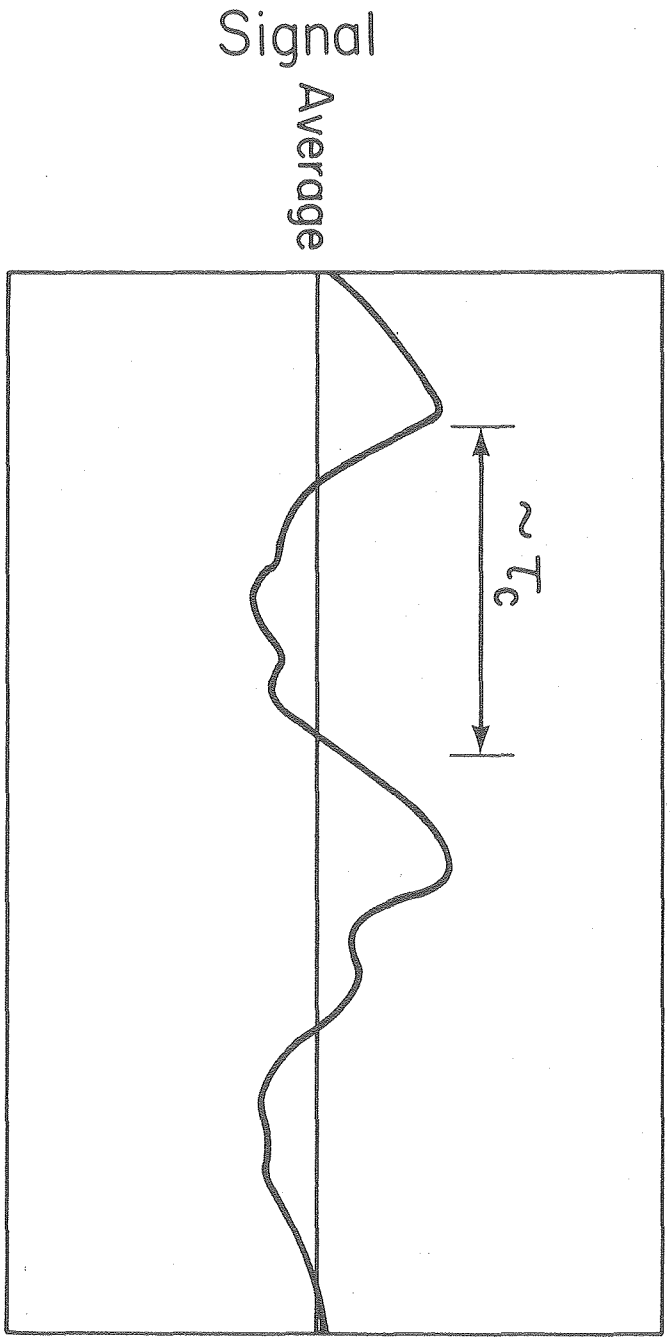

XBL 7910-5060

perturbation technique. If the system is intrinsically slow, then spontaneous fluctuations will be slow to decay. One can imagine, then, analyzing a long record like the one in figure 1, and arriving at an "average fluctuation" which is interpreted in terms of the kinetic parameters of the equilibrium.

The averaging process used to generate the "average fluctuation" is the calculation of the autocorrelation function, $G(\tau)$. The information contained in the autocorrelation function is equivalent to the information in the power spectrum, since the two functions are a Fourier transform pair. The autocorrelation function is used instead of the power spectrum partly because of the availability of a hardwired minicomputer capable of computing autocorrelation functions quickly. Also, the results in terms of the power spectrum can not be stated in closed form, but contain tabulated integrals.

Fluctuations contain information about the size of the system, as well as kinetic information.[4,5] Consider the case of an open volume, which contains a number of particles that may enter and leave. The particles in the open volume are in equilibrium with a reservoir of particles. The state of the system is taken to be the number of particles in the volume. The mean squared fluctuation in the number of particles in the volume will equal the average number of particles in the volume. Thus, the typical fluctuation amplitudes are the size of the square root of the number of particles in the volume. If the system is increased in size, then the amplitude of the fluctuations will also increase, but not so quickly.

This result may be more familiar when stated in terms of coin tosses. If a fair coin is tossed four times, it is likely that it

will land head up one two or three times. On the average, it should land twice with its head up. The average fluctuation in the number of heads after four tosses is 1, which is 50% of the average number of heads after four tosses. Tossing the coin 100 times, it is likely that the number of heads will be "close to 50." The average fluctuation from 50 will be 5 or 10%. It is in this sense that the fluctuations get larger as the system increases in size, but the relative fluctuations get smaller.

In the same way, molecular concentrations are related to number fluctuations.[6] The process by which concentrations fluctuate is indicated in the relaxation spectrum. Fundamental theorems generalize this point by guaranteeing that every dynamic process capable of having an equilibrium is associated to a fluctuation mode.

These theorems state the extreme generality of fluctuation spectroscopy. Any system in dynamic equilibrium can be studied, in principle, by watching it fluctuate. For example, ion channels in nerve tissue have been studied actively by observing fluctuations in electrical conductance as channels in the nerve membranes open and close.[7-10] Scattered light can be used to monitor number fluctuations in the same way that fluorescence is used in fluorescence correlation spectroscopy.[3,11] Rotational diffusion has been considered in much the same way as translational diffusion.[12,13] Fluctuation measurements of slow rotational diffusion have the important feature that the rotational correlation time should be much longer than the fluorescence lifetime.

In each of these experiments, it is important that a fairly strong signal can be detected from each fundamental unit of the system,

over each correlation time. For example, suppose many ion channels exist in a nerve membrane, and that each opens and closes, leading to the observed fluctuations in the electrical conductance of the membrane. Fluctuations will persist over a period of time determined by the opening and closing rates of the ion channels. In order to observe the channels opening and closing, many ions must pass through an open channel before it closes. If zero one or two ions pass through the channel, the correlation time will be poorly defined.

Similarly, if a rotating molecule emits many fluorescent photons as it diffuses rotationally, then each fluorescent photon from that molecule will be correlated with other fluorescent photons from that molecule. Rotational correlations can be measured accurately as long as many photons are detected from each molecule in each correlation time.

Signals from different ion channels or from different diffusing molecules are presumed to be independent. Thus, cross-correlations will not be present. Non-ideal situations may exist, of course. They have been considered theoretically.[14]

In real experiments, noise will usually be present. By noise it is meant fluctuations with correlation times that are short compared to the time scale of interest. In photon detection, for instance, there will be shot noise. Shot noise has a correlation time of zero, and will always be faster than the time scale of interest. Johnson noise plays a similar role in conductance experiments. Experimental design will have to take into account contributions of noise to the observed autocorrelation function.

There are two counter-intuitive aspects of fluctuation experiments

that are illustrated in figure 2. One is that, in most experiments, one attempts to filter out the fluctuations and average the time independent signal. In fluctuation experiments, the time independent part of the signal is usually removed from the autocorrelation function, and the fluctuations are averaged, instead. In figure 2, the time independent part of the autocorrelation function has a value of $\langle i \rangle^2$. It is removed electronically, in pratice. The noise associated with the time independent part can not be removed, since it is in the form of fluctuations. The noise from the time independent part of the signal must be prevented from obscuring the desired signal.

The manner of doing this is the second counter-intuitive aspect of fluctuation experiments. To get acceptable signal to noise, the sample is made as small as possible, within the limits of detectability. The time varying part of the autocorrelation function is proportional to the size of the sample. The time independent part is proportional to the square of the sample size. Thus, the smaller the sample, the larger are the relative fluctuations, and the greater is the time varying part compared to the time independent part.

Figure 2. The autocorrelation function, $G(\tau)$, of a signal has a maximum at $\tau = 0$. For a fluctuating signal with non-zero mean, it decays to the square of the average signal, in the absence of long term correlations. The decay amplitude and the average signal are both proportional to the size of the system.

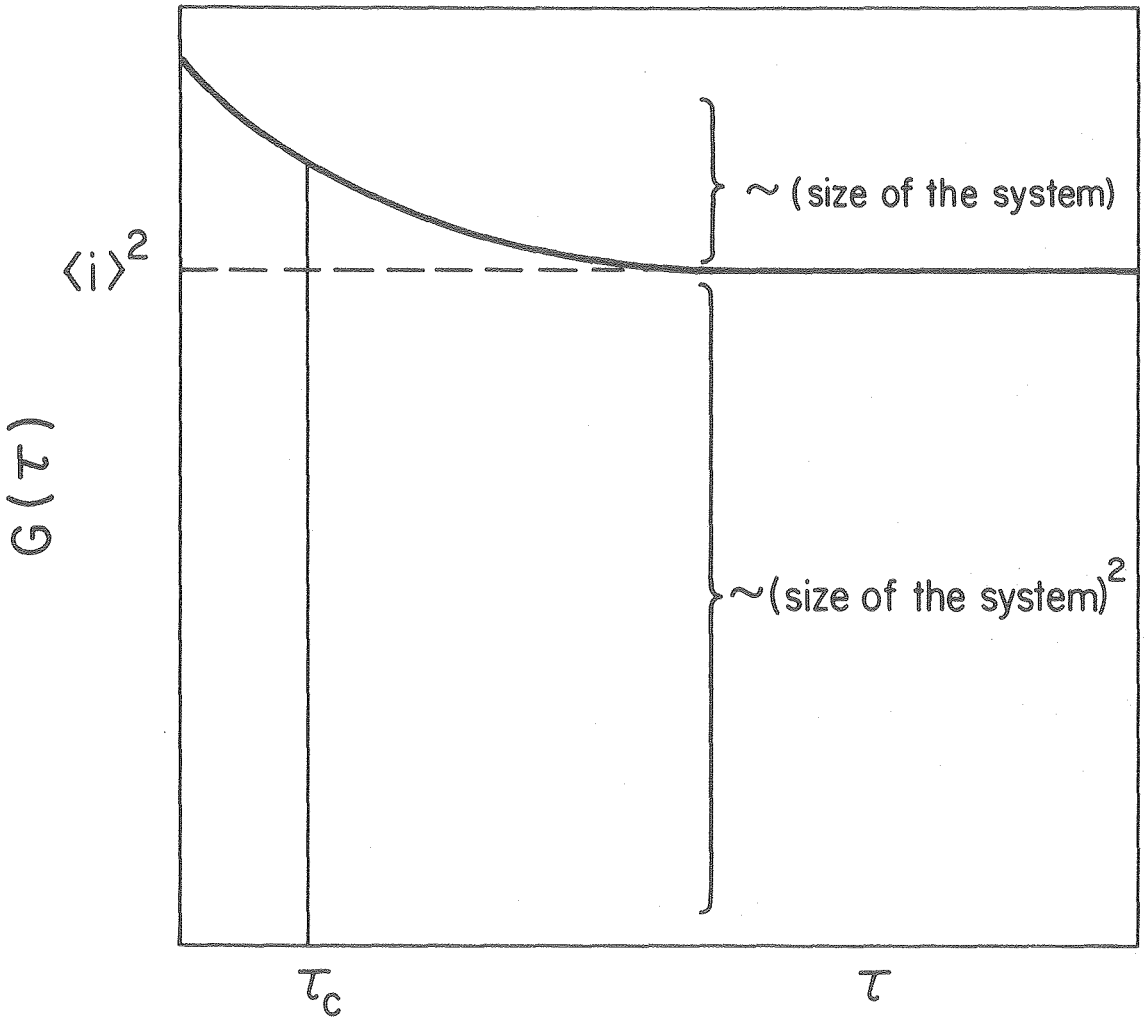

XBL 7910-5059

References

1.) D. Magde, Quarterly Reviews of Biophysics 9, 35 (1976).

2.) W. Webb, Quarterly Reviews of Biophysics 9, 49 (1976).

3.) E. Elson, and W. Webb, Annual Reviews of Biophysics and Bioengineering, 4, 311 (1975).

4.) L. Landau, and E. Lifshitz, Statistical Physics sect. 117-118, 2nd Ed. (Addison-Wesley, Reading, Mass. 1964).

5.) F. Reif, Fundamentals of Statistical and Thermal Physics ch. 15, (McGraw Hill, New York, New York 1965).

6.) G. Feher, and M. Weissman, Proc. Nat. Acad. Sci. 70, 870 (1973).

7.) E. Bamberg, and P. Läuger, J. Membrane Biol. 11, 177 (1973).

8.) H.-A. Kolb, P. Läuger, and E. Bamberg, J. Membrane Biol. 20, 133 (1975).

9.) H. Zingsheim, and E. Neher, Biophys. Chem. 2, 197 (1974).

10.) C. Stevens, Nature 270, 391 (1977).

11.) D. Schafer, Science 180, 1293 (1973).

12.) S. Aragon, and R. Pecora, Bioploymers 14, 119 (1975).

13.) M. Ehrenberg, and R. Rigler, Quarterly Reviews of Biophysics 9, 69 (1976).

14.) G. Phillips, Bioploymers 14, 499 (1975).

DERIVATION OF AUTOCORRELATION FUNCTIONS

The form for autocorrelation functions of fluctuations in fluorescence intensity has been derived for several important cases.[1-5] Some of the results are relevant to experiments described below. Those results will be reviewed, here.

Elson and Magde derived autocorrelation functions for the cases of translational diffusion and diffusion coupled with simple chemical reactions involving diffusing species. The photocurrent due to diffusing fluorescent molecules is denoted $i(t)$. If the average photocurrent is $\langle i \rangle$ then fluctuations in the photocurrent are denoted $\delta i(t) = i(t) - \langle i \rangle$. The autocorrelation function, $G(\tau)$ is defined by

$$G(\tau) = \lim_{T \to 0} \int_0^T \delta i(t) \delta i(t+\tau) dt$$

For a stationary random process, $G(\tau)$ can also be written $G(\tau)$

$$G(\tau) = \langle \delta i(0) \delta i(\tau) \rangle$$

where the brackets indicate ensemble averaging.

Among the important results found in reference 1, is the expression for $G(\tau)$ in the case of simple translational diffusion.

$$\frac{G(\tau)}{\langle i \rangle^2} = \frac{1}{\pi w^2 LC} \frac{1}{1 + \tau/\tau_D} \qquad (1)$$

The characteristic diffusion time, τ_D, can be thought of as the time to diffuse across the illuminated region. In fact, $\tau_D = w^2/4D$, where D is the diffusion coefficient. In deriving expression (1), it is assumed that the open illuminated volume is defined by a laser beam with gaussian intensity profile having e^{-2} radius of w. Then the intensity profile can be written as $I(r) = I_0 \exp(-2r^2/w^2)$. It is further assumed that the sample absorbs a negligible fraction of the

beam power, and that the beam radius is constant over the depth of the sample, L. C is the average number concentration of diffusing molecules in the sample. We see that $\langle i \rangle^2/G(0)$ can be thought of as the number of molecules in the beam.

Another result is that, in the presence of many diffusing species, G(0) can be expressed as

$$\frac{G(0)}{\langle i \rangle^2} = \frac{\sum_i (\varepsilon_i Q_i)^2 C_i}{\pi w^2 L \left(\sum_i \varepsilon_i Q_i C_i \right)^2}$$

where the index, i, runs over the different diffusing species. C_i is the number concentration of the i^{th} species, which has a decadic extinction coefficient, ε_i, and quantum efficiency for fluorescence, Q_i. Again, the sample depth is L, and the beam e^{-2} radius is w. Strongly fluorescent species contribute to G(0) to a greater extent than to $\langle i \rangle^2$.

Another useful result refers to the case of diffusion of molecules coupled by a bimolecular reactio of the form

$$A + B \underset{k_b}{\overset{k_f}{\rightleftharpoons}} C \ .$$

Forward and backward reactiom rates are k_f and k_b, respectively. If one assumes that A and C are large molecules and that B is small, the the diffusion coefficient of B will be much greater than the ones for A and C. In many experiments, it will also be true that $\varepsilon_A Q_A$ and $\varepsilon_B Q_B$ will be much smaller than $\varepsilon_C Q_C$. That is, only the complex is strongly fluorescent. One additional condition to make is that the rate of relaxation of the chemical reaction should be much faster than the characteristic diffusion rate. Bimolecular reactions relax exponentially

to equilibrium, following small perturbations, with a rate R, such that

$$R = k_b + k_f([A] + [B]) \ .$$

Then the last condition can be restated as $R >> D/w^2$.

Each of these conditions is satisfied in the case of binding of the fluorescent dye, ethidium bromide to DNA. Making the above assumptions, an approximate expression for the autocorrelation function is stated in three terms.

$$\frac{G(\tau)}{\langle i \rangle^2} = \frac{G_0(\tau)}{\langle i \rangle^2} + \frac{G_+(\tau)}{\langle i \rangle^2} + \frac{G_-(\tau)}{\langle i \rangle^2}$$

$G_0(\tau)$ can be thought of as describing diffusion of large DNA molecules, each one bearing dye molecules. DNA molecules with no bound chromophores would not be observed. In the case of strong binding,

$$\frac{G_0(\tau)}{\langle i \rangle^2} = \frac{1}{\pi w^2 LD} \frac{1}{1 + \tau/\tau_0}$$

where D is the concentration of stained DNA molecules. The characteristic diffusion time, τ_0, corresponds to τ_D, the characteristic time for free diffusion.

$$\tau_0 = w^2/4D_{DNA}$$

Here, D_{DNA} is the diffusion constant for DNA.

$G_+(\tau)$ can be thought of as describing diffusion of individual dye molecules, slowed as they bind to and release from DNA binding sites. In the case of strong binding, it can be written as

$$\frac{G_+(\tau)}{\langle i \rangle^2} = \frac{1}{\pi w^2 LC} \frac{1}{1 + \tau/\tau_+} \ .$$

In this case, C is the average concentration of bound dye molecules. The diffusion time, τ_+, should depend on the strength of the binding. If dye molecules spend most of their time bound, the diffusion time will be relatively long. Binding strength can be expressed in terms of the binding constant, K. For the bimolecular reaction of interest,

$$K = \frac{k_f}{k_b} = \frac{[C]}{[A][B]} .$$

The diffusion time, τ_+ can be expressed in terms of K and τ_D, the diffusion time for free dye.

$$\tau_+ = \tau_D(1 + K[A])$$

K[A] is the ratio of bound to free dye. Thus, the rate of diffusion in $G_+(\tau)$ is slower than free diffusion by the proportion of time the dye is free.

$G_-(\tau)$ describes the binding and release of dye molecules to individual binding sites. The relaxation rate, R, appears only in the $G_-(\tau)$ term. In the case of strong binding,

$$\frac{G_-(\tau)}{\langle i \rangle^2} = \frac{e^{-R\tau}}{\pi w^2 LC} \frac{1}{1 + \tau/\tau_-} .$$

Here, $\tau_- = \tau_D(1 + 1/K[A])$. Thus, the rate of diffusion in the $G_-(\tau)$ term is slower than the rate for free diffusion by the proportion of time the dye is bound.

The condition for strong binding has been that $K[A] \gg 1$. If this condition is not satisfied, then $G_+(\tau)$ and $G_-(\tau)$ will contain additional terms of appreciable magnitude.

Rotational diffusion has also been considered.[2-4] Fluorescence intensity fluctuation autocorrelation functions can be written as the sum of exponential decays in the case of purely rotational diffusion. The coefficients of the terms depend on the geometry of the illuminating and detecting devices.

The expected autocorrelation function for coupled translational and rotational diffusion has been reported, but the results vary somewhat in important aspects. A simple and direct derivation will be presented here, that accounts for the essential features of the autocorrelation function. It will be instructive to rederive the results for translational and rotational diffusion illustrating the approach that will be used for coupled diffusion.

Translational diffusion. It is important that no cross correlations be considered between photons emited by different molecules. Therefore, we suppose that only one fluorescent molecule is present in the sample. Initially, it is at point r_0. Fluorescence is detected by a photomultiplier. The ensemble average of the photocurrents from many such systems can be written in the notation of reference 1.

$$i(t) = g\varepsilon Q \int P(r,t)I(r)\, d^2r$$

The gain of the photomultiplier is represented by the factor g. $I(r)$ is the illuminating intensity profile, $P(r,t)$ is the probability of finding the molecule at the point r after time $t>0$. The symmetry of the problem is 2-dimensional throughout these calculations.

$P(r,t)$ will obey the 2-dimensional diffusion equation.

$$\frac{\partial P(r,t)}{\partial t} = D\,\nabla^2 P(r,t) \qquad (1)$$

D is the diffusion coefficient. We introduce the Fourier transform pair.

$$P(r,t) = \frac{1}{2\pi}\int e^{ikr}\, p(k,t)\, d^2k$$

$$p(k,t) = \frac{1}{2\pi}\int e^{-ikr}\, P(r,t)\, d^2r$$

Transforming Eq.1, we see that

$$\frac{\partial p(k,t)}{\partial t} = -k^2 D p(k,t)$$

so that $$p(k,t) = p(k,0)\exp(-k^2Dt)$$

$p(k,0)$ can be expressed in terms of $P(r,0) = \delta(r - r_o)$.

$$p(k,0) = \frac{1}{2\pi}\int e^{-ikr''}\, P(r'',0)\, d^2r'' = \frac{1}{2\pi}\, e^{-ikr_o}$$

Then, $$P(r,t) = \frac{1}{4\pi^2}\int e^{ik(r-r_o)}\, e^{-k^2Dt}\, d^2k$$

and, $$P(r,t) = \frac{1}{4\pi Dt}\, \exp(-(r-r_o)^2/4Dt)$$

As expected, $P(r,t)\, d^2r = 1$.

The autocorrelation function for one molecule, $G_1(\tau)$ is

$$G_1(\tau) = \langle \delta i(0)\delta i(\tau)\rangle = g^2\varepsilon^2Q^2 \int P(r,0)P(r',\tau)I(r)I(r')\, d^2r\, d^2r'$$

$$= \frac{g^2\varepsilon^2Q^2}{4\,Dt}\int I(r_o)I(r')\, e^{-(r-r_o)^2/4D\tau}\, d^2r'$$

Taking $I(r) = I_o\exp(-2r^2/w^2)$, and performing the integrals, we find

$$G_1(\tau) = \frac{g^2\varepsilon^2Q^2{I_o}^2}{1 + 8D\tau/w^2}\, \exp\left(- \frac{4r^2\,(1 + 4D\tau/w^2)}{w^2\,(1 + 8D\tau/w^2)}\right)$$

The autocorrelation function for a uniform distribution of many

independent molecules would be the superposition of autocorrelation functions having the form of $G_1(\tau)$. Thus,

$$G(\tau) = C \int G_1(\tau)\, d^2r_o \ .$$

where C is the average 2-dimensional number concentration of chromophores. Then,

$$G(\tau) = \frac{\pi w^2\, g^2\varepsilon^2 Q^2 I_o^2\, C}{4\,(1 + 4D\tau/w^2)} \ .$$

The average photocurrent for many chromophores is

$$\langle i \rangle = g\varepsilon Q\, C \int I(r)\, d^2r = g\varepsilon Q\, C\, I_o \frac{\pi w^2}{2} \ .$$

In agreement with reference 1, we find,

$$\frac{G(\tau)}{\langle i \rangle^2} = \frac{1}{\pi w^2 C} \frac{1}{1 + 4D\tau/w^2}$$

Rotational diffusion. We may borrow from the notation of reference 2 to compute the fluorescence intensity autocorrelation function for rotational diffusion. Let $H(\Omega)$ be the probability that a molecule with orientation Ω will absorb and emit a detectable photon. Thus, $H(\Phi$ includes information about the orientations of both the emission and absorption dipole moments. We take one fluorescent molecule to be present at position r_o initially at orientation Ω_o The ensemble average photocurrent for many such systems will be

$$i(t) = g\varepsilon Q \int P_\rho(r_o,\Omega,t) H(\Omega) I(r)\, d\Omega,$$

where $P_\rho(r_o,\Omega,t)$ is the probability that the molecule at position r_o will have orientation Ω after time $t>0$. $P_\rho(r_o,\Omega,t)$ obeys the rotational

diffusion equation. We may take a high order of symmetry for the purpose of illustrating the derivation.

$$\frac{\partial P_\rho(r_o,\Omega,t)}{\partial t} = D_\rho \, L^2 P_\rho(r_o,\Omega,t)$$

where $L^2 = \frac{1}{\sin^2\theta}\frac{\partial^2}{\partial\phi^2} + \frac{1}{\sin\theta}\frac{\partial}{\partial\theta}\left(\sin\theta\frac{\partial}{\partial\theta}\right)$, and D_ρ is the rotational diffusion coefficient. $P_\rho(r_o,\Omega,t)$ can be expressed in terms of the spherical harmonics, $Y_{\ell m}(\Omega)$.

$$P_\rho(\Omega,\tau) = \sum_{\ell,m} \exp(-\ell(\ell+1)D_\rho\tau)\, K_{\ell m}\, Y_{\ell m}(\Omega)$$

Then, $$K_{\ell m} = \int P(\Omega'',0)Y^*_{\ell m}(\Omega'')\, d\Omega'' = Y^*_{\ell m}(\Omega_o)$$

and, $$P_\rho(\Omega,\tau) = \sum_{\ell,m} \exp(-\ell(\ell+1)D_\rho\tau)\, Y_{\ell m}(\Omega)Y^*_{\ell m}(\Omega_o).$$

The autocorrelation function for one molecule, $G_1(\tau)$, is

$$G_1(\tau) = g^2\varepsilon^2Q^2 \int P_\rho(r_o,\Omega,0)P_\rho(r_o,\Omega',\tau) \times I^2(r_o)H(\Omega)H(\Omega')\, d\Omega d\Omega'.$$

$$G_1(\tau) = g^2\varepsilon^2Q^2\, I^2(r_o) \sum_{\ell,m} \exp(-\ell(\ell+1)D_\rho\tau)\, Y_{\ell m}(\Omega_o) \int Y_{\ell m}(\Omega') \times H(\Omega_o)H(\Omega')\, d\Omega'$$

If many chromophores are present and uniformly distributed in initial orientation, then we may write the combined autocorrelation function, $G(\tau)$, as

$$G(\tau) = C \int G_1(\tau)\, d\Omega_o/4\pi \, .$$

$$G(\tau) = (C/4\pi)g^2\varepsilon^2Q^2 \int I^2(r_o)\, d^2r_o \sum_{\ell,m} \exp(-\ell(\ell+1)D_\rho\tau) \times \left| \int H(\Omega)Y_{\ell m}(\Omega)\, d\Omega \right|^2$$

The average photocurrent, $\langle i \rangle$, will be

$$\langle i \rangle = (C/4\pi)\, g\varepsilon Q \int I^2(r)\, d^2r \int H(\Omega)\, d\Omega$$

and $$G(\tau)/\langle i \rangle^2 = (4\pi/\pi w^2 C) \sum_{\ell,m} \exp(-\ell(\ell+1)D_\rho \tau) \times \frac{\left| \int H(\Omega) Y_{\ell m}(\Omega)\, d\Omega \right|^2}{\left[\int H(\Omega)\, d\Omega \right]^2}$$

This result extends the computations in reference 2 to the case of an open volume with gaussian illumination. It corresponds to the result of reference 2 with the understanding that $\pi w^2 C$ is the number of molecules in the beam.

Coupled translational and rotational diffusion. Again, we consider one molecule in the sample, initially at point r_0 and orientation Ω_0. Rotational and translational motion are taken to be independent, so the probability function factors into translational and rotational parts.

$$P(r,\Omega,t) = P_r(r,t) P_\rho(\Omega,t)$$

As in the previous two cases,

$$P_r(r,t) = \frac{1}{4\pi Dt} \exp(-(r-r_0)^2/4Dt)$$

and $$P_\rho(\Omega,t) = \sum_{l,m} \exp(-\ell(\ell+1)D_\rho t)\, Y_{\ell m}(\Omega) Y^*_{\ell m}(\Omega_0)$$

The ensemble average photocurrent and the autocorrelation function also factor.

$$\langle \delta i(t) \rangle = g\varepsilon Q \int I(r) P_r(r,t)\, d^2r \int H(\Omega) P_\rho(\Omega,t)\, d\Omega$$

$$G(\tau) = (g^2\varepsilon^2Q^2/4\pi D\tau) \int I(r_o)I(r')\exp(-(r'-r_o)^2/4D\tau)\, d^2r'$$
$$\times \sum_{\ell,m} \exp(-\ell(\ell+1)D_\rho\tau)\, H(\Omega_o)Y^*_{\ell m}(\Omega_o)\, H(\Omega')Y_{\ell m}(\Omega')$$

Performing the indicated spatial integrals,

$$G_1(\tau) = \frac{g^2\varepsilon^2Q^2}{1 + 8D\tau/w^2}\exp\left(-4\,\frac{r_o^2}{w^2}\,\frac{1 + 4D\tau/w^2}{1 + 8D\tau/w^2}\right)$$

$$\times \sum_{l,m} \exp(-\ell(\ell+1)D_\rho\tau)\, H(\Omega_o)Y^*_{\ell m}(\Omega_o) \int H(\Omega')Y_{\ell m}(\Omega')\, d\Omega'$$

Other independently diffusing molecules can be taken into account. The overall photocurrent fluctuation autocorrelation function and average photocurrent become

$$G(\tau) = (C/4\pi) \int G_1(\tau)\, d^2r_o\, d\Omega_o$$

and
$$\langle i\rangle = g\varepsilon Q\,(C/4\pi) \int I(r)\, d^2r \int H(\Omega)\, d\Omega$$

$$\frac{G(\tau)}{\langle i\rangle^2} = \frac{1}{\pi w^2 C}\,\frac{1}{1 + 4D\tau/w^2}\; 4\pi \sum \exp(-\ell(\ell+1)D_\rho\tau)$$
$$\times \frac{\left|\int H(\Omega)Y_{\ell m}(\Omega)\, d\Omega\right|^2}{\left[\int H(\Omega)\, d\Omega\right]^2}$$

Several points may be noted. One is that rapid rotational motion has no effect on the translational part of the autocorrelation function. This is because the ℓ=0 term in the rotational part is the time independent part, and has magnitude one. The other point is that rapid translational motion <u>will</u> effect the observed autocorrelation function, making it impossible to observe rotational motion.

There is a simple intuitive argument that favors the result

arrived at, here. The autocorrelation function measures correlations between photons. Correlated photons from one molecule cease to be measured when that molecule leaves the beam. Thus, the observed time scale can be no slower than the scale of translational diffusion. If rotational diffusion were slower than translational diffusion, the observed autocorrelation function would be dominated by faster translational motion.

References

1. E. Elson, and D, Magde, Biopolymers 13, 1 (1974).

2. J. T. Yardley, and L. Specht, Chem. Phys. Letters 37, 543 (1976).

3. S. Aragon, and R. Pecora, J. Chem. Phys. 64, 1791 (1976).

4. M Ehrenberg, and R. Rigler, Chem. Phys. 4, 390 (1974).

5. D. Magde, W. Webb, and El Elson, Biopolymers 17, 361 (1978).

HEATING OF THE SAMPLE BY ABSORBED LIGHT

The question of heating naturally arises when fluorescence is excited in a very small volume. In fluctuation experiments using a pulsed exciting beam, an estimate of heating has been reported of considerably less than one degree.[1] In experiments described below, beam power ranges from about 0.01 to 1 millewatt. For photons with a wavelength of 500 nm., that is equivalent to 2.5×10^{13} to 2.5×10^{15} photons/sec. This flux will be directed through an area as small as 3×10^{-8} cm^2. It is true that heat will diffuse away from a small volume quickly, but some quantitative estimate is called for to rule out the possibility of excessive heating in the sample.

The temperature will vary radially from the beam axis. That is, we may assume cylindrical symmetry. For simplicity, we also assume that the glass boundaries will conduct away no heat. This makes the problem 2-dimensional.

The temperature profile will obey the diffusion equation.

$$\frac{\partial T(r)}{\partial t} = D\ \nabla^2 T(r) + Q(r)/\rho c \qquad (1)$$

where $T(r)$ is the temperature at a radial displacement, r, from the beam axis, D is the thermal diffusivity of the solution, $Q(r)$ is the power per unit of volume entering the system at point r, ρ is the mass density, and c is the heat capacity. We define the flux, $\vec{J}$, to be

$$\vec{J} = -k\vec{\nabla}T(r) \qquad (2)$$

where k is the thermal conductivity. Energy conservation can be stated in terms of the flux and the temperature change by the expression

$$\vec{\nabla}\cdot\vec{J} + \rho c \frac{\partial T(r)}{\partial t} = Q(r). \qquad (3)$$

These three expressions can be combined to show that $k = \rho cD$.

In the case of illumination by a focussed laser beam, the temperature increase will be computed in two steps. First the temperature rise at a location r and time t due to the deposition of energy at a location r_0 at an earlier time t_0 will be computed. Next, all points in the illuminated region will be allowed to contribute energy by diffusion to a point r, in effect summing up contributions from a distribution of energy sources.

From the diffusion equation, we know that energy deposited instantaneously at a position r_0 at a time t_0 will diffuse to a position r in a time $\Delta t = t - t_0$ according to the expression

$$T(r,t) = T(r_0,\Delta t)\exp(-(r-r_0)_2/4D\Delta t). \qquad (4)$$

$T(r_0,\Delta t)$ can be evaluated given the amount of energy deposited at r_0 at time t_0. If an amount of energy, Q is deposited, then

$$Q = c \int \rho(r)T(r,t)\, d^3r = cL\rho \int T(r,t)\, d^2r$$

$$= cL\rho T(r_0,\Delta t) \int \exp(-(r-r_0)^2/4D\Delta t)\, d^2r$$

$$= 4\pi cL\rho D\, T(r_0,\Delta t)\Delta t,$$

where L is the sample depth. Then, $T(r_0,\Delta t) = Q/(4\pi cL\rho D\Delta t)$. Thus, we can write the temperature rise at a point r after a time Δt, due to an amount of energy Q placed at point r_0, as

$$T(r,\Delta t) = \frac{Q}{4\pi DLc\rho\Delta t} \exp(-(r-r_0)^2/4D\Delta t) \qquad (5)$$

Next, we express the energy deposited in terms of the laser power absorbed, P. $Q = P\tau$, where τ is a short interval of time, during which energy is delivered to a point r_0 at the rate P. We may allow energy to be delivered with a spatial density I(r), so that the power passing through an area ΔA is $\Delta P = \int_{\Delta A} I(r)\, d^2r$.

In the experiments of interest, the laser illumination has a gaussian intensity profile. Given a beam with e^{-2} radius of w, the intensity profile can be written $I(r) = I_0 \exp(-2r^2/w^2)$. If the total power in the beam is P, then we can write

$$P = \int I(r)\, d^2r = I_0 \pi w^2/2. \tag{6}$$

Then, $I_0 = 2P/\pi w^2$. Of the total amount of power incident on the sample, a fraction, α, will be absorbed. We can write the temperature rise at a point r after time Δt in terms of the above quantities as

$$T(r,\Delta t) = \int_{-\infty}^{t} dt' \int_0^{\infty} d^2r_0 \frac{\alpha I_0 \exp(-2r_0^2/w^2)}{4\pi Dt' L c\rho} \exp(-(r-r_0)^2/4Dt'. \tag{7}$$

$$= \frac{P}{4\pi DLc\rho} \int_a^b \exp(-x)/x\, dx, \tag{8}$$

where $a = 2r^2/(w^2(1 + 8Dt/w^2))$, and $b = 2r^2/w^2$. No closed form solution exists for the integral in equation (8). A series solution may be written for the temperature rise.

$$T(r,\Delta t) = \frac{\alpha P}{4\pi DLc\rho}\left(\log\left(1+\frac{8D\Delta t}{w^2}\right) + \sum_{n=1}^{\infty}(-2r^2/w^2)\frac{1}{n\ n!}\left(1 - \left(1+\frac{8D\Delta t}{w^2}\right)^{-n}\right)\right) \tag{9}$$

On the beam axis, $T(0,\Delta t) = \frac{\alpha P}{4\pi DLc\rho} \log\left(1 + \frac{8D\Delta t}{w^2}\right)$. The expression for $T(r,\Delta t)$ can be confirmed by computing the flux, $\vec{J} = -k\vec{\nabla}T(r,\Delta t)$, its divergence, and the quantity $\rho c\, \partial T(r,\Delta t)/\partial t$.

We find $\vec{\nabla}\cdot\vec{J} + \rho c \frac{\partial T}{\partial t} = \frac{2P\alpha}{\pi w^2 L} \exp(-2r^2/w^2)$. Since the power per unit volume, absorbed by the system is $I(r)/L = \frac{2P\alpha}{\pi w^2 L} \exp(-2r^2/w^2)$, wee see that equation 9 is the proper expression for the temperature rise due to heating from power absorbed from the illuminating beam.

We can now apply this expression to the experiments of interest. The samples studied never had an extinction coefficient of more than 10^6 liter/mole-cm. They were less concentrated in dye than 10^{-6} M, and were usually thinner than 10^{-3} cm. If absorption follows Beer's law, then one photon in 10^3 would be absorbed. Thus, when one milliwatt of power was incident on the sample, less than 10^{-6} watts was absorbed. Most of this was emitted as fluorescence in the case of Rhodamine 6G. Ethidium bromide samples were all more dilute than 10^{-6} M by almost two orders of magnitude, but had quantum efficiencies for fluorescence of only about 20%. The remaining 80% was converted to heat, for the most part. Overall then, the value of 10^{-6} watts for the power absorbed is a generous overestimate.

For dilute aqueous samples, the thermal properties will be the same as for water. We may take[2]

$$D = 1.4 \times 10^{-3} \text{ cm}^2/\text{sec}$$

$$c = 4.18 \text{ joules/gm-K}$$

$$\rho = 1.0 \text{ gm/cm}^3.$$

For a gaussian beam, with e^{-2} radius of 1 μ, the termperature rise on the beam axis will be less than 1.36×10^{-2} K $\log(1 + t/8.9 \times 10^{-7} \text{ sec})$. After 500 seconds, the temperature rise will be about 1/4 K.

To review the assumptions made in this estimate, we recall that cylindrical symmetry was used, the glass boundaries of the sample conducted away no heat, and absorbed no light. One milliwatt of power was incident on the sample, 0.1% of which was absorbed, and all the absorbed power was converted to heat. After one second under these conditions, the temperature rise would be about 1/5 K. After 500

seconds, the temperature rise would be about 1/4 K. The logarithmic increase in time of the temperature would be even less noticeable after 500 seconds. Computer calculations of the radial temperature increase profiles are shown in figure 3 for various times of exposure to illumination. We may conclude from this calculation that very small heating effects may be expected. Generous overestimation of possible heating effects leads to a very low upper bound on the amount of heating, even along the beam axis.

It is remarkable that heating effects as small as those computed here cause index of refraction changes that have been measured.[3-5] Experiments of the kind reported in references 3, 4, and 5 have been used to estimate optical absorption coefficients and their rates of change with temperature in apparently transparent liquids. Given those values, it would actually be possible to measure heating effects, in situ, in samples prepared for fluctuation correlation experiments. Such measurements were not attempted.

Figure 3. Computed temperature rise for a gaussian beam with e^{-2} radius of 1 μ. Beam power is 1 mW. Absorbed power is 1 μW in a 10 μ deep sample. Curves correspond to different illumination times. a) 15 μsec, b) 4 msec, c) 1 sec, d) 500 sec.

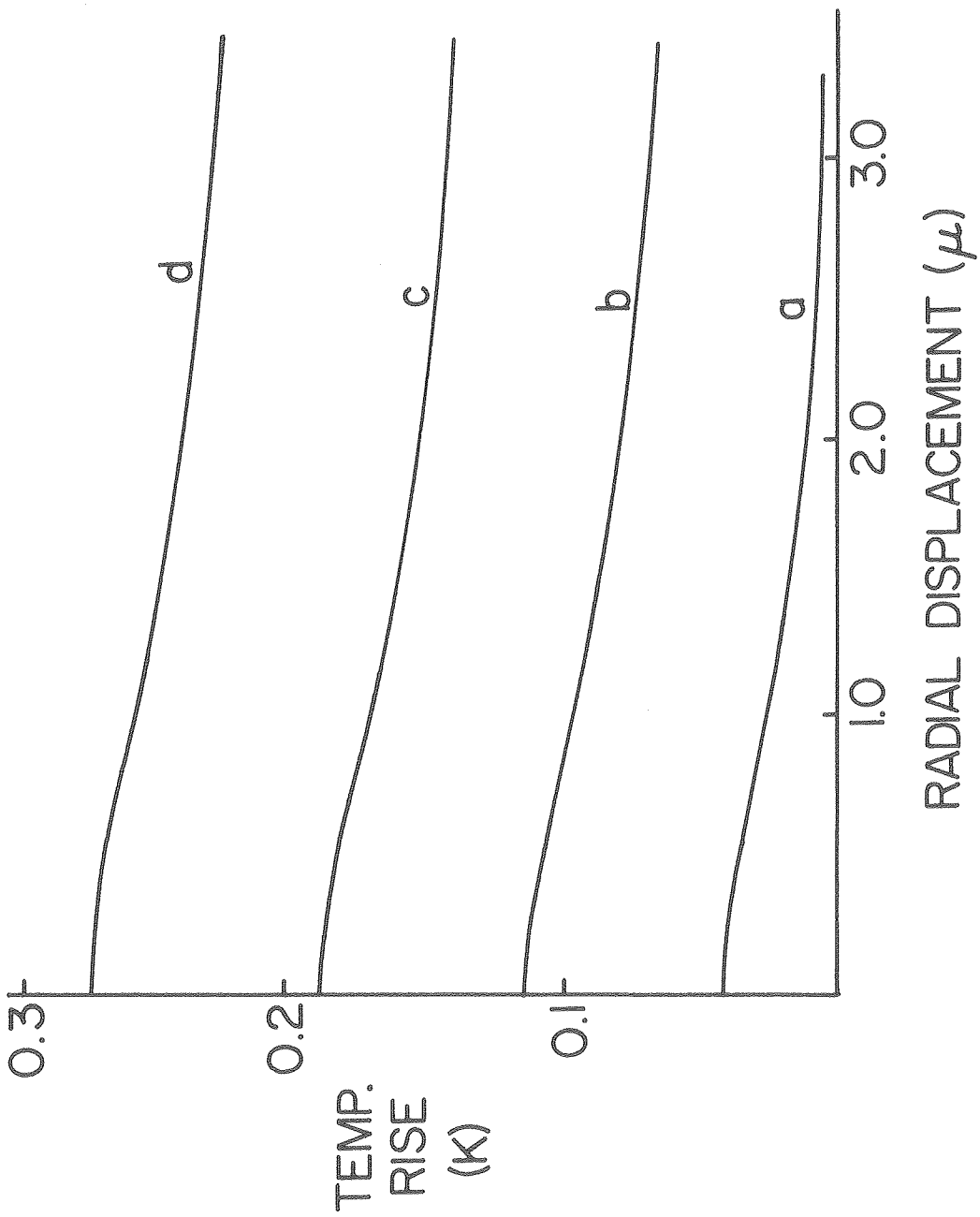

XBL798-4968

References

1.) D. Axelrod, Biophysical Journal 18, 129 (1977).

2.) Handbook of Chemistry and Physics 51st ed. (Chemical Rubber Co. Cleveland, Ohio. 1971)

3.) F. Dabby, R. Boyko, C. Shank, and J. Whinnery, IEEE J. of Quantum Electronics QE-5, 516 (1969).

4.) C. Hu, and J. Whinnery, Applied Optics 12, 72 (1978).

5.) J. Whinnery, Accounts of Chemical Research 7, 225 (1974).

MEASUREMENTS BASED OF VARYING THE BEAM SIZE

Analysis of autocorrelation functions of the fluctuations of fluorescence light intensity leads to the kinetic parameters, provided the focal spot size is known.[1-3] In this section, a simple method is presented for the determination of the focal spot size which circumvents the difficulties encountered by previous practitioners of this technique.

Generally, when it is desired to determine the size of a focal spot it is compared with an object whose dimensions have been determined previously by other methods. The difficulty increases as the beam size becomes smaller. Weissman, Schindler, and Feher describe a fluctuation correlation experiment in which a large sample volume is calibrated with polystyrene spheres.[4] Other approaches involve knife edges and thin fibers being translated across the focal spot.[5-7] By measuring the amount of light scattered by the fiber or knife edge, the profile of the beam intensity can be inferred. This is also a calibration step. The sample is subsequently placed in the beam and the sample and beam are brought into focus simultaneously, so that the sample is illuminated at the beam waist. Thus, the beam dimensions are measured in one experiment and the fluctuation measurements are made in a separate experiment or experiments.

It is possible to perform both measurements simultaneously. Near the focal plane, the beam shape varies in a known way. The fluctuation parameters will vary correspondingly so that the size of the beam waist and other experimental parameters can be estimated from the same data.

In fluorescence fluctuation experiments, one measures the

autocorrelation function, $G(\tau)$, of the photomultiplier current, $i(t)$. For the case of translational diffusion in an open volume,[2]

$$G(\tau) = G(0)/(1 + \tau/\tau_D) \tag{1}$$

which is completely specified by the two parameters, $G(0)$ and τ_D, where

$$\tau_D = \frac{w^2}{4D} = \frac{w_o^2}{4D}\left(1 + \frac{\lambda^2 \Delta z^2}{\pi^2 w_o^4}\right) \tag{2}$$

$$G(0) = \frac{\langle i \rangle^2}{\pi w^2 LC} = \frac{\langle i \rangle^2}{\pi L C w_o^2 (1 + \lambda^2 \Delta z^2 / \pi^2 w_o^4)}, \tag{3}$$

and w_o is the radius of the beam in the focal plane, D is the diffusion coefficient, C is the average concentration of fluorescent diffusing molecules in the illuminated volume, $\langle i \rangle$ is the average photocurrent, and Δz is the distance between the sample position and the position of the beam minimum.

Thus, both τ_D and $\langle i \rangle^2/G(0)$ depend on Δz in essentially the same way. If measurements of the parameters are expressed in the form

$$\tau_D = a\Delta z^2 + b \text{ and } \langle i \rangle^2/G(0) = c\Delta z^2 + d,$$

then, $$w_o^4 = \frac{\lambda^2 b}{\pi^2 a} = \frac{\lambda^2 d}{\pi^2 c}, \quad D = \frac{\lambda}{4\pi\sqrt{(ab)}}, \text{ and } \quad CL = \frac{\sqrt{(cd)}}{\lambda}.$$

In this way, measurements of the autocorrelation function at different values of Δz lead to essentially independent estimates of w_o, while simultaneously giving values for the diffusion coefficient, D, and the two-dimensional concentration, CL.

Before demonstrating the technique, we will first characterize the beam profile in front of the focussing lens. We can then predict the beam shape near the focal plane, after which the beam shape near

the focal plane will be measured directly. Finally, we will infer the beam shape from parameters measured by fluorescence fluctuation spectroscopy and compare the values obtained for the beam waist radius.

Beam Profile The illuminating beam is that of an argon ion laser operating at 488 nm. After spatial filtering, to reject higher modes, and recollimation, the beam is primarily gaussian in profile. To measure the intensity profile of the recollimated beam in the plane normal to the beam axis, a pinhole was translated across the beam. A photosensitive field-effect-transistor measured the light intensity transmitted by the pinhole. The pinhole and detector were driven by a micrometer. Figure 4 shows the beam intensity profile measured in this way. The points are measured values, while the solid curve is the fit of a gaussian to the observed values.

If $I(r) = I_0 \exp(-2r^2/d^2)$, then $d = 3.08$ mm.

Size of the focussed beam; prediction and direct measurement Scalar diffraction theory[8] predicts that the laser beam intensity in a plane perpendicular to the propagation direction remains gaussian in profile near the focal plane, so that

$$I(r) = I_0 \exp(-2r^2/w^2) \tag{4}$$

and

$$w^2 = w_0^2\left(1 + \frac{\lambda^2 \Delta z^2}{\pi^2 w_0^4}\right) \tag{5}$$

where w_0 is the beasm radius measured in the focal plane, λ is the wavelength of the laser light, and Δz is the displacement along the beam axis from the focal minimum.

The recollimated beam is focussed by a lens of focal length, $f = 25.4$ cm. The beam radius in the focal plane will be

Figure 4. The laser beam intensity profile is gaussian, with e^{-2} radius of 3.08 mm.

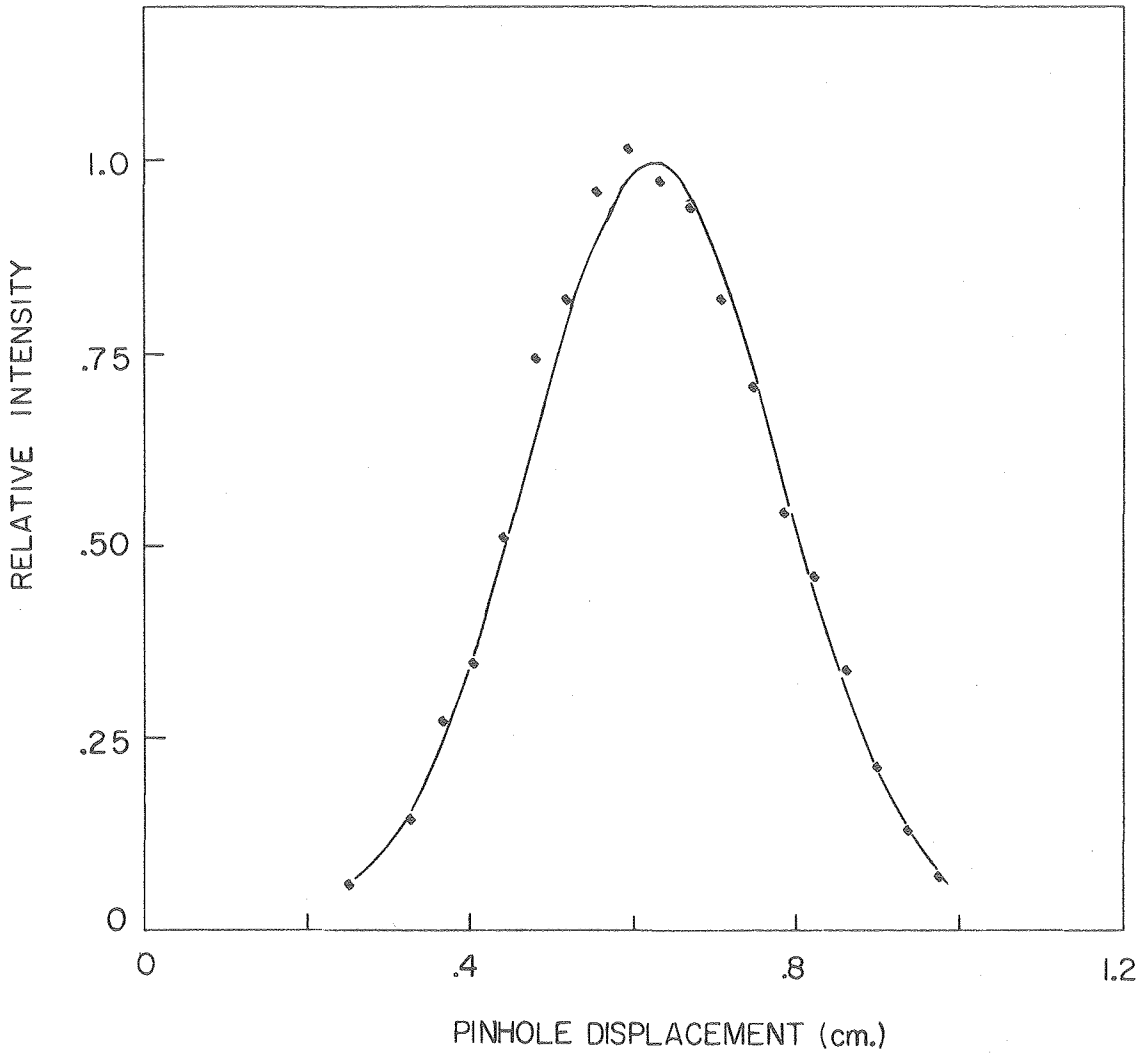
RELATIVE INTENSITY
1.0
.75
.50
.25
0
0
.4
.8
1.2
PINHOLE DISPLACEMENT (cm.)

XBL796-4855

$$w_0 = \frac{\lambda f}{\pi d}. \qquad (6)$$

Thus, we expect w_0 = 12.8 μ. The uncertainty in this value is about 0.5 μ.

When the beam is focussed, the pinhole used to characterize it will no longer be small compared to the dimensions of the beam. Translating the pinhole across the focussed beam would give a distorted measure of the intensity profile. Rather than translating the pinhole <u>across</u> the beam, the pinhole is translated <u>along</u> the beam to confirm the shape of the beam near the focal plane. The pinhole is centered on the beam axis, and the transmitted light intensity is measured as a function of displacement of the pinhole along the beam axis. The arrangement is shown in figure 5.

If we let T be the fraction of light transmitted, then

$$T = \frac{\int_0^{r_0} \exp(-2r^2/w^2)\ r\ dr}{\int_0^{\infty} \exp(-2r^2/w^2)\ r\ dr} \qquad (7)$$

where r_0 is the radius of the pinhole.

Next, we define $W^2(T) = -2/\ln(1-T)$. From the expression for T, we see that W(T) is the beam radius stated in units of r_0. That is, $W^2(T) = \frac{w_0^2}{r_0^2}(1 + \frac{\lambda^2 \Delta z^2}{\pi^2 w_0^4})$. Microphotographs of the pinhole indicate that it is roughly circular, with radius $r_0 = (23 \pm 1)\mu$. Airy diffraction rings of light transmitted by the pinhole give a value for r_0 of $(23.5 \pm 0.5)\mu$. Figure 6 shows how $W^2(T)$ varies with the position of the pinhole along the beam axis. The solid line is a computer fit to the data, assuming the parabolic dependence of $W^2(T)$ on Δz. From

Figure 5. Near the focal plane, a pinhole transmits part of the beam. A photodetector behind the pinhole measures transmitted light intensity.

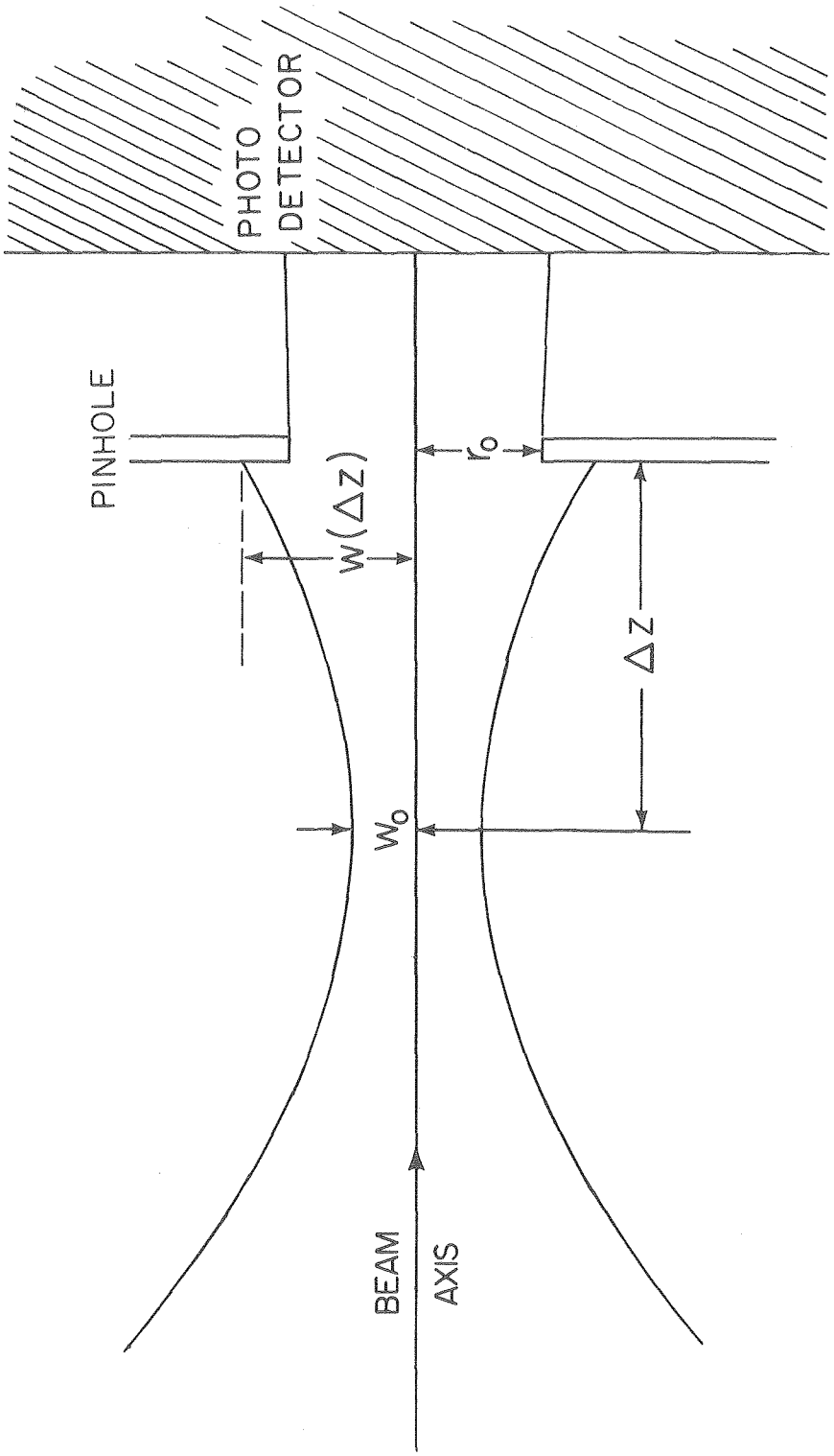

XBL-796-4856

Figure 6. The square of the beam e^{-2} radius near the focal spot is plotted in units of the pinhole radius, r_o. It depends quadratically on the displacement of the pinhole from the beam waist.

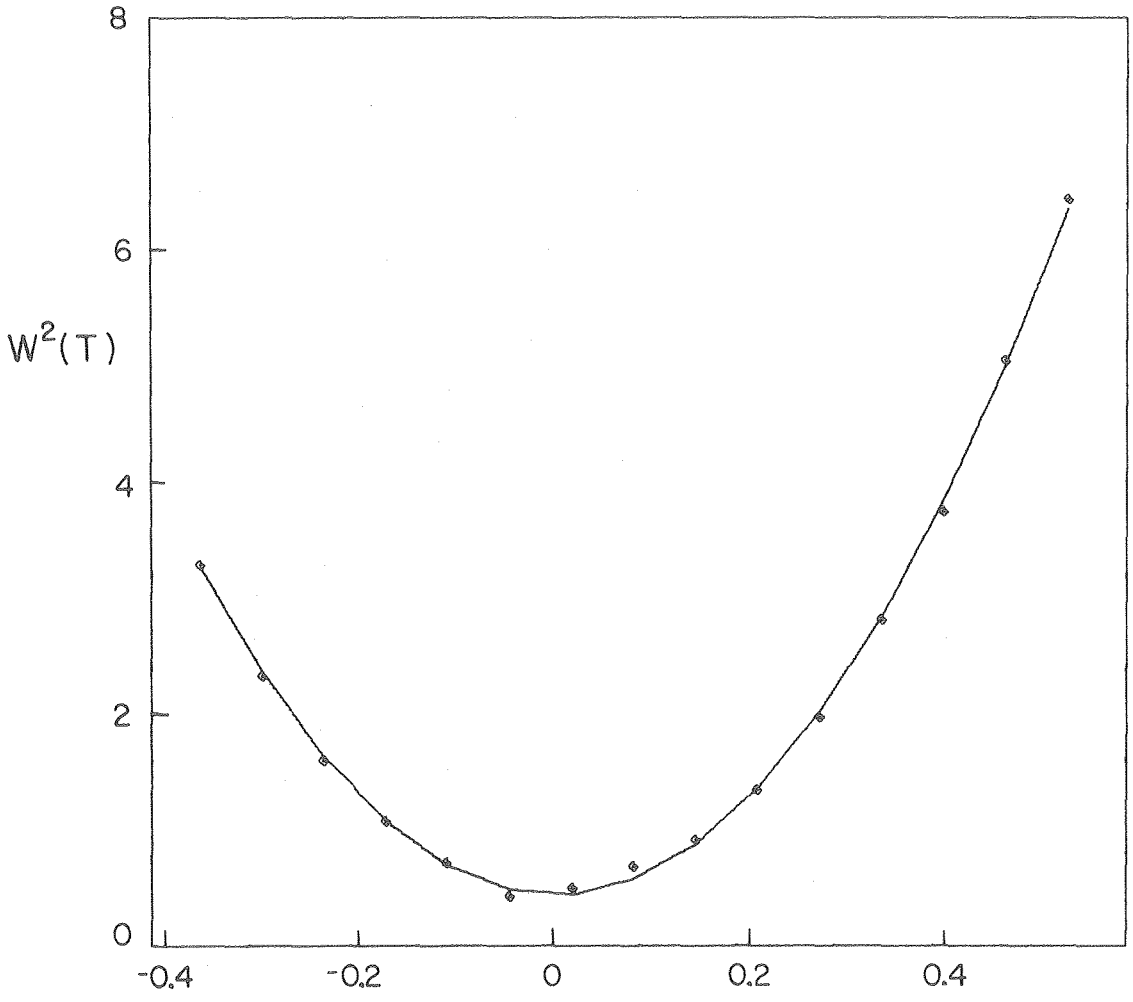

XBL796-4857

these data, we find w_o = 14μ and r_o = 22.6μ, which compare favorably with the expected values of 12.8μ for w_o and 23.4μ for r_o.

Beam shape inferred from fluctuation experiments The apparatus used for fluorescence fluctuation measurements is shown in figure 7. It is essentially the same as the one described in reference 3, except that our system contains an external servo for additional stabilization of the beam intensity. The beam power is monitored by a photosensitive field-effect-transistor. The sample is a dilute solution of Rhodamine 6G. It is situated at the focus of a paraboloidal mirror which directs fluorescent light to a photomultiplier. The photocurrent is converted to a voltage and amplified, so that the photomultiplier and the beam monitor show equal average voltages. A difference amplifier subtracts the beam monitor signal from the photomultiplier signal in an effort to minimize the effect of fluctuations in the beam intensity. The difference is correlated by a Saicor model SAI-43A Correlator and Probability Analyzer. The output of the autocorrelator is punched on paper tape. A computer finds the least squares fit of the data to a function of the form $G(\tau) = G(0)(1 + \tau/\tau_D)^{-1} + B$, where B is a constant. Correlations imposed on the signal by electronic filters are not considered in the computations.

Measurements are made for various displacements of the beam. From each individual autocorrelation function, estimates of τ_D and $\langle i \rangle^2/G(0)$ are made. These values of τ_D and $\langle i \rangle^2/G(0)$ are then plotted against position, Δz, and are shown in figures 8 and 9, respectively.

Error bars shown in figures 8 and 9 are computed from the differences between observed values of $G(\tau)$ and fitted values. Consequently, they reflect only the precision of the fit. The observed

Figure 7. Apparatus for Fluorescence Correlation Spectroscopy. Details are given in the text.

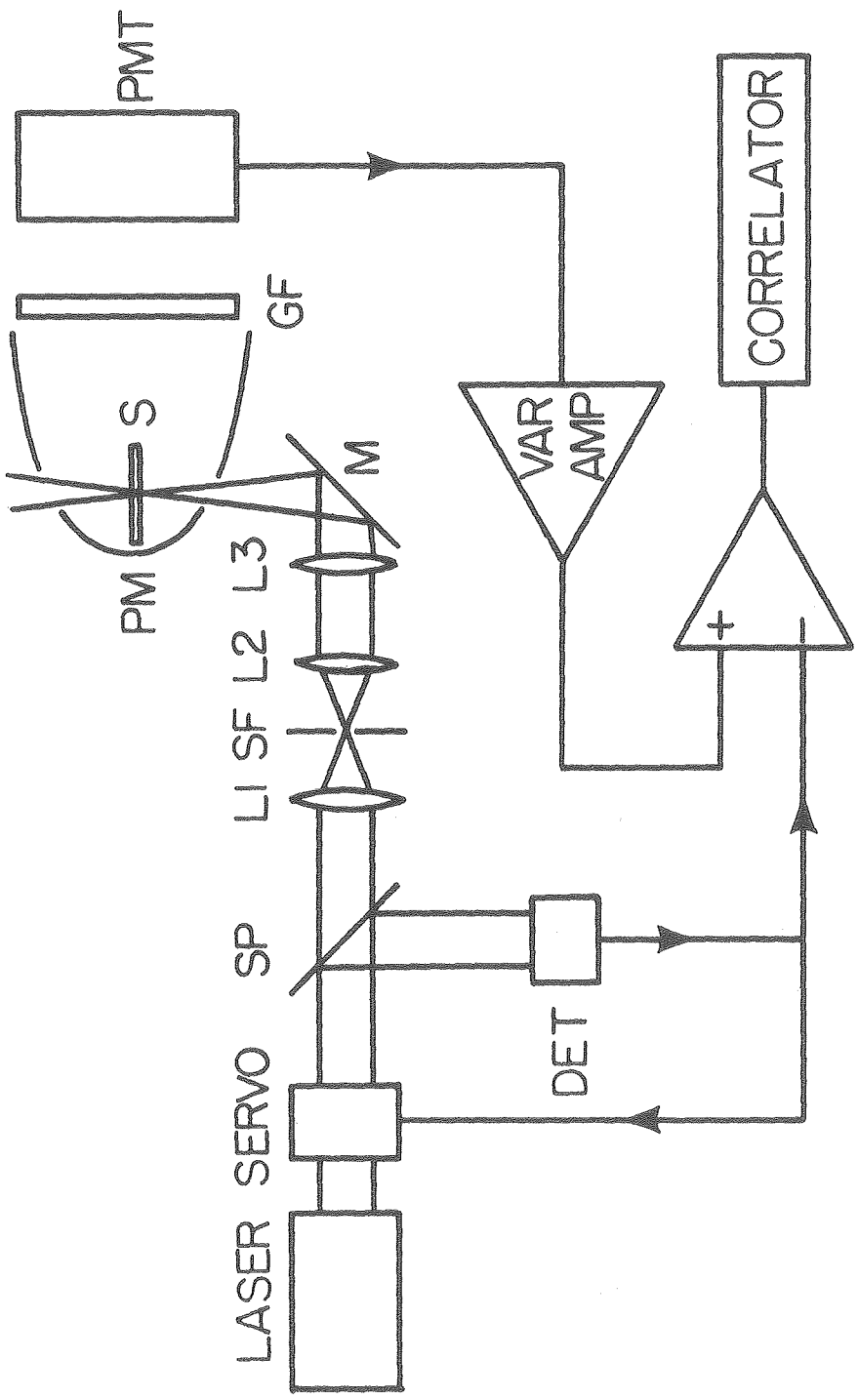

XBL796-4858

Figure 8. Diffusion times are plotted as a function of displacement of the beam focal plane through the sample. Error bars indicate only the precision of the computer fits of the autocorrelation functions. The solid line is the weighted least squares fit of a quadratic polynomial.

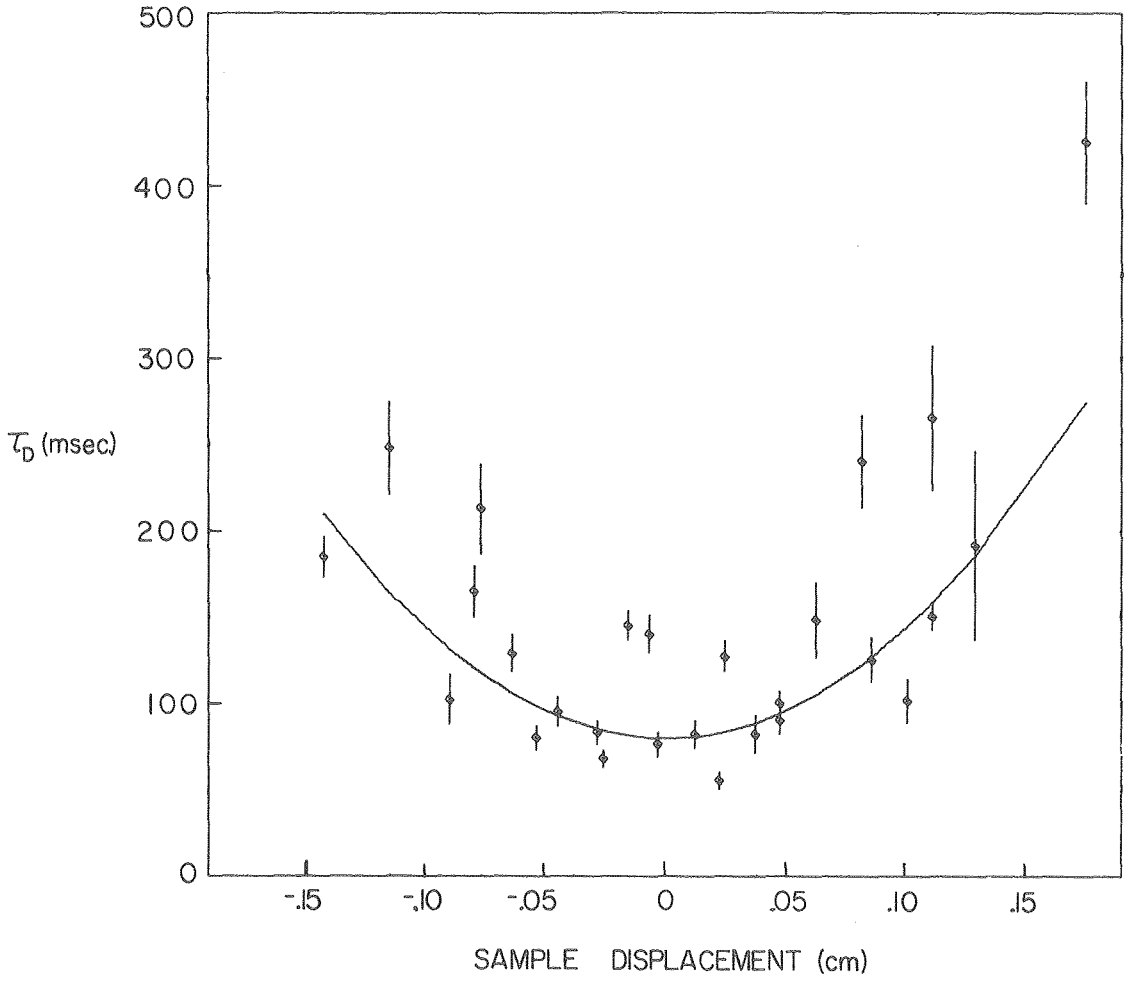
500
400
300
200
100
0
τ_D (msec)
-.15
-.10
-.05
0
.05
.10
.15
SAMPLE DISPLACEMENT (cm)

XBL796-4859

Figure 9. $\langle i \rangle^2/G(0)$ is plotted as a function of displacement of the beam focal plane through the sample. Error bars indicate only the precision of the computer fits of the autocorrelation functions. The solid line is the weighted least squares fit of a quadratic polynomial.

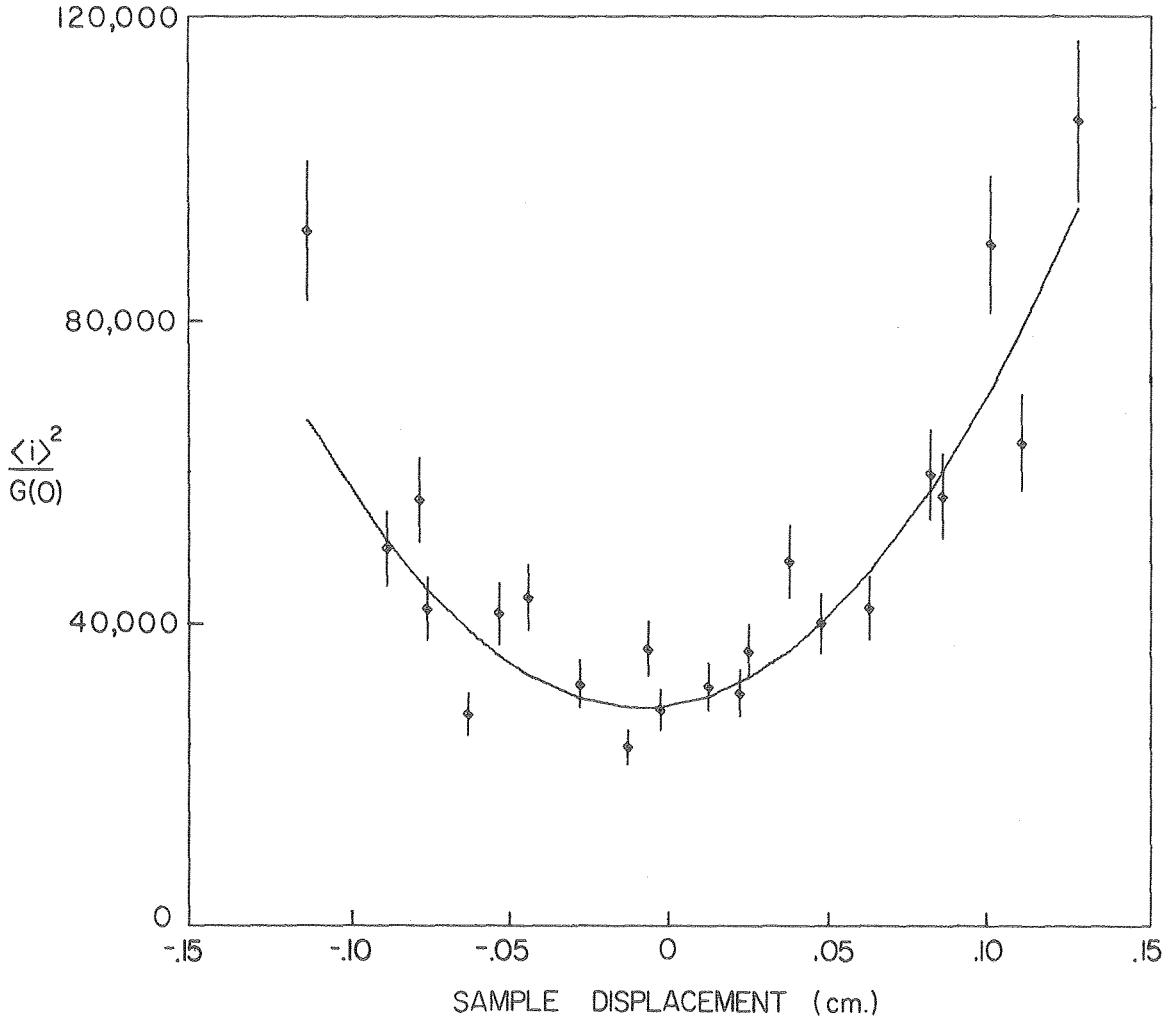
120,000
80,000
40,000
0
$\frac{\langle i \rangle^2}{G(0)}$
-.15
-.10
-.05
0
.05
.10
.15
SAMPLE DISPLACEMENT (cm.)

XBL796-4860

values of $G(\tau)$ are, themselves, subject to uncertainties which would limit the accuracy of values derived from computer estimates. Thus, the error bars in the figures take into account only a fraction of the relevant uncertainties. The error bars were used to weight the data in the least squares estimates of parameters used to compute w_o, D, and CL. The data were not weighted in computations of the variances of w_o, D, and CL.

Assuming the stated dependence of τ_D and $\langle i \rangle^2/G(0)$ on Δz, these data lead to estimates for the diffusion coefficient, D, the 2-dimensional concentration, CL, and to two estimates of w_o. The results are summarized in table I. L, the depth of the cell, was 100μ.

The uncertainties stated for w_o, r_o, D, and C are estimated from the differences between the observed and fitted values. Consequently, any systematic errors are excluded from consideration in arriving at the stated uncertainties. For example, measurements using the pinhole near the focal plane are subject to uncertainties in the determination of the total light intensity in the beam. If the total light intensity were inaccurately measured, the fraction of light transmitted, T, would contain a small scale factor error.

Near the focal minimum, the fraction of light transmitted was essentially 1.0. Since the quantity plotted in figure 3 includes the factor $\ln(1-T)$, it would be sensitive to such systematic errors in T. Thus, the stated uncertainty for the value of w_o measured in this way is probably an underestimate.

Nonetheless, the results presented here are about as expected. The values given for the beam radius in the focal plane are in close agreement. It is significant that scale factor errors in τ_D and

TABLE I

	w_o (μ)	r_o(μ)	D(cm^2/sec)	C (moles/liter)
EXPECTED VALUE	12.8 ± 0.5	23.4 ± 0.5	2-5 X 10^{-6}	5 X 10^{-9}
OBSERVED VALUES				
Transmission through pinhole	14 ± 0.4	22.6 ± 0.5	_____	_____
τ_D versus Δz	13 ± 1	_____	(5.5 ± 0.8) X 10^{-6}	_____
$\langle i \rangle^2/G(0)$ versus Δz	12 ± 1	_____	_____	(1.1 ± 0.1) X 10^{-9}

Values are shown for beam waist radius, w_o; the radius of the pinhole, r_o; the diffusion coefficient for Rhodamine 6G in water, D; and the concentration of fluorescent molecules, C. Each type of microscopic measurement gives an estimate of w_o and one other physically significant parameter.

$\langle i \rangle^2/G(0)$ have no effect on the estimate of w_0. This is in contrast to the sensitivity to scale factor errors of the estimate of w_0 obtained by transmission through the pinhole.

The value for the diffusion coeeficient of Rhodamine 6G is consistent with the size of the molecule,[9] although reports exist of somewhat lower values.[3] The value obtained for the radius of the pinhole agrees satisfactorily with dimensions obtained from the microphotograph and Airy rings. The measured 2-dimensional concentration of the fluorescent molecules is also about as expected. The dye solution was prepared to be 5×10^{-9} M by serial dilution from stock solutions. During the course of the experiments, some of the molecules are destroyed by the exciting light, and thus do not appear in $\langle i \rangle^2/G(0)$. This leads to an underestimate of the two-dimensional concentration. We consider an underestimate by a factor of five to be reasonable.

The results presented here demonstrate that the focussed beam behaves as predicted by scalar diffraction theory and that the beam shape can be characterized by measurements made with fluorescence correlation spectroscopy. It was mentioned above that other methods exist for determining beam size down to microscopic dimensions. In fact, one such measurement was presented here. The advantages of the correlation method are three-fold by comparison with direct physical measurements.

This method helps confirm that the autocorrelation functions arise from translational diffusion. In the case of rotational diffusion, for instance, the correlation time would not depend on beam size, while $\langle i \rangle^2/G(0)$ would.[10,11]

This method also arranges for τ_D and $\langle i \rangle^2/G(0)$ to be estimated at the focal minimum even though no measurements need be performed at that precise location. A third advantage is that the beam waist is measured with the sample in situ. The last two points are especially important in practice. Typically, the fluorescent light is collected by an optical system different from the system that focusses the exciting beam onto the sample. Both systems must be properly focussed relative to each other and to the sample if reliance is to be placed on direct physical measurements of the beam shape.

References

1. D Magde, E. Elson, and W. Webb, Phys. Rev. Lett. 29, 705 (1972).

2. E. Elson, and D. Magde, Biopolymers 13, 1 (1974).

3. D. Magde, E. Elson, and W.Webb, Biopolymers 13, 29 (1974).

4. M. Weissman, H. Schindler, and G. Feher, Proc. Nat. Acad. Sci. USA 73, 2776 (1976).

5. Y. Suzaki,, and A. Tachibana, Appl. Opt. 14, 2809 (1975).

6. D. Axelrod, D. Koppel, J. Schlessinger, E. Elson, and W. Webb Biophys. J. 16, 1055 (1976).

7. D. Magde, W. Webb, and E.Elson, Biopolymers 17, 361 (1978).

8. J. Goodman, Introduction to Fourier Optics (McGraw-Hill, New York, 1976).

9. L.G. Longworth, J. Am. Chem. Soc. 74, 4155 (1952).

10. M. Ehrenberg and R. Rigler, Chem. Phys. 4, 390 (1974).

11. S.R. Aragon, and R. Pecora, Biopolymers, 14, 119 (1975).

BIOLOGICAL REIVIEWS

The Biology of DNA in the Cell Cycle

The long range motivation for the research discussed in this thesis is the hope that this work will help answer questions about the character of DNA in living cells. It would be helpful, then, to review some of what is known about DNA in cell nuclei. This review is certainly not meant to be definitive, and parts of it may prove to be false. However, it is important to have a suitable biological context to refer to when considering the results that follow. The ideas found in this brief survey can be found in recent textbooks and review articles.[1-7] It should be understood that what follows applies to the more complex eukaryotic cell types.

Cell Growth Cycle Cell growth is described as taking place in four stages. Once a cell divides, the daughter cells do not resume synthesizing DNA for several hours. This latent period is denoted G_1, meaning the first apparent gap in DNA activity. Late in G_1, protein is being synthesized to de-repress DNA replication. DNA synthesis follows, and continues for 10-18 hours. This is called S phase. Synthesis continues at a more or less constant rate during S. At the end of S, two copies of DNA are present, but motosis does not start for several hours. This second gap in DNA activity is called G_2. Mitosis is denoted M. During mitosis, the nuclear membrane disappears, chromosomes become closely bound to elaborate structural proteins, and are drawn apart. The cell membrane is pinched into two halves, and the cell cylce is ready to repeat.

When cells have not been growing for some time, it is believed that they enter a resting state, denoted G_0, which is difficult to

distinguish from G_1. When stimulated to grow, cells leave G_0, enter G_1, and proceed through the cell growth cycle. DNA synthesis usually starts 12-15 hours after stimulation. G_1 is different from G_0 in the sense that the biochemical apparatus for growth and DNA synthesis is activated in G_1, but is inactive in G_0. Certain dyes are bound differentially by the DNA of cells in G_0 and G_1.

Chromatin Most cellular DNA is found in the nucleus. During cell division, the chromosomes are organized into highly ordered compact form. This so-called metaphase form is widely popularized because it is easily visualized with stain. When the cell is not dividing, the chromosomes assume interphase form, which is relatively diffuse, and poorly visualized with stain. In this form, chromosomes are called chromatin. Chromatin refers to a complex of DNA, RNA, and various proteins. The proteins include the histones, which are believed to be primarily structural proteins, as well as enzymes involved with transcription of DNA into RNA, replication of DNA, and repair.

The enzymes associated with chromatin are incompletely characterized. Among them are expected to be such enzymes as polymerases nucleases, ligases, unwinding enzymes and repair enzymes. Polymerases work at the replication fork, to attach nucleotides to the growing daughter strands. They also insert nucleotides into gaps between adjacent DNA segments. Nucleases can break DNA molecules by nicking one strand or cutting both strands of the double helix. Enzymes which connect nucleotides in adjacent DNA segments of DNA molecules are called ligases. Since DNA molecules are wound as helices, and the helices themselves are known to be strongly twisted, there will have to be some way to separate the two strands of DNA during replication,

or the RNA from the DNA during transcription. This would be accomplished by unwinding enzymes. Rewinding the two new double strands is also fairly complicated, but is probably accomplished in a manner completely different from the replication process. Repair enzymes are often present. They can recognize some gross structural abnormalities and correct them, given time. Once a base pair is in place, however, it is unlikely that repair enzymes can recognize or correct an error. Other proteins will be present, as well, and the ones mentioned may exist in various forms and combinations.

Nucleosomes The histones are proteins that occur in five distinguishable forms. Of the five, four can combine to form a tetramer. These histones are denoted H2a, H2b, H3, and H4. Two tetramers will join to form an octamer. The octamer is associated with a characteristic unit of chromatin. One copy of the fifth histone, denoted H1, is also associated with the chromatin unit, which is called a nucleosome, ν-body, or nucleohistone particle. Nucleosomes have been studied by electron microscopy, neutron diffraction, and by partial digestion with nucleases, among other techniques. It has been found that nucleosomes vary slightly from cell type to cell type, and that they can be reconstituted from isolated DNA and histones with moderate success. Common to all nucleosomes is a core segment of DNA that is 140 base pairs long. It is believed that the DNA winds around the outside of the octamer of histones, making a flattened sphere about 50 A high and 100 A in diameter. There would be two rings of DNA at the top and two at the bottom, probably with a tetramer of histones inside each set of double rings.

These nucleosomes are connected to each other by a strand of DNA

that varies in length from 0 to 100 base pairs. Within the nucleosome particle, some base pairs are more accessible to attack by nucleases than others. In general, every tenth base pair along the strand of 140 in the core is relatively sensitive to nuclease digestion. The connecting strands between the core particles are particularly sensitive to attack, especially when their histone, H1, is missing.

There is evidence that the core particle can split into halves, possibly as part of the replication process. Each half would then have one histone tetramer. Calculations involving the energy of interaction between histones and DNA suggest that folding and unfolding of DNA around hidstone tetramers can be accomplished by making or breaking one or two pairwise interactions between histones and DNA molecules.

The nucleohistone particles are involved in higher orders of structure. They are connected by strands to each other, giving the appearance of beads on a string, especially when the histone associated with the connecting strand is missing. When all the histones are present, the beaded string appears as a 100 Å fiber. Fibers of 300 Å diameter have been isolated, which probably are solenoids of 100 Å fibers with a 100 Å hole down the middle. It appears that eight nucleosomes form a stable unit. Additional organization is presumed to exist, but direct observation is particularly difficult because of problems in isolating the particles intact.

Biological activity can be used to give a somewhat different perspective of the structure and function of chromatin. The process of replication of DNA is a subject of considerable controversy, but many elements are now understood. At the level of the nucleosome, nuclease digestion patterns of transcriptionally active chromatin are similar

to the patterns from inactive chromatin, when staphylococcal nuclease is used. Pancreatic nuclease preferentially digests active chromatin. Chromatin that was recently active, or that is about to become active is also more sensitive to pancreatic nuclease. This is reasonable, since the processes of replication and transcription should involve disruption of the nucleosome and changes in the amount of protection provided by the histones.

DNA Synthesis As new DNA strands are synthesized from the parent strands, new histones must be combined with the new strands to make nucleosomes. In fact, histone synthesis usually coincides with DNA synthesis. If histone synthesis is blocked, the old histones will be distributed evenly between the two new double strands. The octamers making up the individual histones remain intact over at least four cells divisions. It is possible that histones from small groups of adjacent nucleosomes remain together on one of the new strands, but for the most part, new and old histones are found on both new strands.

DNA synthesis proceeds simultaneously at many points in the cell nucleus. All chromosomes are involved in DNA synthesis all through S. Different organisms replicate DNA at different rates as they proceed through S. Most eukaryotes spend about the same amount of time in S in spite of considerable differences in total DNA contents. Individual replication forks have been observed to move at rates of 0.1 μ/min. to 2 μ/min. This is equivalent to 0.2 to 4 X 10^6 daltons/min. or 300 to 6000 base pairs/min. In 10 hours, one replication fork polymerizing 3000 base pairs per minute would make a DNA strand 2 X 10^6 base pairs long. Since there are 5 X 10^9 base pairs in each human cell, there would be of the order of 1000's of replication forks simultaneously

synthesizing DNA at that rate in each cell, all through S.

Replication Units Replicating chromatin is thought of as being organized in pieces of increasing size. The pieces can be characterized in genetic or molecular terms. Some DNA segments can be identified genetically, but it is usually not obvious which genetically characterized particles correspond to which biochemically isolated particles.

One fairly well characterized particle is called the replication unit. The replication unit presumably includes unwinding enzyme, polymerases, nucleases, ligating enzymes and structural proteins. The DNA involved ranges from 4 μ in length, weighing about 8×10^6 daltons, containing about 1.3×10^4 base pairs, up to 280 μ in length, weighing 560×10^6 daltons, containing 9×10^5 base pairs. Thus, the replication unit would contain between 50 and 7000 nucleosomes. The particle weights refer to DNA weight, and do not include proteins, and other chromatin constituents.

Replication units can cluster in groups of 2 to 250. These are probably genetic units of some kind. For example, the small chromosomes of simple organisms may be made up of one replication unit cluster. Stains sometimes reveal bands on chromosomes which can be seen in a microscope. One or a few bands may be made up from one or a few replication unit clusters, depending on the complexity of the organism.

The Replication Process The replication process includes synthesis of DNA, regulation of the rate and location of synthesis, as well as reorganization and assembly of newly synthesized DNA strands.

The two DNA single strands in a double helix are complementary, rather than identical. In addition, each single strand is oriented by the assymetry of the sugar backbone. The carbon atoms in the sugar are

numbered from 1' to 5'. A phosphodiester bridge connects the 3' carbon in one nucleotide to the 5' carbon in the next nucleotide. Thus, one end of the DNA single strand segment is called the 3' end, and the other is the 5' end.

It is known that DNA polymerase can add nucleotides only to the 3' end of a daughter strand. That is, the polymerases are all unidirectional, working from the 5' end toward the 3' end of the daughter single strand. Every replication fork will expose two daughter strands, one with a 3' end and the other with a 5' end. This is shown schematically in figure 10. The process by which both strands are polymerized is not completely understood.

Initiation of DNA replication is believed to take place at specific sites. An initiation protein presumably recognizes an initiation sequence of base pairs. It now appears that replication is initiated in given replication units in a particular order. That is, certain units always begin replicating before others. Different chromosomes start and stop replicating in the same order. In most cases, replication proceeds in both directions from the individual initiation sites. Termination of replication may occur at specially coded sequences, or may occur when replication forks meet. Each replication unit will usually have many replicating forks.

Recent evidence suggests that both daughter strands are assembled in discontinuous steps, from intermediate sized segments. Many possible mechanisms are under consideration. Other evidence suggests only one of the daughter strands is assembled discontinuously, the other being assembled continuously, one nucleotide at a time.

One can think in terms of three stages of DNA replication, in S

Figure 10. The orientation of strands of DNA molecule is determined by position of 3' and 5' carbon atoms in the sugar backbone.

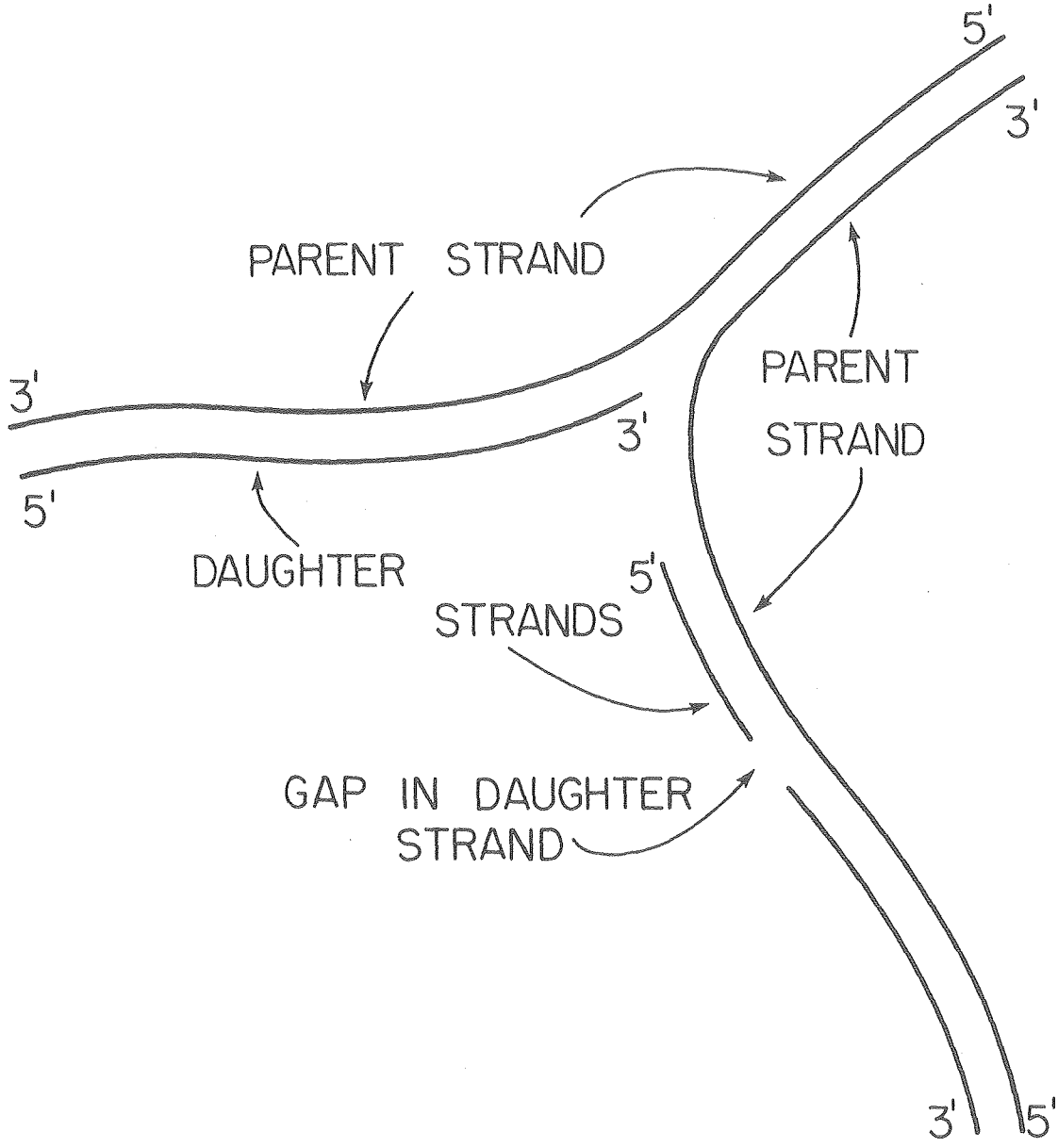
5'
3'
PARENT STRAND
3'
3'
5'
PARENT
STRAND
DAUGHTER
5'
STRANDS
GAP IN DAUGHTER
STRAND
3'
5'

XBL798-4965

phase. In the first stage, daughter strands 220-280 nucleotides in length are produced. These strands are longer than the DNA in a nucleosome, but nucleosomes are probably made from these segments. Nucleosomal maturation seems to take 2-15 minutes. In the second stage, the primary intermediates are elongated into increasingly larger segments until replication units appear. This elongation process is accomplished by ligating enzymes. In the third stage, mature chromosomal units are made from clusters of replication units. The first two stages proceed steadily all through S. Until the chromatin matures in the thrid stage, it is relatively fragile, especially to shearing forces. The third stage of DNA synthesis is relatively rapid, but may occur long after the first two stages.

Regulation Regulation of DNA synthesis occurs at many levels. One important point of regulation is the activity of the initiator protein that creates replication forks. Protein synthesis late in G_1 includes the initiator proteins. Once a replication fork is created, replication usually proceeds at one rate until that fork terminates. RNA is needed to make DNA polymerase start, serving as a primer. Thus, RNA activity can be a point of regulation. Elongation proteins must be synthesized all through S, and their synthesis and activity can be regulation points. Conversion of second stage intermediates into chromosomes is also believed to be involved in regulation.

References

1. A. Lehninger, Biochemistry (Worth Publishers Inc. New York, 1970).

2. L. Stryer, Biochemistry (W. H. Freeman & Co., San Francisco, Ca. 1975).

3. R. Scheinin, and J. Humbert, Annual Rev. of Biochem. 47, 277 (1978).

4. G. Felsenfeld, Nature 271, 115 (1978).

5. R. Baserga, and C. Nicolini, Biochimica & Biophys. Acta 458, 109 (1976).

6. T. Igo-Kemens, and H. G. Zachau, Cold Spring Harbor Symposium 42, 109 (1977).

7. T. R. Cech, D. Potter, and M. L. Pardue, Cold Spring Harbor Symposium 42, 191 (1977).

Dye Binding to DNA

Biological stains are dyes that are used for making objects more clearly visible. This is ironic, in a way, because the field of biological staining is particularly dense. Before 1850, a few natural stains were used for microscopy, mainly carmine and indigo. Leeuwenhoek wrote in 1719 of using saffron to see small particles. In 1856, aniline dye chemistry began rapid commercial development, motivated by the textile industry. Introduction of these dyes revolutionized microscopy. Nomenclature in the field became highly confused at an early point because of commercial interests in the chemical and textile industries. It has never really recovered.

The chemical structures of biological stains are well documented. The nature of the binding of popular stains has only recently come to light.[1-3] One classification of dyes is by the acidic or basic nature. In basic dyes, the part of the molecule that is important in staining will be positively charged. Acidic dyes have negatively charged character. The dyes are rarely acids or bases, but usually salts. Basic dyes are often accompanied by chloride negative ions, and acidic dyes often have sodium as an accompanying positive ion. Amino groups ($-NH_2$), for instance, give a molecule basic character, while carboxyl groups (-COOH) contribute acidic character. Some dyes have both types of groups, each contributing to the overall character of the dye.

DNA is stained by basic dyes. RNA is stained by some of the same dyes. A few dyes stain DNA with one color and RNA with a different color. Among the stains used for DNA are pararosaniline, also known as basic fuchsin, basic rubin, and aniline red. It stains DNA magenta. With methyl green, DNA appears green. Pyronine gives a red brown or

purple color. Toluidine blue stains DNA blue or reddish purple. With azure B, DNA appears blue. Fast green FCF and cresyl fast violet are also used. None of these stains is strongly fluorescent.

Several fluorescent dyes stain DNA, and have well characterized properties.[4] They include ethidium bromide, propidium iodide, acridine orange, quinacrine, actinomycin D, mithramycin, acriflavine and proflavine. Sturctures of some of these molecules are shown in figure 11. Acridine orange is of special interest, in that it fluoresces in the green when bound to DNA, but is red when bound to RNA.[5,6] All of these dyes require lethal preparations for the cells, although reports of staining live cells with ethidium bromide have been published.[7] DNA stains that fluoresce and can be used in living cells have recently been released, but are not widely available at this time.[8]

DNA possesses native fluorescence which could be monitored, in principle, instead of introducing dye molecules. Each of the nucleotides absorbs with a maximum around 250-290 nm. Emission maxima fall between 360-390 nm. Quartz optics would be required for observation and illumination, and UV excitation from a laser would be almost essential. Quantum efficiencies for fluorescence tend to be .005 or less. Still native fluorescence may be considered as a potential indicator for DNA molecules in fluorescence fluctuation experiments.

Flow Microfluorimetry One popular application of fluorescent DNA stains is in the measurement of DNA content per cell in large populations of cells.[8,9] Cells are grown in culture, harvested and stained. Frequently, the stains used are ethidium bromide, propidium iodide and acridine orange. In flow microfluorimetry,[10-13] cells are harvested, made permeable to the dye, and treated with an excess of dye, so that all

Figure 11. Stuctures of five commonly used DNA stains. All bind by intercalation.

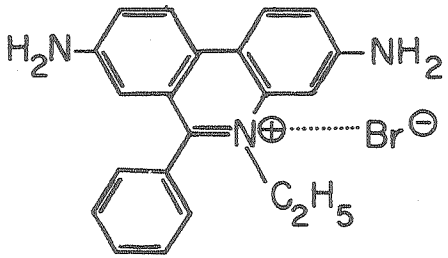

ETHIDIUM BROMIDE

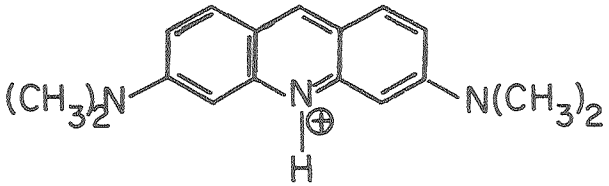

ACRIDINE ORANGE

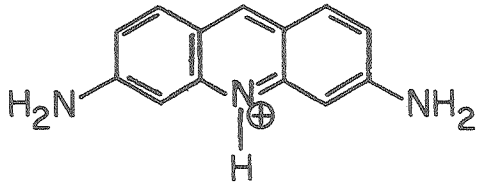

PROFLAVINE

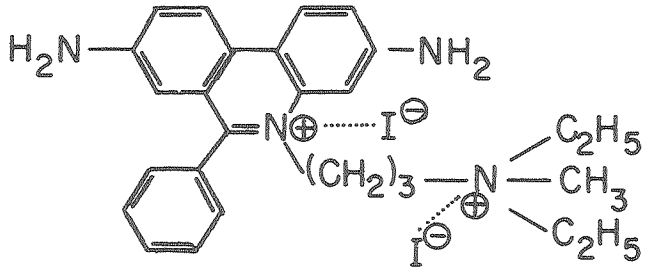

PROPIDIUM IODIDE

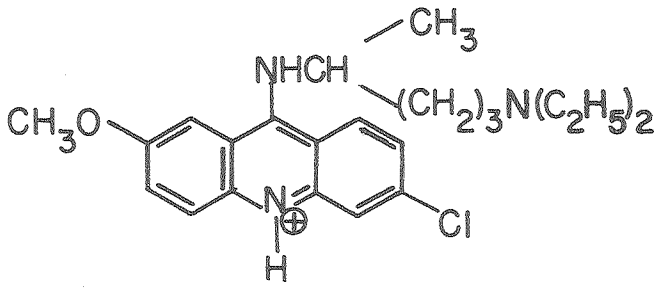

QUINACRINE

XBL798-4969

accessible binding sites are occuppied with dye molecules. Cells are suspended, and made to pass through a narrow flow chamber in such a way that they pass one at a time through a focussed laser beam which propagates across the path of the cells. Fluorescence is excited from the cellular DNA and is collected by a photomultiplier. The photocurrent, less background, will be proportional to the number of dye molecules in the cell, which should be proportional to DNA content. In a few seconds, several thousand cells can be examined in this manner. As cells are examined, a histogram can be compiled in a pulse height analyzer which shows the distribution of cells with given DNA contents.

In a population of growing cells, the cells in G_1 will have one copy of DNA, cells in G_2 and M will have two copies, and the cells in S will have between one and two complete copies. A histogram from an unsynchronized population would, in principle, have the appearance of figure 12a. In fact, the variability in fluorescence intensity is such that the peaks are somewhat broadened, and histograms similar to the one in figure 12b are typical.

Cell populations can be synchronized so that most of the cells are at the same point in the cell growth cycle. As the cells proceed through the cycle, the histograms of samples taken from the population at successive times will reveal a peak that moves to increasingly higher fluorescence intensity, then jumps back to lower intensity as the cells divide. Fluorescence intensity is not an exact measure of position in the cell cycle, but is usually accepted as a good approximation.

Figure 12. a) Ideal histogram of a population of growing cells, showing the number of cells with a given DNA content. b) Typical histogram, in which peaks are broadened by instrumental and biological variability.

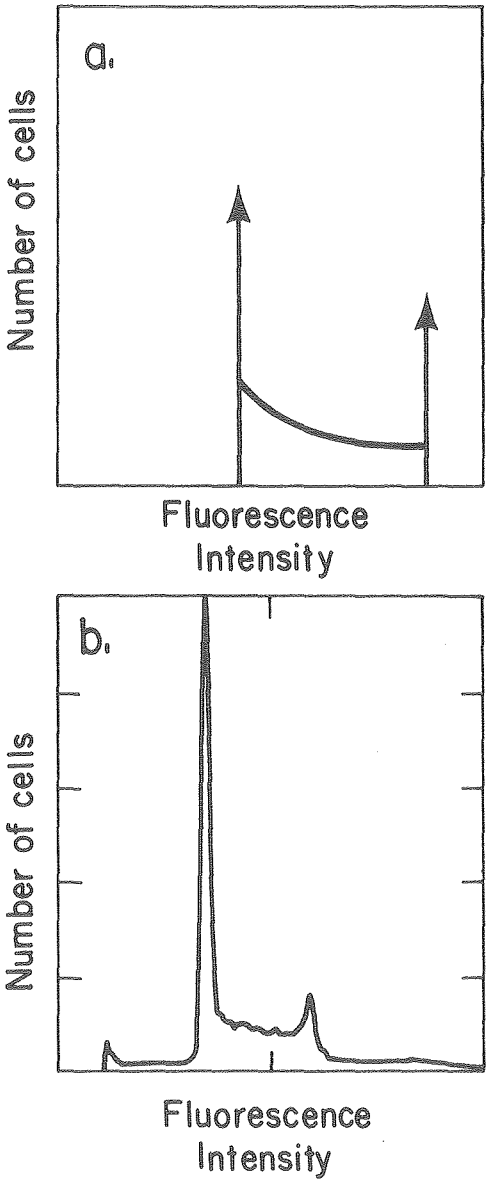

XBL 7910-5061

References

1. E. Gurr, Rational Use of Dyes (Williams and Wilkins Co., Baltimore, Md., 1966).

2. H. J. Conn, Biological Stains (Williams and Wilkins & Co., Baltimore, Md., 1961).

3. E. Gurr, Staining, Practical and Theoretical (Williams and Wilkins Co., Baltimore Md., 1962).

4. E. Gurr, Synthetic Dyes (Academic Press, New York, New York, 1971).

5. Z. Darzynkiewcz, F, Traganos, T. Sharpless, and M. Malamed, Proc. Nat. Acad. Sci. 73, 2881 (1976).

6. F. Traganos, Z. Darzynkiewcz, T. Sharpless, and M. Malamed, J. Histochem. and Cytochem. 25, 46 (1977).

7. C. Nicolini, F. Kendall, R. Baserga, C. Dessaive, B. Charleson, and J. Fried, Exp. Cell Res. 106, 111 (1977).

8. D. Arndt-Jovin, and T. Jovin, J. Histochem. and Cytochem. 25, 585 (1977).

9. S. Udenfriend, Fluorescence Assay in Biology and Medicine (Academic Press, New York, New York, 1969).

10. D. Holm, and L. Cram, Exp. Cell Res., 80, 105 (1973).

11. J. Friend, A. Perez, and B. Clarkson, J. Cell Biol. 71, 172 (1976).

12. H. Crissman, and J. Steinkamp, J. Cell Biol. 59, 766 (1973).

13. J. Bartholemew, A. Pearlman, J. Landolph, and K. Straub, Cancer Res. 39, 2538 (1979).

Binding of EtBr to DNA

Ethidium Bromide, was intoduced as a drug for cattle in the late 1950's in Africa. It was found to kill trypanosomes, bacteria that are carried by flies. It was recognized fairly quickly that EtBr interferes with DNA synthesis. The trypanosomes are relatively simple, and suffer DNA synthesis problems that more complex cells are able to survive. Nevertheless, EtBr is known to cause mutations in complex organisms, presumably by the same interference with DNA synthesis that is fatal to trypanosomes.

Choice of EtBr as a probe of DNA Among all the dyes that bind to DNA, EtBr is of particular importance because of its optical properties.[1,2] It has an absorption band in the visible, with a relatively large extinction coefficient. The absorption shifts appreciably when the dye is bound, allowing measurements of both bound and free dye concentrations.[3] Of considerable importance is the quantum efficiency for fluorescence.[4] Bound EtBr has a quantum efficiency for fluorescence that is about 0.2, while free EtBr has a quantum efficiency for fluorescence of approximately 0.01. Under conditions where the bound dye concentration is comparable to or greater than the free dye concentration, detected fluorescence will overwhelmingly be from bound dye.

EtBr also has remarkable staining selectivity. It is known to bind strongly to DNA and RNA, but interactions with other biological molecules are not significant. RNA bound EtBr has an absorption spectrum similar to DNA bound EtBr.[3] At low dye concentrations, RNA binding is weaker than DNA binding.[3] Furthermore, the quantum efficiency for fluorescence of EtBr bound to single stranded RNA is much lower than for

EtBr bound to double stranded RNA and DNA.[4] Thus, fluorescence detected from EtBr in the presence of RNA and DNA is limited, to a remarkable degree, to double stranded RNA and DNA.

Another important advantage of EtBr is that illumination is available from argon ion lasers at 514.5 nm., which is close to the absorption maximum of bound EtBr. Light of this wavelength isn't likely to be absorbed by anything else in the cell. Absorption and emission bands are both at visible wavelengths, and are easily separated from each other by dielectric optical devices. EtBr is fairly stable under intense illumination, and is not known to form reactive photoproducts.

Absorbance Spectrum of EtBr-DNA Complex Shown in figure 13 are the absorption spectra of EtBr in the presence of different concentrations of DNA. They have what is called an isosbestic point at about 510 nm. The significance of this feature can be demonstrated by a simple calculation. Suppose there are two optically distinct forms of EtBr, which will be referred to as the bound and free forms. If we prepare several samples of EtBr-DNA mixtures, each with the same concentration of EtBr, but with different DNA concentrations, the absorbance of a sample can be written, using Beer's law, as

$$A(\lambda) = [\varepsilon_f(\lambda)C_f + \varepsilon_b(\lambda)C_b)L,$$

where ε_f and ε_b are the extinction coefficients for free and bound dye, C_f and C_b are the concentrations of free and bound dye, and L is the length of the light path through the sample. If we take $C = C_f + C_b$, to be the total EtBr concentration in the sample, then

$$A(\lambda) = [\varepsilon_f(\lambda)(C-C_b) + \varepsilon_b(\lambda)C_b]L.$$

At some wavelength, λ_i, the graphs of ε_f and ε_b may cross. Then, $\varepsilon_f(\lambda_i) = \varepsilon_b(\lambda_i) = \varepsilon$, and $A(\lambda) = \varepsilon CL$. The absorbance at λ_i is then

Figure 13. Absorbance spectra for various mixtures of EtBr and calf thymus DNA. All samples contain 10^{-4} M EtBr. The spectrum with a peak at 475 nm. contains no DNA. The peak at 520 nm. corresponds to a sample with 5 X 10^{-4} M DNA base pairs. Intermediate DNA concentrations are 0.25 X 10^{-4} M, 1.0 X 10^{-4} M, 1.5 X 10^{-4} M, 2.0 X 10^{-4} M, and 2.75 X 10^{-4} M.

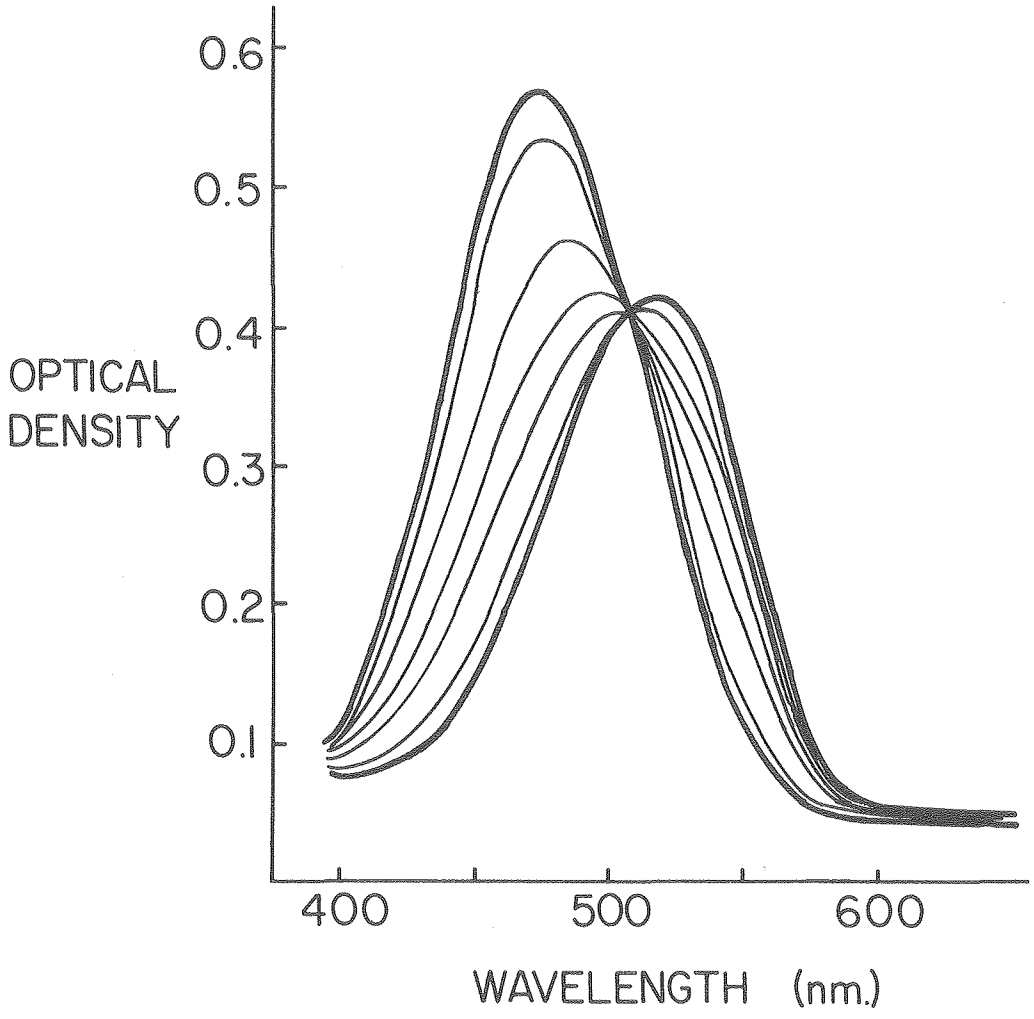

XBL798-4966

independent of DNA concentration. In this example, λ_i is an isosbestic point.

This argument shows that the presence of only two optically distinct absorbing species will result in an isosbestic point, at any wavelength where the two extinction coefficients are equal. If one observes an isosbestic point at a wavelength where the two extinction coefficients are equal, it is taken as strong evidence that only two optically distinct forms of the absorbong species are present.

Binding Constant and Scatchard Plots From a series of spectra such as the one shown in figure 13, one should be able to deduce the binding constant for the binding of EtBr to DNA. A graphical method for such a determination was developed by Scatchard.[5] The method presumes a reversible reaction of the form

$$A + B \underset{k_b}{\overset{k_f}{\rightleftharpoons}} C$$

Here, A and B are free reactants, and C is the complex of A with B. Forward and backward reaction rate constants, k_f and k_b describe the flow of mass from one side of the reaction to the other. That is,

$$\frac{d}{dt}[C] = k_f[A][B] - k_b[C].$$

The first term on the right hand side represents flow in the forward sense. The second term represents flow in the backward sense. At equilibrium, the flows are equal, and

$$\frac{[C]}{[A][B]} = \frac{k_f}{k_b} = K.$$

K is the binding constant. We can rearrange the expression for K, making certain substitutions.

Let [A] be the concentration of free binding sites,

let [B] be the concentration of free dye,

let n be the number of binding sites per DNA nucleotide,

and let r be the number of bound dye molecules per nucleotide.

Then, $$r = \frac{[C]}{[C] + [A]}, \quad \text{and} \quad n - r = \frac{[A]}{[C] + [A]}.$$

Also, $$K = \frac{r}{[B](n - r)}, \text{ so that } \frac{r}{[B]} = K(n - r).$$

In a Scatchard plot, r/[B] is plotted as a function of r. The slope is a measure of the binding constant, K, and the point on the r axis where the curve crosses is the number of binding sites per nucleotide. In the experiment, one physical property is varied; the DNA concentration. From each sample, an absorbance measurement is made. Two physical parameters are deduced; the binding constant and the number of binding sites per nucleotide.

To finish the procedure, we need expressions for r and [B] in terms of the known or measured quantities. Sufficient information is available at any wavelength for which the extinction coefficients of bound and free dye are different. We can write

$$A = \alpha A_b + (1 - \alpha)A_f$$

where α is the fraction of dye bound, A_b is the absorbance one would measure if all the dye were bound, A_f is the absorbance one would measure if all the dye were free, and A is the measured absorbance. We may express α as

$$\alpha = \frac{A - A_f}{A_b - A_f}.$$

We express r and [B] in terms of α and the total concentrations of dye

and DNA. Then,

$$r = \frac{\alpha B_T}{DNA_T}, \quad [B] = B_T(1 - \alpha), \text{ so } \frac{r}{[B]} = \frac{\alpha}{(1 - \alpha)DNA_T},$$

where B_T is the total dye concentration and DNA_T is the total DNA concentration. A similar procedure may be used if measurements had been made of fluorescence intensity instead of absorbance.[4] The flourescence intensity can be written

$$I = \alpha I_b + (1 - \alpha)I_f.$$

Then,

$$\alpha = \frac{I - I_f}{I_b - I_f},$$

where I_f is the fluorescence intensity one would measure if all the dye were free, I_b is the fluorescence intensity one would measure if all the dye were bound, and I is the measured intensity.

Once the fraction of dye bound is computed, the procedure for the Scatchard plot is the same for fluorescence measurements as the case where absorbance was measured. An example of a Scatchard plot of the binding of EtBr to calf thymus DNA is shown in figure 14. The value obtained for the binding constant is 1.2×10^6 M^{-1}. The number of binding sites per nucleotide is about 0.20. These values are in close agreement with values reported in the literature.[3,4,24,26]

One might expect that the binding constant, K, would depend on many biochemical factors.[4] K decreases by an order of magnitude as salt concentration increases to 0.5 M, but the effect of pH change is very small, until the DNA is denatured at extreme pH. Base pair composition is not important. Raising the temperature decreases binding strength. For low salt concentrations, at physiologic pH, and room temperature, values of K have been reported in the range of $1\text{-}2 \times 10^6$ M^{-1}. Values

Figure 14. Scatchard plot for binding of EtBr to calf thymus DNA.

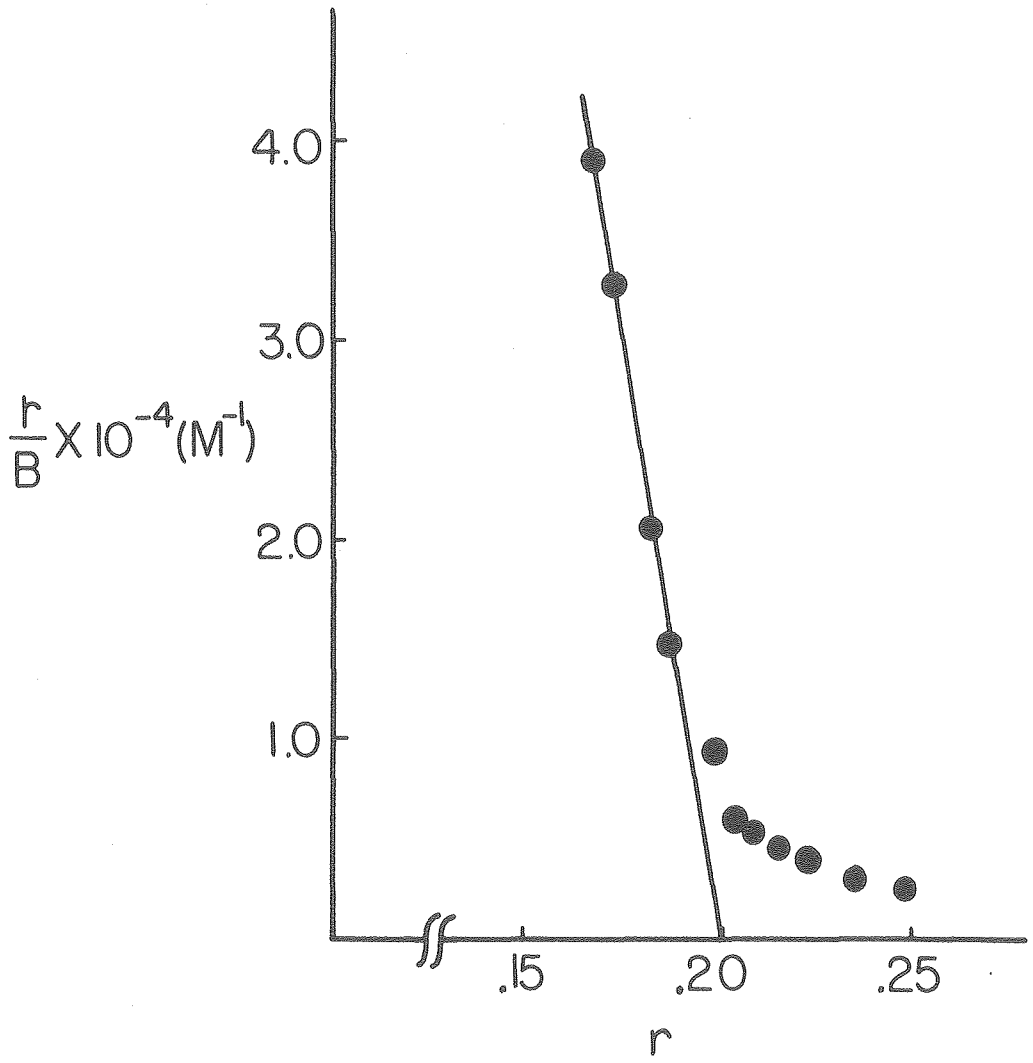

XBL 798-4967

for the number of binding sites per nucleotide, n, range from .18 to .22, depending on the source of the DNA and preparation of the samples.

Nature of the binding of EtBr to DNA Figure 14 shows the expected behavior of r/[B] as a function of r, only when there is an excess of DNA binding sites. As r approaches 0.2, and most of the available binding sites become occuppied, r/[B] decreases more slowly. Interactions of other drugs with DNA have shown similar behavior.[7-9] It is interpreted as meaning that a second type of binding site exists with a lower affinity for dye. At high DNA concentrations, the sites with higher affinity or stronger binding are the ones most likely to be occuppied. As DNA concentration goes down, high affinity sites fill up, and weaker binding sites become apparent. If only the strong binding sites existed, then the value of r would never increase beyond 0.2, and the value of r/[B] would reach a limiting value, as well. In figure 14, the limiting value for r/[B] would be 2×10^3 M^{-1}, because the total dye concentration in all samples for that experiment was 1.0×10^{-4} M.

The secondary binding is believed to be an electrostatic effect between the positively charged dye molecules and the negatively charged phosphate groups in the sugar backbone of DNA. The DNA base pairs must separate slightly to allow the dye molecules to intercalate, and the electrostatic binding is regarded as an intermediate step, in which the dye molecules are kept close to the base pair until an opening presents itself.

The binding of EtBr is compared to the binding of acridines which are generally believed to intercalate between base pairs.[10,11,18] EtBr competes with acridines for binding sites. Competition with some

acridines involves the intermediate sites, with the number of intercalation sites, n, remaining unaffected. In these cases, the binding constant goes down. More strongly binding acridines compete with EtBr by occuppying the intercalation sites, reducing the number available to EtBr. In these cases, the binding constant is unaffected.

The number of binding sites per nucleotide, n, is measured to be about 0.2. That is, one dye molecule binds for every 2 1/2 base pairs. This is interpreted to mean that binding to a given site makes it impossible to bind at adjacent sites. This is known as the excluded site model. Conformational studies of DNA conclude that intercalation leads naturally to the excluded site property.[19] Binding studies of chromatin reveal more complex binding behavior, and the excluded site property is taken into account explicitly. This matter will be discussed more fully when describing the binding of EtBr to chromatin.

Evidence for intercalation as the mechanism for binding starts with comparison to acridines. The acridine structure is similar to the purines and pyrimidines in the base pair, and they would be expected to interact strongly. The phenanthridinium ring of EtBr would also be expected to match the structure of a base pair and interact strongly. EtBr binds to double stranded DNA and RNA, but not to single stranded RNA. In single stranded RNA, there are no base pairs, and intercalation would be impossible. DNA molecules can be aligned in flow chambers. Studies with aligned DNA molecules using polarized light indicate that EtBr molecules bound to DNA are aligned in a manner consistent with intercalation.[4] Energy transfer is known to occur between bound dye molecules when they are bound to nearby sites.[4,12] Calculations of the energy transfer based on intercalation agree with observations.[12-14]

Steric considerations indicate that intercalation results in an unwinding of the DNA helix. Closed circular DNA, isolated from certain viruses, is known to have a tightly twisted structure. When EtBr binds to such DNA molecules, the DNA unwinds and becomes less compact. Addition of more EtBr causes the DNA to rewind in the opposite sense and become compact again. This effect is useful as a means of separating closed circular DNA from linear DNA and from closed untwisted DNA, using centrifugation.[15] The observed unwinding is consistent with the unwinding expected from intercalation.[16]

The intercalation mechanism accounts for the increase in quantum efficiency for fluorescence when the dye is bound.[17] It is agrued that proton transfer from the excited singlet state is the process primarily responsible for the quenching of fluorescence in solution. Intercalated molecules would be more isolated from solvent molecules and would be less able to transfer protons. These conclusions are supported by measurements of fluorescent lifetimes in different solvents, and in the presence of proton acceptors. Fluorescence lifetimes increase when amino protons in the dye are deuterated, and when D_2O is used as the solvent instead of H_2O.

The structural dynamics of DNA can give some insight into dye binding.[19] The natural flexibiltiy of DNA has been recognized for some time,[20] and is becoming more widely appreciated. DNA is resistant to forces that would bend the molecule away from the helical axis. Nevertheless, the hydrogen bonds between the base pairs are said to "breathe," so that, at any time, a small fraction of them are accessible to solvent molecules as they separate briefly.[21-23] Conformational fluctuations are also described in terms of bending, stretching,

unwinding, and sliding motions.[19] These can give rise to a kink or flexible hinge in the helical structure, through which the dye molecules might intercalate. From stuctural models of DNA, one can see that the two strands of DNA are not equivalent in the helix. The grooves between the two strands have different sizes, and are called the major and minor groove. As the DNA structure fluctuates, the kinks that develop present different aspects to the major and minor groove. Some dyes would intercalate by approaching from the minor groove. Actinomycin D and EtBr are believed to be of this type.[19,27] The intermediate binding referred to earlier may be associated with a particular kink in the helix which commonly arises. Other molecules intercalate by approaching from the major groove. Acridine orange and proflavine are examples of this type. In other cases, approach from either groove is possible.

References

1. S. Udenfriend, Fluorescence Assay in Biology and Medicine, vol II, (Academic Press, New York, New York, 1969).
2. P. Lurquin, Chem.-Biol. Interactions 8, 303 (1974).
3. M. Waring, J. Mol. Biol. 13, 269 (1965).
4. J.-B. LePecq, and C, Paoletti, J. Mol. Biol. 27, 87 (1967).
5. G. Scatchard, Ann. New York Acad. Sci. 51, 660 (1949).
6. D. Doenecke, Exp. Cell Res. 109, 309 (1977).
7. A. Peacocke, and J. Skerrett, Trans. Far. Soc. 52, 261 (1956).
8. L. Cavalieri, and G. Nemchin, Biochim. Biophys. Acta 87, 641 (1964).
9. M. Gellert, C. Smith, D. Neville, and G. Felsenfeld, J. Mol. Biol. 11, 445 (1965).
10. L. Lerman, J. Mol. Biol. 3, 18 (1961).
11. G. Weil, and M. Calvin, Biopolymers 1, 401 (1963).
12. D. Genest, and P. Wahl, Biocim. Biophys. Acta 259, 175 (1972).
13. P. Wahl, J. Paoletti, and J.-B. Lepecq, Proc. Nat Acad. Sci. USA 65, 417 (1970).
14. P. Genest, P. Wahl, and J. Auchet, Biophys. Chem. 1, 266 (1974).
15. W. Bauer, and J. Vinograd, J. Mol. Biol. 33, 141 (1968).
16. M. Waring, J. Mol. Biol. 54, 247 (1970).
17. J. Olmsted, and D. Kearns, Biochemistry 16, 3647 (1977).
18. P. Lurquin, Chem.-Biol. Interactions 8, 303 (1974).
19. H. Sobell, B. Reddy, K. Bhandary, S. Jain, T. Sakore, and T. Seshadri, Cold Spring Harbor Symposium 42, 87 (1977).
20. H. Li, and D. Crothers, J. Mol. Biol. 39, 461 (1969).
21. H. Teitelbaum, and S. Englander, J. Mol. Biol. 92, 55 (1975).
22. J. McGhee, and P. von Hippel Biochemsitry 14, 1568 (1975).

23. J. McGhee, and P. von Hippel, Biochemistry 14, 1297 (1975).

24. T. Shih, and J. Bonner, J. Mol. Biol. 48, 469 (1970).

25. A. Chitre, and K. Korgaonkar, Biochem. J. 179, 213 (1979).

26. J.-J. Lawrence and M. Daune, Biochemistry 15, 3301 (1976).

27. C. Tsai, S. Jain, and H. Sobell, Proc, Nat. Acad. Sci. USA 72, 628 (1975).

EtBr Binding to Chromatin

EtBr is used as a probe of DNA. The DNA in chromatin is in an environment very different from that of isolated DNA, free of all proteins. Consequently, EtBr should bind to chromatin differently from the way it binds to DNA, if it is to be useful as a probe.

Optical properties In fact, the optical properties of EtBr bound to chromatin are very similar to the optical properties of EtBr bound to isolated DNA.[1-3] This feature simplifies interpretation of the important differences that do exist between the two bound forms. The absorption spectra, fluorescence emission spectra, fluorescence lifetimes, and quantum efficiencies for fluorescence are essentially identical for EtBr bound to DNA and to chromatin. In both cases, dye molecules will interact with each other if they bind to nearby sites, so that the quantum efficiency for fluorescence drops as more binding sites become occuppied.

Binding sites, binding constants Optical properties give some indications of structural features of the binding site. There is some evidence from fluorescence studies that the bound dye molecules may cluster together more in chromatin than in DNA.[2] Rotational relaxation rates inferred for the two types of binding sites suggest that chromatin is stiffer than isolated DNA, so that rotation is allowed through a smaller angular range for chromatin.[2]

One actively studied feature of EtBr binding is that chromatin binds less dye than isolated DNA.[2-4] That is, for a fixed concentration of nucleotides, chromatin bound dye gives a smaller signal than DNA bound dye. The magnitude of the difference depends on the concentration of the reactants. This matter will be discussed in detail, below. The

effect is observed in measurements made of absorbance, fluorescence intensity, and circular dichroism. Since the optical properties of the two binding sites are so similar, it is probable that the intercalation binding mechanism applies to chromatin binding as well as to binding to DNA. Two immediate explanations for the difference in the signals from the two types binding sites are that chromatin has fewer binding sites, or that the binding constant for chromatin is lower than for DNA.

In fact, the situation is somewhat more complex. The most convincing evidence so far is that at least two important binding sites are present in chromatin.[2,5,6] Scatchard plots of EtBr binding to chromatin are not really linear at any level of dye binding. In this case, it becomes necessary to revise the simple Scatchard formalism to allow for more complicated binding.[6] The first revision we will consider, explicitly takes into account the excluded site model.[7,8] We assume that binding at one site precludes binding at n' nearest neighboring sites. In the case of the excluded site model, n'=2, so that sites on either side of the occuppied site may not accept a dye molecule. The simple Scatchard model predicts

$$\frac{r}{[B]} = K(n - r),$$

where r is the number of bound molecules per base pair,

n is the number of binding sites per base pair,

K is the binding constant, and

[B] is the concentration of free dye.

If we explicitly take into account the excluded site model, the parameter n is eliminated, because each base pair is assumed to be a potential binding site. The revised expression for r/[B] is

$$\frac{r}{[B]} = K \frac{(1 - n'r)^{n'}}{(1 - (n'-1)r)^{n'-1}}$$

where r, [B], and K are as before, and n' is the number of nearest neighboring excluded sites.

More alterations may be made.[6] We may assume that not all the base pairs represent potential binding sites. If some fraction, α, of the sites is accessible to dye molecules, then

$$\frac{r}{[B]} = K \frac{(\alpha - n'r)^{n'}}{(\alpha - (n'-1)r)^{n'-1}}$$

We assume $0 \leq \alpha \leq 1$. The remaining fraction, $(1-\alpha)$, of the binding sites is presumed to be completely inaccessible to dye molecules. In the case of two binding sites, each with different binding constants, K_1 and K_2, and different fractions of accessible sites, α_1 and α_2, we can define r_1 and r_2 to be the number of dye molecules bound per base pair to the first and second types of binding sites, respectively. Then, $r = r_1 + r_2$. Assuming $n'=2$, we can write

$$\frac{r_i}{[B]} = K \frac{(\alpha_i - 2r_i)^2}{\alpha_i - r_i)} \quad \text{for } i=1,2.$$

This can be rewritten as

$$r_i = \frac{\alpha_i}{2}(1 - \frac{1}{\sqrt{(1 + 4K_i[B])}})$$

Limiting behavior includes the case where $K_i[B] \ll 1$, so that most of the binding sites are free. In that case, r_i approaches zero. For the case of excess dye, the upper bound on r_i is $\alpha_i/2$, which is consistent with the excluded site model.

With these alterations to the Scatchard theory, we now have five adjustable parameters. Not surprisingly, binding of EtBr to chromatin

can be described very well in terms of these five parameters. In particular, observed values of r/[B] as a function of r are consistent with n'=2, the excluded site model, in every case considered.

Data for chromatin isolated from calf thymus are consistent with two binding sites. One binding site would involve about 13% of the base pairs, and would have a binding constant considerably greater than the single binding constant observed for isolated DNA. The other binding site would involve about 80-85% of the base pairs and would have a smaller binding constant than isolated DNA. The free DNA binding constant is about 1.5×10^6 M^{-1}. The chromatin high affinity site binding constant has been reported as being about 14 times,[5] and about 700 times[6] the value of the binding constant for free DNA. The lower affinity site binding constant has been reported as being 1/16 and 1/10 the free DNA binding constant.[5,6]

The effect of chromatin structure on EtBr binding EtBr binding to chromatin has been analyzed by varying the structure of the complex. Very high orders of structure can effect binding. Mild nuclease digestion can break chromatin into oligomers of nucleosomes, and into individual nucleosomes. It is found that longer chains of nucleosomes bind slightly less EtBr (10-20%) than oligomers, and that oliogmers bind less than individual nucleosomes.[9] Presumably, non-histone proteins, more likely to remain in longer chromatin fragments, hinder dye binding.

The binding of EtBr is strongly influenced by histone proteins. To avoid confusion, it is important to distinguish between the effects of different histones on the two binding sites. The binding constant for the weak binding site increases as histones are slowly extracted,

approaching the value for protein-free DNA as all the histones are removed.[6,10] More than 80% of the base pairs are involved in this type of binding. The strong binding site is observed only when all the histones are present.[6] If the histones are removed, the strong binding vanishes. When the histones are replaced, strong binding returns. About 15% of the base pairs are involved in this type of binding. If non-histone proteins are removed, both sites remain. If histone H1 is removed, and the others remain, strong binding vanishes. If the histone H1 is left intact, and the four other types of histones are removed, strong binding decreases. Strong binding vanishes altogether when 15-20% of the four histones in the nucleosome remain. As more nucleosomal histones are removed, leaving the H1 histones in place, the strong binding vanishes, leaving only weak binding.

Of the five histones, H1 has the greatest net positive charge. Electrostatic considerations would suggest that H1 would interfere with the binding of EtBr, a basic dye. On the other hand, of the five histones, H1 has the greatest effect on long-range ordering of the nucleosome core particles. Thus, the association of the high affinity sites with H1 may be related to conformational effects.

One final point may be kept in mind about binding and binding sites. Most of the results mentioned above were obtained using relatively high dye concentrations, so that a significant fraction of the binding sites are occuppied. At high EtBr concentrations, the structure of chromatin is opened up.[11] It is clear that most of the DNA in chromatin is accessible to EtBr. Exceptions may be small segments where histones bind directly to DNA strands. Intercalation unwinds the DNA helix. This means that unwinding will occur in essentially all

segments of the nucleosome core bodies. and connecting strands. Chromatin opens up in the sense that histone-DNA interactions weaken when EtBr binds, releasing some of the histones and making histones more susceptible to extraction with NaCl. Also, nuclease digestion is more rapid in the presence of large amounts of EtBr, and tends to be more random, cleaving inside the core body more often than when no EtBr is present.[9,12] It is not clear how significant it is that DNA unwinds or that chromatin opens up; it is something that may be kept in mind.

Dye binding to chromatin from growing and resting cells Another interesting aspect of EtBr binding to chromatin is its dependence on the growth state of the cells from which the chromatin was isolated. One of the first observations about EtBr binding to chromatin was that the amount of dye bound to chromatin correlated strongly with transcriptional activity.[15,16]

The gross morphology of chromatin in intact cell nuclei has also been considered as a function of growth state.[13,14] Measurements were made of fluorescence from Feulgen stained HeLa cells using a microscope equipped with a photomultiplier. The apparatus was able to map fluorescence intensity over the cell nucleus, and characterize the shape and size of nuclei. Claims are made that cells harvested in different stages of growth have measureably different spatial distributions of stain in the nucleus. Resolution is not ideal in these measurements. Simply stated, it appears that chromatin in G_1 cells is relatively dispersed, while chromatin in early S cells appears more condensed. As the HeLa cells continue toward G_2, dispersion increases to the level observed in G_1 cells.

A number of reports exist concerning dye binding to chromatin in

which measurements were made of circular dichroism. Circular dichroism can be very sensitive to conformational changes of macromolecules. Information about proteins can be seen in an absorption band ranging from 200 to 250 nm. DNA is optically active around 260-290 nm. Intercalated EtBr has a CD spectral band from 300-350 nm, while free EtBr is not optically active.[3]

Two observations are made from CD measurements.[18-21] The first is that chromatin isolated from cells stimulated to grow has greater optical activity in the band from 260-290 nm. than chromatin isolated from resting cells. The other observation is that when EtBr is bound to chromatin isolated from cells stimulated to grow, the CD spectrum of EtBr has a greater amplitude than for EtBr bound to chromatin from resting cells. It is presumed that the amplitude of the CD spectrum is a direct measure of the amount of bound dye.[3] When 8-10% of the proteins are extracted in 0.25 M NaCl, the spectral differences vanish.[18] When the extracted proteins are replaced, the spectra return to their original appearance. If the extract of one type of chromatin is mixed with the other type of chromatin, some spectral features of the extract's original chromatin can be preoduced, but only with a large excess of the extracted protein. Chromatin from cells in S phase seem to bind more EtBr than chromatin from G_1 cells.[19] Both types of chromatin bind more EtBr than chromatin from cells in mitosis. The CD changes in the band from 260-290 nm. follow changes in dye binding, as cells go through the cell growth cycle. Optical activity in the 200-250 nm. band behaves similarly.

These results are consistent with increased dye binding to transcriptionally active chromatin, since mitotic cells are not

transcriptionally active, while G_1 and S phase cells are synthesizing RNA. It has also been found that methylating carcinogens have the effect of increasing dye binding and increasing circular dichroism in the 260-290 nm. band.[22]

All of these experiments involve fairly high concentrations of EtBr, so that a significant fraction of the sites contain bound dye. Binding constant determinations were not reported. Different chromatin preparations show different levels of dye binding, with the magnitude of the effect varying somewhat from one report to the next. Dye binding in different chromatin samples was effected by as much as a factor of three in a few cases, and by as little as 30% in other cases.

References

1. L. Angerer, and E. Moudrianakis, J. Mol. Biol. 63, 505 (1972).

2. L. Angerer, S. Georghiou, and E. Moudrianakis, Biochemistry 13, 1077 (1974).

3. R. Williams, P. Lurquin, and V. Seligy, Eur. J. Biochem. 29, 426 (1972).

4. C. Nicolini, K. Ajiro, T. Brown, and R. Baserga, J. Biol. Chem. 250, 3381 (1975).

5. J. Lawrence, and M. Louis, FEBS Letters 40, 9 (1974).

6. J. Lawrence, and M. Daune, Biochemistry 15, 3301 (1976).

7. D. Poland, and H. Scheraga, Theory of Helix-Coil Transitions (Academic Press, New York, New York, 1976).

8. D. Crothers, Biopolymers 6, 575 (1968).

9. D. Doenecke, Exp. Cell Res. 109, 309 (1977).

10. A. Chitre, and K. Korgaonkar, Biochem. J. 179, 213 (1979).

11. W. Stratling, and I. Seidel, Biochemistry 15, 4803 (1976).

12. J. Paoletti, Biochem. Biophys. Res. Comm. 81, 193 (1978).

13. C. Nicolini, W. Linden, S. Zeitz, and C. Wu, Nature 270, 607 (1977).

14. F. Kendall, R. Swenson, T. Borum, J. Rowinski, and C. Nicolini, Science 196, 1108 (1977).

15. V. Seligy, and P. Lurquin, Nature New Biology 243, 20 (1973).

16. N. Ringertz, and L. Bolund, Exp. Cell Res. 55, 205 (1969).

17. C. Nicolini, and R. Baserga, Chem.-Biol. Interact. 11, 101 (1975).

18. C. Nicolini, S. Ng, and R. Baserga, Proc. Nat. Acad. Sci. USA 72, 2361 (1975).

19. C. Nicolini, K. Ajiro, T. Borum, and R. Baserga, J. Biol. Chem. 250, 3381 (1975).

20. T. Ide, and R. Baserga, Biochemistry 15, 600 (1976).

21. N. Chin, and R. Baserga, Biochemistry, 14, 3126 (1975).

22. C. Nicolini, R. Ramanathan, F. Kendall, J. Murphy, S. Parodi, and D. Sarma, Cancer Res. 36, 1725 (1976).

EXPERIMENTAL PROCEDURE

Description of the Apparatus

In a previous section, experiments were described in which Rhodamine 6G was used to demonstrate how to measure the beam waist radius of a focussed laser beam. Additional information was simultaneously acquired regarding the diffusion coefficient and number concentration of fluorescent molecules diffusing through the open volume defined by the beam. The optical arrangement used in that experiment has several attractive features. One is that the focal spot is large enough to be measures directly, and predicted accurately. Another advantage is that a paraboloidal reflector can collect almost all the fluorescent light and direct it to a photomultiplier.

These features have aspects that prevent successful measurements on small biological samples. The focal spot is larger than ideal when a cell nucleus is the experimental subject. As small a spot as possible is preferred. The very efficient paraboloidal reflector rejects almost all information about the spatial characteristics of the illuminated object. In order to get high optical resolution, the detection apparatus was incorporated into a microscope as indicated in figure 15.

The basic arrangement from before is maintained. The optical components are mounted on a vibration isolation table. The cooling fan for the laser and all fan cooled electrical equipment are placed away from the table. The microscope is mounted in a steel frame to reduce the effect of any possible vibrations.

In the revised apparatus, the image of lens L1 is now cast toward the microscope instead of onto the sample. The sample is viewed in focus in the microscope. The lens L1 is then translated along the beam

Figure 15. Apparatus for Fluorescence Correlation Spectroscopy. Revisions from original apparatus involve the incorporation of a microscope for observing the sample directly.

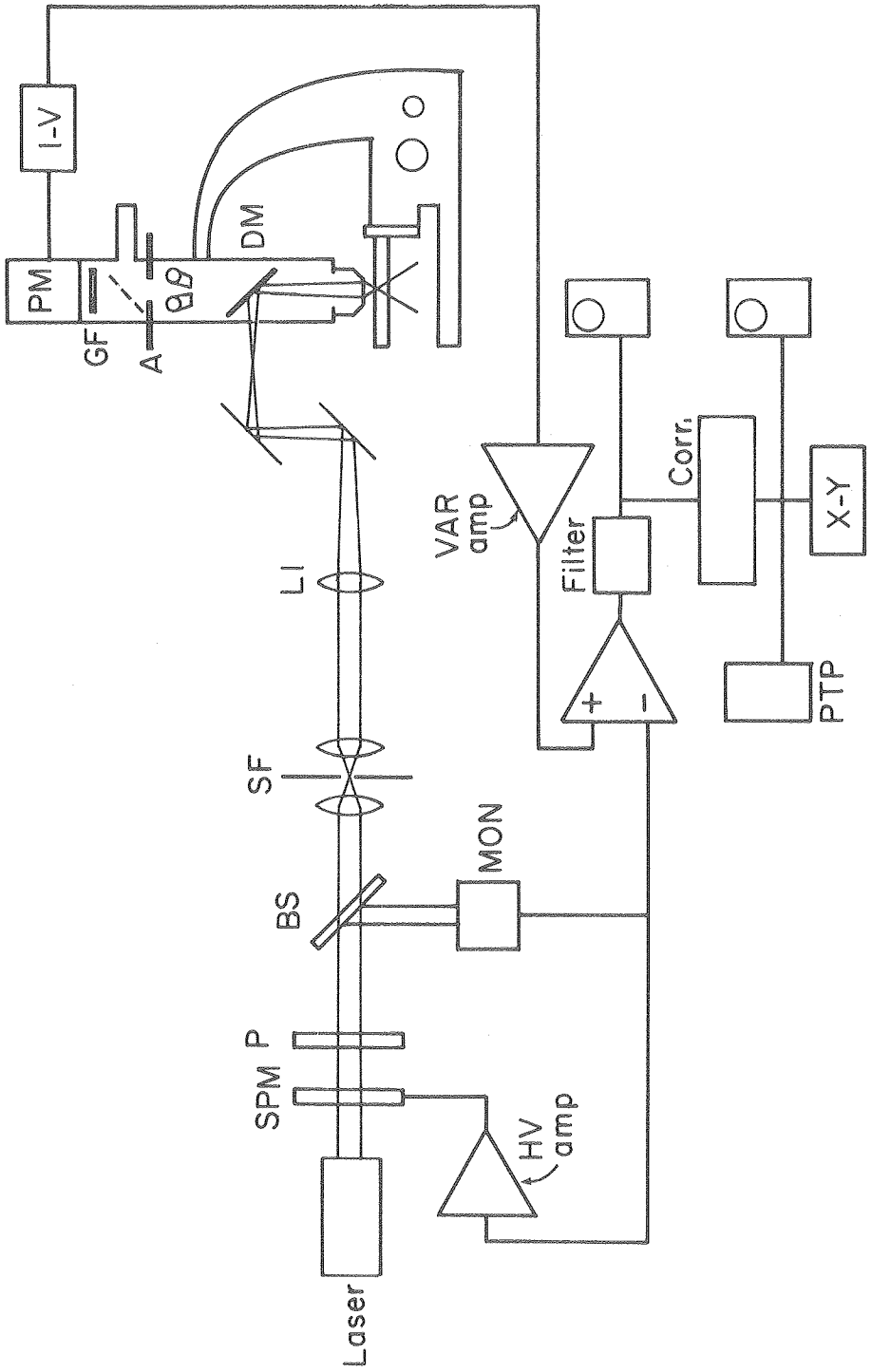

XBL7812-13067

until it casts its image of the beam onto a point slightly in front of the body of the microscope. At one position of the lens L1, the beam and the sample may be viewed in focus simultaneously. The beam and sample can now be moved relative to one another in two ways. Lens L1 can be translated along the beam axis. This will move the position of the beam focus to a point above or below the sample. The sample will remain in focus. Alternatively, the sample stage can be moved, while the beam focal plane stays in focus in the microscope. Moving L1 involves a transformation of the position of L1 to the corresponding displacement of the beam relative to the sample. L1 movement will be a matter of centimeters, while the beam moves a few microns relative to the sample.

The excitation beam is directed to the objective lens of the microscope by a mirror with specially prepared dielectric coatings. The mirror reflects essentially all of the excitation beam intensity. Fluorescent light, at longer wavelenghts, is transmitted by the same mirror with up to 95% efficiency. Some of the incident light is reflected or scattered from the sample, collected by the objective lens, and directed toward the photomultiplier. Most of it is rejected by the dichroic mirror. Some is absorbed by the mirror and a small fraction is transmitted. Glass filters are placed before the photomultiplier. They remove most of the remaining non-fluorescent light.

An aperture is placed in the body of the microscope to reject all light except that coming from an area immediately surrounding the beam in the center of the field of view. This eliminates substantial background signal. The light transmitted through the aperture can be

viewed in a monocular eyepiece, or allowed to pass to the photomultiplier.

Signal processing is done basically as described before. Versatility was provided by introducing a variable band low pass electronic filter after the difference amplifier. The filter and the attenuator in the correlator now have to be adjusted for each measurement of an autocorrelation function at a new time scale. Both settings depend on the characteristic time scales to be observed. The experimenter decides what time scale is of interest. The low pass filter will not allow fluctuations to decay away in a time shorter than the filter's time constant. Thus, the filter's time constant is chosen so that fluctuations will persist for at least several correlator time increments, $\Delta\tau$. In practice, the filter is usually set so that the first 10-20 delay increments in the autocorrelation function are dominated by correlations imposed by the filter. In fact, the transfer function or the impulse response of the filter can be seen in these first few points of the autocorrelation function.

This procedure has two objectives. One is to ensure that the digitizer in the correlator sees a representative value when it samples input voltage for a brief moment during the delay increment, $\Delta\tau$. The filter will smooth the input so that no appreciable variations occur over the time $\Delta\tau$.

The other objective is to allow the largest possible signal to reach the digitizer without distorting the computed autocorrelation function. The correlator has an adjustable attenuator that scales the input signal so that fluctuations do not exceed the capacity of the digitizer. If the low pass filter rejects all but the lowest

frequencies, then the root mean square fluctuation is reduced, and the attentuator can be set to attenuate very little of the remaining input. If an identical photocurrent had been filtered to pass higher frequencies, then the root mean square fluctuation would have been larger, the attenuator would be set to scale the input to lower values, and the computed autocorrelation function would have had a lower amplitude.

If the input fluctuations have amplitudes with a gaussian distribution, then the manufacturer of the correlator recommends that the attenuator be set so that at least one standard deviation from the mean falls within the limits of the digitizer. The actual distribution of fluctuation amplitudes was measured routinely. Between one and two standard deviations were made to fall within the limits of the digitizer.

Proper settings of the filter and attenuator will <u>not</u> effect values of the diffusion time or $\langle i \rangle^2/G(0)$. The filter time constant should be much faster than the diffusion time, and attenuator settings are taken into account when computing $\langle i \rangle^2/G(0)$.

To review, the experimenter decides what time scale is to be observed, and chooses the delay time, $\Delta\tau$ so that the range from 0 to 400 $\Delta\tau$spans the time scale of interest. The low pass filter is set so that fluctuations are smoothed out over several delay increments, $\Delta\tau$. Next, the attenuator in the correlator is set so that the root mean square fluctuation amplitude is comparable to, but does not exceed the limits of the digitizer. Finally, autocorrelation functions can be measured. Whenever the value of $\Delta\tau$ is changed, the filter and attenuator are adjusted accordingly.

Analysis of the Data

Algorithm for measuring $G(\tau)$ The Saicor model 43A Correlation and Probability Analyzer uses one basic algorithm for computing $G(\tau)$. Variations on the basic scheme can be chosen by adjusting settings on the front panel. Those variations will not be discussed.

The autocorrelation function of the photocurrent can be approximated by an integral.

$$G(\tau) \approx \frac{1}{T}\int_0^T i(t)i(t+\tau)\, dt$$

The parameter t is a dummy variable of integration. The important temporal parameter is τ. $G(\tau)$ measures the correlations in $i(t)$ as a function of the delay interval, τ. The Saicor correlator computes the the integral shown above, for 400 values of τ.These values are 0, $\Delta\tau$, $2\Delta\tau$, ... , $399\Delta\tau$. The quantity $\Delta\tau$ is chosen from settings on the front panel of the device.

Near the beginning of each increment, $\Delta\tau$, the input signal is sampled briefly. During the rest of the delay increment, a series of computations takes place. At the end of the computations, the input voltage is sampled again and the computations are repeated.

The computations are ordered in two arrays, each stored in a memory containing 400 elements. In the initial 399 delay intervals, 399 consecutive values of the input are sampled and digitized. The measurements are stored in consecutive locations in one of the 400 element arrays. We may denote these values i_1, i_2, ... , i_{399}. Accumulated values of $G(\tau)$ are stored in the other 400 element storage array. These elements may be denoted $G(0)$, $G(\Delta\tau)$, ... , $G(399\Delta\tau)$. For the first 399 delay increments, the $G(\tau)$ array contains only zeros. In the 400th increment, the input signal is

sampled, digitized, and stored in the input array as i_{400}. Next i_{400} is multiplied byitself and the product is addeddto the value of G(0). The result is stored in the G(0) element of the $G(\tau)$ array. The product of i_{400} with i_{399} is computed and added to the contents of the $G(\Delta\tau)$ element of the $G(\tau)$ array. Similarly, i_{400} is multiplied by the other elements of the input array, and the products are added to the corresponding elements of the $G(\tau)$ array, and the results stored in the $G(\tau)$ array.

Then, the elements of the input array are all shifted down by one location, and the value stored in the first element is lost. Thus, the first 399 elements of the input array now contain $i_{2, 3, \ldots, i_{400}}$. Next, the 401st sample of the input signal is made, digitized, and stored in the 400th element of the input array. The cycle is repeated in this way. A new value of the input is obtained. Then 400 multiplications and additions are performed, followed by 400 shifts in the input array.

It may be noted that the $G(\tau)$ array will actually contain values approximating $TG(-\tau)$. That is, the correlator computes

$$\sum_{j=0}^{M} i(t_j)i(t_j-n\Delta\tau)\Delta\tau \approx \int_0^T i(t)i(t+\tau)\,dt \approx TG(-\tau),$$

where $M\Delta\tau=T$, $t_0=0$, $t_{j+1}-t_j=\Delta\tau$, $n\Delta\tau=\tau$, and $n=0,1, \ldots, 399$. The resulting approximation to the autocorrelation function can be normalized for accumulation time by noting the number of cycles of the real time data are being collected.

If $\Delta\tau$ is less than 400 microseconds, the the computations are still in progress when the delay increment ends. For $\Delta\tau$ less than 400 microseconds, the correlator continues to sample input in every delay

increment, but performs the calculation cycle every 400 μsec. Thus, there is a loss of efficiency at high sampling rates.

Analysis of measured autocorrelation functions The output of the Saicor model 43A Correlation and Probability Analyzer is 400 points, representing the autocorrelation function, evaluated at 400 delay times, usually starting with zero delay. Once the data are colected, the 400 values for $G(\tau)$ are punched on paper tape. The paper tape is read by a computer which fits the 400 values to a function of the form $A(1 + \tau/T)^{-1} + B$, using the least squares method.

The parameter will usually be τ_0 or τ_+, depending on the experimental circumstances. The parameter A is closely related to G(0). The parameter B is a first order approximation of the effect of various slowly varying voltages that are included in the input to the correlator. Examples of these slowly varying inputs are a 10 mV DC offset, known to be present in the output of the difference amplifier. Another example is the slow loss of photocurrent due to bleaching of the chromophores in the sample. High pass electronic filters minimize this problem, but do not eliminate it in many cases. A third example is an intermittent drift introduced in the correlator itself, which may be associated with the internal 12 volt power supply.

Given the least squares fit to the data, uncertainties can be estimated for the parameters A, B, and T. These uncertainties reflect only the precision of the fit. They do not take into account the fact that one autocorrelation function will differ somewhat from another collected under identical experimental circumstances. While computed uncertainties are admittedly underestimates of the true uncertainties, they do provide some measure of the relative uncertainties of the

parameters from one measurement to the next. Thus, they are used to weight the data in some cases.

The computations proceed in this fashion. We define

$$g(t_i;A,B,T) = A(1 + t_i/T)^{-1} + B,$$

and $$S^2(A,B,T) = \sum_{i=1}^{400} (g(t_i;A,B,T) - G(t_i))^2 ,$$

where $G(t_i)$ is the observed value of the autocorrelation function at the delay interval t_i. The best least squares estimators of A, B, and T are the values $\tilde{A}$, $\tilde{B}$, and $\tilde{T}$ that satisfy the conditions

$$0 = \frac{\partial S^2}{\partial A} = \frac{\partial S^2}{\partial B} = \frac{\partial S^2}{\partial T} .$$

These three equations are linear in $\tilde{A}$ and $\tilde{B}$, but non-linear in $\tilde{T}$. The preocedure for arriving at the values for $\tilde{A}$, $\tilde{B}$, and $\tilde{T}$ is iterative. A guess is made of $\tilde{T}$. Using the first two conditions above, and the guess of $\tilde{T}$, conditional estimates can be made for $\tilde{A}$, and $\tilde{B}$. Then the third condition above can be evaluated, conditionally. The result is compared to zero. More guesses are made of $\tilde{T}$, and values obtained for $\frac{\partial S^2}{\partial T}$. When $\frac{\partial S^2}{\partial T}$ assumes a value regarded as being close to zero, the process is finished. In practice, "close to zero" means that the true value of $\tilde{T}$ is within $\Delta\tau/5$ of the current guess of $\tilde{T}$.

During the iteration process, new guesses of $\tilde{T}$ are made in a clumsy but straightforward manner. The first guess is $2\Delta\tau$. The second guess is $22\Delta\tau$. New guesses are made at intervals of $20\Delta\tau$, until $\frac{\partial S^2}{\partial T}$ changes sign. The previous guess of $\tilde{T}$ is recalled, and $2\Delta\tau$ is added to it. The process is repeated, each time taking smaller steps in the parameter T.

For example, if $\frac{\partial S^2}{\partial T}$ is less than zero for $T=2\Delta\tau$, $22\Delta\tau$, ... , but

is greater than zero for $T=82\Delta\tau$, then the guess following $82\Delta\tau$ is $64\Delta\tau$. subsequent guesses are $66\Delta\tau$, $68\Delta\tau$, and so on, until $\frac{\partial S^2}{\partial T}$ is again positive. In this manner, increasing resolution in T is achieved. Computation time is not the rate limiting step in the analysis of the data.

Fitting in this manner has always found a minimum of S^2 rather than a maximum. If the data are very noisy, it is possible that no solution is found. Every fit found in this way is graphed and visually inspected. In all cases, the solutions found have been reasonable and appropriate, given the data.

On some occaisions, periodic noise is present in addition to the desired fluctuations. The resulting autocorrelation function will then contain a term of the form $C \cos \omega\tau$, where C is a constant and ω is the angular frequency of the periodic noise. When the periodic noise is severe enough so that ω can be evaluated by inspection, the computer estimates will include a value for $\tilde{C}$, the best estimator for C. C is treated computationally in the same way that A and B are treated.

Uncertainties are computed by the method of maximum likelihood.[1] A likelihood function, L, is defined.

$$L(t_i;A,B,T) = \left(\prod_{i=1}^{N} \sigma_i^{-n}\right) \exp\left(-\frac{1}{2}\sum_{i=1}^{N} \frac{(g(t_i;A,B,T) - G(t_i))^2}{\sigma_i^2}\right)$$

Here, σ_i is the uncertainty associated with the measurement of $G(t_i)$, and there are N data points. The variances and covariances of the estimated parameters are expressed in matrix form by

$$(\mathrm{cov}(X,Y))_{i,j} = \left(-\frac{\partial^2 \ln L}{\partial X \partial Y}\right)^{-1}_{i,j}.$$

In practice, all of the uncertainties, σ_i are assumed to be equal.

Diffusion times When simple diffusion is the only process contributing to the observed autocorrelation function, then T may be interpreted as the characteristic diffusion time, τ_D. When the fluctuations of interest arise from EtBr-DNA binding, the the expected autocorrelation function consists of three terms.

$$G(\tau) = G_0(\tau) + G_+(\tau) + G_-(\tau)$$

$G_0(\tau)$ describes the diffusion of DNA molecules. $G_+(\tau)$ can be thought of as arising from the diffusion of EtBr molecules from one binding site to the next. By "next" binding site, it is meant the next site to which the molecule binds, not the neighboring site. It is extremely unlikely that a dye molecule will hop its way along a DNA double strand. $G_-(\tau)$ can be thought of as reflecting fluctuations due to EtBr molecules binding to and releasing from a binding site. Both $G_0(\tau)$ amd $G_+(\tau)$ have the same general appearance.

$$G_0(\tau) = \frac{G_0(0)}{1 + \tau/\tau_{DNA}}$$

$$G_+(\tau) = \frac{G_+(0)}{1 + \tau/\tau_+}$$

In these expressions, τ_+ and τ_{DNA} are the characteristic diffusion times of the processes from which $G_+(\tau)$ and $G_0(\tau)$ arise.

In all the experiments described below, the autocorrelation function will be dominated either by $G_0(\tau)$ or $G_+(\tau)$. This means that all the experiments can be described in terms of the parameters estimated from the general form $G(\tau) = A(1 + \tau/T)^{-1} + B$.

The third term, $G_-(\tau)$ is not observed in the measurements discussed here for at least three reasons. $G_-(\tau)$ has very rapid characteristic times. At high concentrations of either free dye or free

binding sites, the on-off rate is considerably faster than once per millisecond. Another reason for not seeing $G_-(\tau)$ is that the amplitude is very small whenthe ratio of bound to free dye is much greater than one. Under conditions of low dye concentration or in the presence of excess DNA, most of the dye will be bound. The third obstacle to observing $G_-(\tau)$ is that signal to noise problems are necessarily more pressing in fast measurements, since fewer photons are detected per correlation time from each fluorescing molecule. Thus, contributions from $G_-(\tau)$ are in a time range outside the scale of most observations, the contributions will have low amplitudes compared to $G_+(\tau)$, and signal to noise problems will be especially severe when trying to resolve $G_-(\tau)$, even if we were looking for it.

Under appropriate conditions, $G_0(\tau)$ can be made to dominate the signal. For instance, making the concentration of bound dye much larger than the concentration of DNA molecules will make $G_0(\tau)/G_+(\tau)$ much larger than one. This condition means that many EtBr molecules will bind to each DNA molecule, providing a great signal to noise advantage to the $G_0(\tau)$ term.

The time scale of observation can also be used to discriminate $G_0(\tau)$ from $G_+(\tau)$. The diffusion time for DNA molecules is not easily altered, but an excess of dye will shorten τ_+ to about the value for free diffusion.

Other conditions are more suitable for observing $G_+(\tau)$ and not $G_0(\tau)$. If the DNA can be immobilized, for instance, then $G_0(\tau)$ will vanish. Low dye concentrations and high DNA concentrations can help make $G_+(\tau)$ more detectable. If there are zero one or a few dye molecules per DNA molecule, then the enormous signal to noise advantage

of $G_0(\tau)$ is lost, since each DNA moleculewould emit relatively few photons per correlation time. The amplitudes of $G_0(\tau)$ and $G_+(\tau)$ would then approach each other.

Computation of $\langle i \rangle^2/G(0)$ The quantity $\langle i \rangle$ is the average photocurrent arising from the fluorescence of diffusing molecules. The average photocurrent is measured by a digital voltmeter while data are being collected. It must be determined what part of the measured photocurrent arises from that fluorescence. Other contributions to the photocurrent include dark current, scattered light, and background fluorescence. Dark current is actually an insignificant factor, being less than one nanoamp. Glass surfaces reflect part of the excitation beam, and about one nanoamp of photocurrent can be attributed to light from each glass water interface, at the laser powers typically used. For samples of about 10 μ depth, both surfaces are well within the depth of focus of the objective lens. About 1 1/2 nanoamps of background photocurrent is a practical lower limit. When observing cell nuclei suspended on a cover slip, one one glass surface is visible, and as little as 0.7 or 0.8 nanoamps of background is not uncommon.

Total fluorescence from samples is sometimes as high as 100's of nanoamps, but it is not unreasonable to attempt to have equal background and fluorescent photocurrents. Thus, one may lower dye concentrations until dye fluorescence approached background levels. In that case, G(0) will be more or less maximized, since very few molecules will be in the beam.

In practice, total background is determined in one of two ways. If data are being collected from a homogeneous sample, then a blank is prepared without dye to estimate background. When looking at nuclei, it

can be measured by displacing the sample a short distance, so that the beam passes through the sample at a point where no EtBr will be bound to DNA. The fluorescence intensity from the displaced sample is taken as background.

The value for G(0) is based on the amplitude $\tilde{A}$ found in the computer fit of the data. Other factors enter. The photocurrent has been converted to a voltage and amplified so that its average value equals the signal from the beam power monitor. A high pass filter then removes the average of the photomultiplier signal, leaving the fluctuations. The fluctuations are amplified 99 times by a second filter and amplifier. The amplified filtered fluctuations are then attenuated in the autocorrelator so that the root mean square fluctuation in the processed photomultiplier signal does not exceed the capacity of the digitizer in the correlator. The output of the correlator is displayed at a resolution set by selecting the most significant bits from 14 bit words stored in memory. The correlator output will always be between -2.5 an 2.5 volts, but the amplitude, A, will depend on the word display position. The correlator output is punched on paper tape. The tape punch scales a voltage of 2.5 volts to be 1.27. Voltages of less than 2.5 volts are scaled proportionately. A should be normalized for the time spent accumulating data; $\langle i \rangle^2/G(0)$ should not depend on accumulation time. Taking all these factors into account,

$$\frac{\langle i \rangle^2}{G(0)} = \frac{1.27\ n\ (99)^2\ V^2\ 2^N}{2.5\ A\ K},$$

where A is the amplitude from the computer fit, K is determined by the attenuator setting, 2^N is the scaling factor specified by the display word position, n is the number of time increments, $\Delta\tau$, measured in

units of 400 X 128 X 1024, and V is the measured average voltage from the photomultiplier, less background. K values are given by the manufacturer, and word position ranges from 1 to 2^8.

Efficiency factor In these fluctuation experiments, total fluorescence intensity is measured and the number of diffusing molecules is determined. It should be possible, then, to calculate the amount of light coming from each diffusing molecule. The collection efficiency of the optical components can be calibrated by using dye molecules of known quantum efficiency for fluorescence. Then, the fluorescence efficiency of less completely characterized samples can be considered. What follows in the next few paragraphs will lead to an expression for the efficiency of fluorecence detection per molecule.

Light is absorbed according to Beer's law.

$$I = I_0\, 10^{-\varepsilon CL} = I_0 \exp(-2.303\varepsilon CL)$$

where I_0 is the incident light intensity, measured in photons per second, I is the transmitted light intensity, ε is the decadic extinction coefficient, C is the concentration of absorbing molecules, and L is the sample depth.

The number of photon absorbed per second is $I_0(1-\exp(-2.303\varepsilon CL))$. The number of fluorescent photons emitted per second is $I_0Q(1 - \exp(-2.303\varepsilon CL))$, where Q is the quantum efficiency for fluorescence. The number of photons detected per second can be written as $I_0a_1a_2a_3Q(1 - \exp(-2.303\varepsilon CL))$, where a_1 is the optical collection efficiency describing the collection of light by the objective lens of the microscope, and the transmission of light to the photocathode of the photomultiplier. The factor a_2 is the photocathode quantum

efficiency, and a_3 is the gain of the photomultiplier, which gives the number of coulombs at the anode for each photoelectron ejected from the photocathode. The photocurrent can be written as

$$i = I_0 Q a_1 a_2 a_3 (1 - \exp(-2.303 \varepsilon CL)).$$

A current to voltage converter is used that has a gain of r. The photomultiplier voltage is set equal to the beam power voltage, V, by adjusting the gain of the current to voltage converter. We may write

$$V = ir = I_0 Q a_1 a_2 a_3 r (1 - \exp(-2.303 \varepsilon CL)).$$

I_0, ε, r, C, and L are known or can be easily measured. Certainly, V, I_0, and r are closely related. The values of $a_1 a_2 a_3$ are not immediately known, but may be estimated roughly. Reasonable <u>a priori</u> estimates are

$a_1 \lesssim 1/4\pi \approx 0.08$. An objective lens might intercept one steradian of solid angle.

$a_2 \approx 0.1$ Photocathode quantum efficiencies quoted by the manufacturer are of this magnitude.

Similarly, $a_3 \sim 10^5$

Then, $a_1 a_2 a_3 \sim 10^{-16}$ coulombs per fluorescent photon. Typically observed values for the other quantities in the expression above are V = 0.1 volt, $I_0 \approx 10^{15}$ photons per second, $r \approx 10^7$ ohms. These would be expected values for a sample of Rhodamine 6G at a concentration of about 10^{-7} M, in a sample about 10 μ deep. R6G has a quantum effeiciency for fluorescence of about 1.0 and an extinction coefficient of around 3×10^4 l/mole-cm. It is the case in this example, and is generally true in what follows that εCL is much less than one. Then, we may expand the exponential term, and find

$$a_1 a_2 a_3 = \frac{V}{2.303\ I_0\ Q\ r\ \varepsilon\ CL} \approx 10^{-17} \text{ coulombs}$$

We see that the observed value for the product $a_1a_2a_3$ is comparable to a priori estimates. It should be noted, in fact, that $a_1a_2a_3$ are functions of wavelength, and these expressions should be regarded ad taking into account the finite bandwidth of the emission spectrum.

Several factors in the expression for $a_1a_2a_3Q$ can be developed further. The quantity V/I_0 is an instrumental constant, that depends on the wavelength of the exciting light. For excitation at 488 nm., it is measured to be 8.13×10^{-16} volt-sec/photon. The factor CL can be derived from $\langle i \rangle^2/G(0)$.

$$CL = \frac{\langle i \rangle^2\ 10^{-12}}{G(0)\ \pi w^2\ 6.02} \text{ cm. mole } \mu^2\text{/liter}$$

where w will be given in microns. Thinking in terms of excitation at 488 nm., we may write

$$a_1 a_2 a_3 = \frac{6.68 \times 10^{-3}\ w^2}{r\ \varepsilon\ \frac{\langle i \rangle^2}{G(0)}} \text{ coulomb-ohm/M-cm-}\mu^2$$

Finally, we may allow for many chromophores to bind to a single diffusing particle. The product of the quantum efficiency for fluorescence with the extinction coeeficient will increase from εQ to $m\varepsilon Q$, where m would be the average number of chromophores per diffusing particle. This assumes that all the chromophores are independent of each other. Thus, m can be thought of as the apparent number of bound chromophores. At this point, we may write

$$ma_1 a_2 a_3 Q = \frac{6.68 \times 10^{-3}\ w^2}{r\ \varepsilon\ \frac{\langle i \rangle^2}{G(0)}} \text{ coul.-ohm-liter/mole-cm-}\mu^2$$

It is understood that w is measured in microns, $\langle i \rangle^2/G(0)$ is the number of particles in the illuminated volume, r is the gain of the current to voltage converter, measured in ohms, and ε is the decadic extinction coefficient in units of liter/mole-cm.

One other consideration might be mentioned. When the chromophore is in the excited state, it will probably not be capable of absorbing light from the beam. This suggests another efficiency factor, a_4, which is the fraction of time a chromophore is in the ground state. It is presumed that a_4 is close to one, and need not be taken into account explicitly. To estimate this factor, we can suppose that 10^{15} photons per second are incident on the sample. Rouphly one in 10^6 is absorbed, making 10^9 absorbed photons per second. If there are 1000 chromophores in the illuminated region, on the average, then each will absorb about 10^6 photons per second. The fluorescence lifetime of EtBr, bound to DNA, is less than 30 nsec., and is relatively large.[2] Thus, the factor a_4 will be about 1.0, and need not be taken into account explicitly. Nevertheless, by changing experimental arrangements slightly, a_4 might be decreased enough so that it becomes important. It should not be ignored altogether.

Precision and accuracy of measured values One can think in two ways about the variability in values of G(0), and the diffusion time. One instinctive measure of variability is, "How do the autocorrelation functions look?" Another is, "How does one measurement compare with another, determined under the same conditions?"

The first measure is closely related to the precision of the measurement. Plots of correlation functions will look good if the 400 data points lie close to a smooth curve of the expected shape.

Correspondingly precise estimates of G(0) and the diffusion time can be computed from such data. Other data will look bad if consecutive points have widely different values. Estimates of G(0) and the diffusion times will be correspondingly imprecise.

Observed correlation functions with small scatter from one point to the next may still give inaccurate values for G(0) and the diffusion time. The diffusion process being studied is statistical in nature. Fluctuations in number concentration can be very precisely measured in some cases, but if those fluctuations are not representative of future and past fluctuations, then estimates derived from only those few fluctuations will be misleading. Even when fluctuations can be characterized with high precision, the data must be collected for many time the characteristic decay time of the system. An empirically determined, but intuitively reasonable lower limit to the data accumulation time is of the order of 1000 correlation times. At this level, uncertainty due to inaccuracies in sampling of fluctuations begins to approach uncertainty due to imprecision in the measurement of the autocorrelation function.

An example may help illustrate this point. DNA molecules can bind many chromophores and can be prepared in dilute solutions. It is possible to have fewer than 100 DNA molecules in the illuminated volume, each one fluorescing very intensely. Even with modest collection efficiency, the fluctuations in fluorescent intensity can be measured very precisely as a function of time. However, if the data are collected for only five diffusion correlation times, then very precise measurements will have been made of fluctuations that may be quite unusual or unrepresentative. In fact, as data are being collected,

one can visually observe just such behavior.

On the other hand, for less intensely fluorescent diffusing molecules, observations made over a long period of time can be surprisingly accurate, even though the data vary considerably from one point to the next.

This question has been studied theoretically.[3] The treatment is very specialized, and won't be discussed here, in detail. One important result is to state a practical limit on the fluorescence intensity necessary for successful measurements. A figure of merit is found, which is the number of detected fluorescence photons from each molecule in one diffusion correlation time. That quantity is denoted $\langle n \rangle \beta$. If many photons are detected from each molecule per correlation time, that is, if $\langle n \rangle \beta \gg 1$, then the experiment is said to be in the high count rate limit. In this limit, the signal to noise is predicted to behave like

$$\frac{S}{N} = \frac{G(\tau)}{\sqrt{\text{var}(G(\tau))}} = \sqrt{\Gamma T}$$

where $\text{var}(G(\tau))$ is the variance of the estimate of $G(\tau)$, Γ is the characteristic decay rate of the system, and T is the data accumulation time.

In the limit where $\langle n \rangle \beta \ll 1$, fewer than one photon per molecule is detected in each correlation time, and signal to noise is proportional to $\langle n \rangle \beta$, as well as to the square root of the accumulation time.

It follows that signal to noise improves with photon counting rate until $\langle n \rangle \beta \sim 1$. Further improvements in detection or more intense fluorescence leads to no improvement in signal to noise. At all photon counting rates, signal to noise improves with the square root of the

data accumulation time.

It is intuitively reasonable that $\langle n \rangle \beta$ be important in assessing signal to noise problems. Fluctuation correlation measurements rely on correlations between detected photons. Photons from different molecules are presumed to be uncorrelated. Thus, correlations can be seen only if more than one photon is detected from at least some of the diffusing molecules. If $\langle n \rangle \beta$ is much less than one, then very few photons will be correlated. If $\langle n \rangle \beta$ is much greater than one, then almost all molecules will emit many detected photons that will be correlated with each other.

References

1. J. Orear Notes on Statistics for Physicists UCRL Pub. #8417, Lawrence Berkeley Laboratory, Berkeley Calif.

2. P. Wahl, and J.-B. LePecq, Proc. Nat. Acad. Sci. USA 65, 417 (1970).

3. D. Koppel, Phys. Rev. A 10, 1938 (1974).

RESULTS

Results for Rhodamine 6G.

In an earlier section, results were discussed involving rhodamine 6G (R6G). It was established that the technique of varying the beam size can be used to determine the beam waist radius and other physically important parameters. These earlier results apply to a focussed beam with a 13 μ waist radius. The optical arrangement for the following results takes advantage of a 60X microscope objective lens that makes a much smaller beam waist. Direct physical measurement of such small focal spots is relatively demanding. Scalar diffraction theory was used to predict the size of the 13 μ focal spot. When applied to the new arrangement, it predicts a focal spot with a 0.12 μ radius. Since the wavelength of the light is about 0.5 μ, it is unlikely that the prediction of scalar diffraction theory will be verified at this level.

In this section, R6G is used to show that the technique of varying the beam size can still be used, with minor modifications. The diffusion coefficient, 2-dimensional concentration, and beam waist radius can be measured in much the same way as before. In addition, the quantity $ma_1a_2a_3Q$ will be discussed. This figure is useful later in arriving at the proper interpretations of other measurements.

Calibration of the beam waist radius A thin sample was prepared containing 10^{-6} M R6G. Autocorrelation functions were obtained at various relative positions of the beam and sample. The data are shown in figure 16. Excitation was at 488 nm. The sample was moved relative to the beam by moving the sample stage of the microscope.

Figure 16. a) Diffusion times are plotted as a function of relative displacement of the beam focus and sample. b) $\langle i \rangle^2/G(0)$ as a function of relative displacement of sample and beam. The sample contains a solution of rhodamine 6G at 10^{-6} M. Error bars represent only the precision of the computer fit of the autocorrelation functions. The solid line is the weighted least squares fit of the data to a quadratic polynomial.

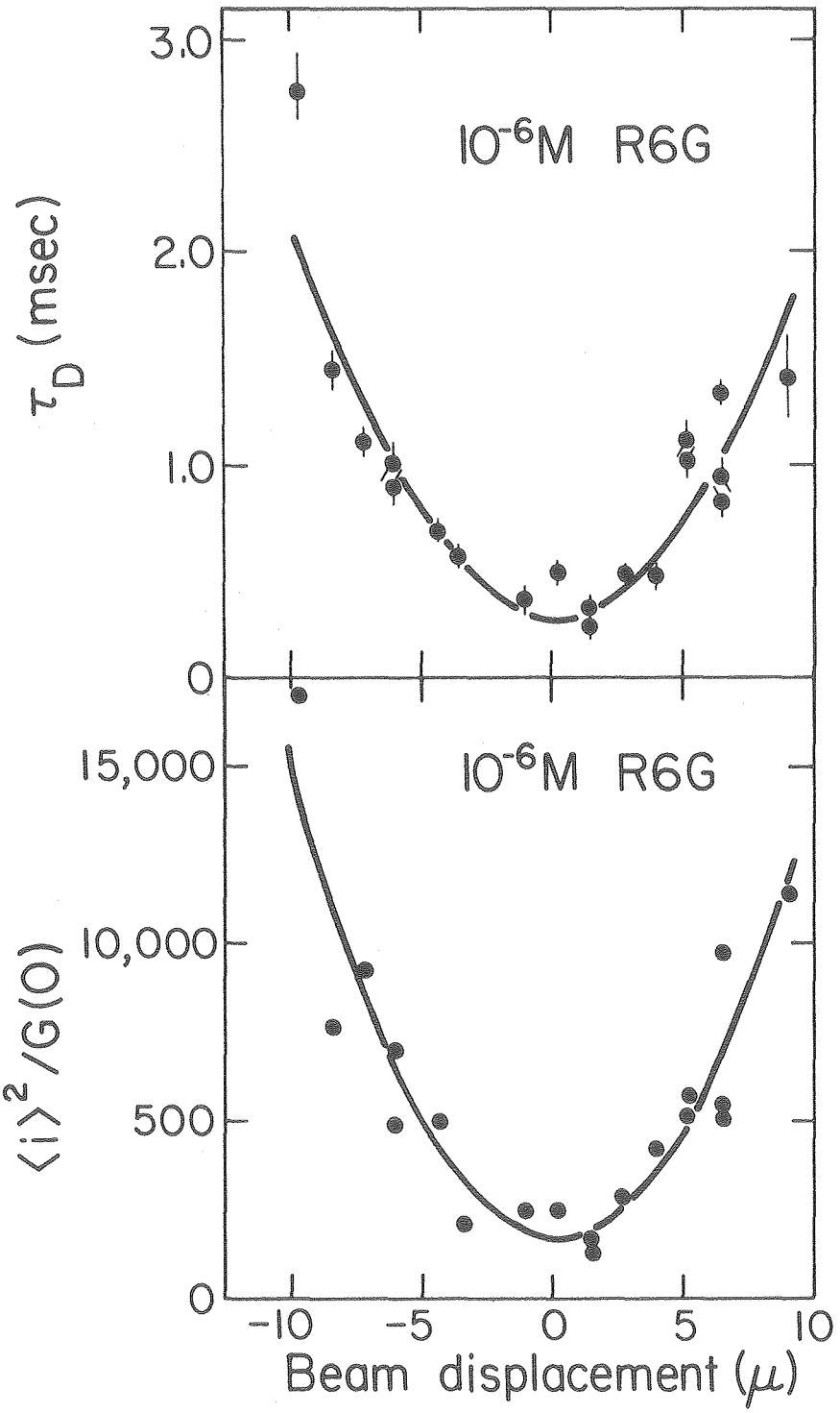
3.0
2.0
1.0
0
τ_D (msec)
10^{-6}M R6G
15,000
10,000
500
0
$\langle i \rangle^2 / G(0)$
10^{-6}M R6G
-10
-5
0
5
10
Beam displacement (μ)

XBL 799-5013

Displacement, measured in microns, was read from the fine focus knob of the microscope. The markings on the knob were checked with a micrometer for large displacements of the sample stage. They were found to be accurate to within a few percent. No determinations of w_0, D, or of the 2-dimensional concentration with this apparatus have been of comparable precision. Thus, no corrections have been made for displacements measured directly from the microscope fine focus knob.

If we assume that the beam varies with relative position in a manner similar to the behavior described before, then we may express the square of the beam radius near the waist as

$$w^2 = w_0^2\left(1 + \frac{\lambda^2 \Delta z^2}{\pi^2 w_0^4}\right)$$

Under this assumption, measurements of τ_D and $\langle i \rangle^2/G(0)$ can be used to estimate the beam waist radius, w_0, the diffusion coefficient, and the 2-dimensional concentration. From the data in figure 16, the values computed for w_0 are $(0.78 \pm 0.05)\mu$ from τ_D values, and $(0.74 \pm 0.05)\mu$ from $\langle i \rangle^2/G(0)$. The diffusion coefficient is $(5.3 \pm 0.7) \times 10^{-6}$ cm^2/sec. The 2-dimensional concentration is $(1.6 \pm 0.2) \times 10^{-6}$ $M\mu$.

In the original apparatus, the diffusion coefficient of R6G was measured to be $(5.5 \pm 0.8) cm^2/sec$. This agrees with the determination here, and is strong evidence that the assumption in the expression above is acceptable.

This experiment has been repeated many times for R6G and other dyes, using water and solvents of other viscosities. It has also been done with EtBr-DNA preparations that will be discussed below. These experiments each lead to values of w_0. Their average is

(0.88 ± 0.12) μ. The standard error of the mean is less than 0.03 μ. The amount of bleaching in the sample is inferred by comparing the known concentration of the dye to the observed number concentration. Comparisons are made difficult by variability in the sample depth. It would appear, however, that the observed number concentrations are smaller than the concentration outside the beam by a factor of 2-5.

Overall efficiency, $ma_1a_2a_3Q$ The quantity $ma_1a_2a_3Q$ has been introduced that is essentially a measure of the amount of light detected from each diffusing particle. It was not measured in the original apparatus. Such measurements would be of no use once the apparatus had been altered, because the collection optics are completely different, and comparisons would provide no important information.

Interpretation of efficiency measurements should take into account several factors. One is that rhodamine and ethidium bromide have different fluorescence emission spectra. This effects a_1, the collection efficiency, and a_2, the quantum efficiency of the photocathode. Optical filters are used to discriminate against scattered light from the excitation beam. The filter pass bands project differently on the two fluorescence emission bands of the dyes. Similarly, photocathode quantum efficiency will differ for the two dyes.

Another point is that data obtained with excitation at 488 nm. should be handled differently from data obtained with excitation at 514.5 nm. The beam monitor responds differently to blue and green beams, with the same photon flux. For excitation at 488 nm, it was shown that the overall efficiency could be expressed as

$$ma_1a_2a_3Q = \frac{6.7 \times 10^{-3}\ w^2}{\frac{\langle i\rangle^2}{G(0)}\ r\ \varepsilon} \quad \frac{\text{coulombs}}{\text{M cm. } \Omega\ \mu^2} \cdot$$

where w is the beam radius in microns, ε is the decadic extinction coefficient, measured in $M^{-1}\ cm^{-1}$, $\langle i\rangle^2/G(0)$ is the number of diffusing particles in the beam, and r is the gain of the amplifiers for the photomultiplier, measured in ohms.

Measurements have been made of $ma_1a_2a_3Q$ for R6G in several experiments. Their weighted average is $(1.03 \pm 0.10) \times 10^{-17}$ coul. In the experiment shown in figure 16, $ma_1a_2a_3Q$ is 1.3×10^{-17} coul. Rhodamine 6G has a quantum efficiency for fluorescence of one. If we assume that m, the number of chromophores per diffusing particle, is also one, then $a_1a_2a_3 = (1.03 \pm 0\ 10) \times 10^{-17}$ coul. for R6G. This should be true for excitation at 488 nm. and 514.5 nm.

Similar measurements using R6G have been made with excitation at 514.5 nm. They indicate that the overall efficiency can be written

$$ma_1a_2a_3Q = \frac{2.9 \times 10^{-3}\ w^2}{\frac{\langle i\rangle^2}{G(0)}\ r\ \varepsilon} \quad \frac{\text{coulombs}}{\text{M cm. } \Omega\ \mu^2} \cdot$$

The numerical coefficient is different from the previous one because the responce of the beam monitor depends on the wavelength of the exciting light. The spectral characteristics of the beam monitor are not available, and were not determined.

Results for Calf Thymus DNA and EtBr

The binding of EtBr to DNA has been studied in great detail, and is discussed in depth elsewhere. Fluctuation techniques have been used to consider EtBr binding,[1,2] and results reported have been consistent with results obtained using steady state absorbance and fluorescence techniques. The results of fluctuation experiments deal with fluctuations arising from the diffusion of dye molecules which are slowed by repeated binding to and release from binding sites. Thus, only $G_+(\tau)$ and $G_-(\tau)$ terms were considered. To make such measurements, it was arranged that a considerable fraction of the dye molecules be unbound. Very low DNA and dye concentrations were used. The reversible binding is described by a simple model.

$$A + B \underset{E}{\rightarrow} C$$

where A and B represent free DNA binding sites and free dye, respectively. Bound dye is represented by C. In the steady state, a binding constant is defined, and denoted K.

$$K = \frac{[C]}{[A][B]}$$

The conditions of low dye and DNA concentrations have the effect of driving down [C]/[B], even in the presence of excess DNA. By balancing total dye and DNA concentrations, while keeping them both low, the ratio of bound to free dye can be kept close to one. This makes the apparent diffusion time decrease, since much of the time, dye molecules are free to diffuse quickly. It also has the effect of separating the time scales of $G_+(\tau)$ and $G_-(\tau)$ from that of $G_0(\tau)$.

The complementary experiment is described, here. Relatively high DNA concentrations are used, resulting in the binding of essentially

all the dye. Most of the correlated photocurrent fluctuations will be due to diffusion of heavily stained DNA molecules. $G_0(\tau)$ will dominate the observed autocorrelation function.

The useful information to be derived from such measurements includes estimates of DNA molecular size from both $\langle i \rangle^2/G(0)$ and τ_+. Also, the measurement of $ma_1a_2a_3Q$ for heavily stained DNA molecules will be very useful later, in distinguishing $G_0(\tau)$ from $G_+(\tau)$ in samples with uncertain properties.

Repeating these experiments with low DNA concentrations in an effort to observe the $G_+(\tau)$ term was never attempted. Consequently, no value of $ma_1a_2a_3Q$ was obtained for individual dye molecule diffusion. It is likely that the measurement would be rather difficult. To make the measurement, [C]/[B] should be kept small, so that τ_{DNA} will be much longer than τ_+. Also, the number of chromophores per DNA molecule should be small, so that $G_0(\tau)$ does not dominate $G_+(\tau)$ in signal to noise. These conditions lead to very low DNA concentrations and even lower dye concentrations. Fluorescence detection then becomes a problem.

Detection was less difficult in the experiments described in reference 2, where a much larger beam was used, more molecules were observed, and considerably more efficient collection optics were possible. Values of $ma_1a_2a_3Q$ are geometry dependent. Measurements must be done with the same arrangement if they are to be compared. Thus it is pointless to alter the apparatus to measure $ma_1a_2a_3Q$ in this way.

It might still be possible to observe the $G_+(\tau)$ term, if the DNA molecules could be immobilized. Agarose and other gels are sometimes

used to immobilize macromolecules. In such a preparation, the $G_0(\tau)$ term would be absent. Small molecules could diffuse freely, for the most part, and $G_+(\tau)$ should be observed. Preliminary experiments along these lines were performed. They involved SV-40 DNA, and will be discussed with other data involving SV-40 DNA.

Preparation of the Sample. Calf thymus DNA,[3] obtained from Cal Biochem was prepared in a solution of 10 mM Tris buffer and 1 mM EDTA at pH 7.9. Such buffers are commonly used for DNA solutions, and are known to stabilize DNA. Tris is an abbreviation for Tris-hydroxymethyl aminomethane. Histone amino groups are believed to be involved in histone-DNA interactions. It is possible that the amino group in Tris buffer stabilizes DNA in a similar fashion.

The concentration of DNA base pairs was 2×10^{-4} M, assuming an average molecular weight of 670 daltons/base pair. EtBr concentration was 1×10^{-4} M. The sample taken for study had a volume of 20 µl. It was placed between a microscope slide and a cover slip having an area of 4.84 cm^2. Thus, the sample depth was approximately 40 µ. The edges of the sample were sealed with wax to retard evaporation of the solution. Excitation was at 488 nm.

It was found that thinner samples were unsuitable; data were not reproducible and were generally uninterpretable. It is believed that surface effects interfered with free diffusion in thin samples, either by imposing local ordering in the solvent, or by creating a gel from the DNA. Similar effects were seen in samples containing only Rhodamine 6G in water. R6G samples were kept at least 10 µ thick to avoid this problem. DNA samples had to be made somewhat deeper.

Results for Calf Thymus DNA Binding with EtBr. Measurements were made at several positions of the beam relative to the sample. Values of τ and $\langle i \rangle^2/G(0)$ for various beam positions are shown in figure 17. From the data in figure 17a, estimates are made of the beam waist radius, w_0, and the diffusion coefficient, D_{DNA}. From the data in figure 17b, estimates are made of w_0 and the 2-dimensional concentration, CL. Some of these results, and similar values from other experiments are summarized in table II.

Beam waist radius. The beam waist radius derived from $\langle i \rangle^2/G(0)$ is (1.1 ± 0.2) μ. The value derived from diffusion times is (1.3 ± 0.2) μ. They are both higher than the values seen for R6G, but this sample is many times thicker than R6G samples. Blurring of the focal spot by thicker samples would have an effect of about this amount. An exact calculation of this effect is possible, starting from the expression for $G(\tau)$ in terms of a three dimensional Fourier transform. The illuminating intensity, I(r), may be allowed to vary along the direction of propagation. The computation is non-trivial, however, because the limits of integration are different for each position of the beam focus relative to the sample.

Diffusion coefficient. From the behavior of τ_0 as a function of beam position, the diffusion coefficient is estimated to be (2.5 ± 0.2) X 10^{-8} cm^2/sec. One might try to determine the molecular weight from the diffusion coefficient. For large spherical molecules, the diffusion coefficient can be expressed as

$$D = \frac{kT}{6\pi\eta a}$$

where k is Boltzmann's constant, T is the absolute temperature, η is the viscosity, and a is the hydrodynamic radius. One may express the

Figure 17 a) Diffusion times as a function of relative displacement of sample and beam. b) $\langle i \rangle^2/G(0)$ as a function of relative displacement of sample and beam. Sample is a solution of EtBr and calf thymus DNA.

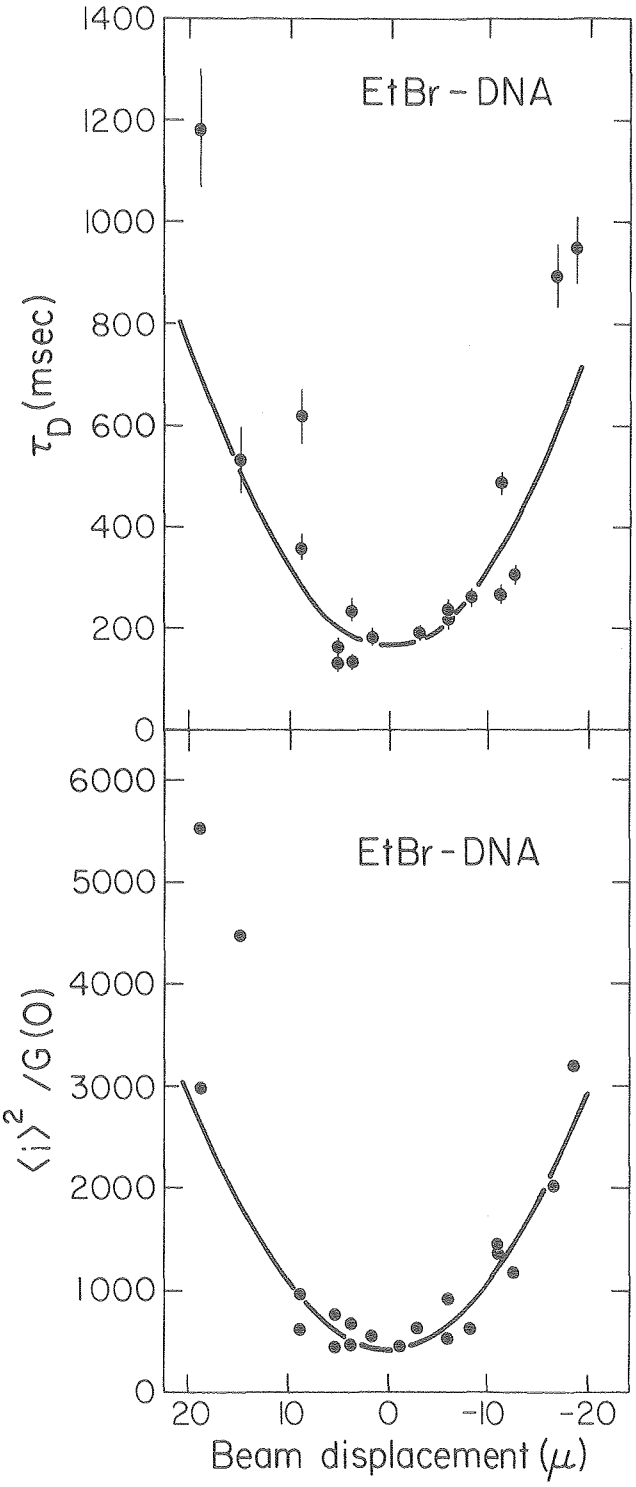
EtBr - DNA
τ_D (msec)
1400
1200
1000
800
600
400
200
0
EtBr - DNA
$\langle i \rangle^2 / G(0)$
6000
5000
4000
3000
2000
1000
0
20
10
0
-10
-20
Beam displacement (μ)

XBL 799-5014

TABLE II

DNA PREPARATION	KNOWN BASE PAIR CONC. (mM)	EtBr CONC. (mM)	EXPECTED NUMBER CONC. (nM)	OBSERVED NUMBER CONC. (nM)	EXPECTED DNA MOL. WT. (10^6 dalton)	INFERRED DNA MOL. WT. (10^6 dalton)	EtBr per OBSERVED DIFFUSER	APPARENT NUMBER OF DYE/DNA	DIFFUSION COEF. (cm^2/sec)
CALF THYMUS DNA	0.2	0.1	13	6	10	22	6000	1300	2.5×10^{-8}
SV-40 DNA	0.07	0.03	13.5	11	3.5	4.3	2100	500	1.5×10^{-8}
SV-40 DNA IN AGAROSE GEL	0.15	0.001	1000	380	———	———	———	2-3	1.3×10^{-8}
SV-40 DNA IN AGAROSE GEL	0.15	0.001	1000	450	———	———	———	3-4	1.5×10^{-8}
CALF THYMUS NUCLEOHISTONE PARTICLES	0.063	0.01	4.3	2.1	10	21	4800	130	3.5×10^{-8}

mass of a spherical molecule as the product of the density with the volume. Finally, one arrives at an expression for the molecular weight in terms of the diffusion coefficient.

$$MW \quad \frac{4\pi\rho}{3} \frac{(kT)^3}{216\ \pi^3\eta^3\ D^3} .$$

If we take the mass density, ρ, to be 1,0 gm/cm^3, the viscosity, η, to be 0.01 gm/cm-sec, the temperature as 300 K, and the diffusion coefficient to be 2.5 X 10^{-8} cm^2/sec, then the hydrodynamic radius is computed to be about 0.09 μ. The corresponding molecular weight is 2 X 10^9 daltons.

The molecular weight of purified calf thymus DNA is about 10^7 daltons. In fact, it is made up of molecules averaging about 10^7 daltons, but the distribution of molecular size may extend half an order of magnitude in both directions. Variations from one sample to the next are observed. Nevertheless, the diffusion coefficient leads to a molecular weight which is a generous overestimate. Several factors account for this. The density won't be 1.0 gm/cm^3. DNA molecules are more or less globular, but fairly loosely packed. The hydrodynamic volume will contain more mass than is attributable to the molecule. Also, the viscosity will be greater than the viscosity of water. DNA solutions are characteristically viscous. Preparations with such high surface to volume ratios as this one can be expected to be even more viscous. These factors both lead to overestimates of the molecular weight. Since the cube of the viscosity appears in the expression for the molecular weight, the effect of its variability should be considerable.

Two-dimensional concentration. The behavior of the 2-dimensional

concentration as a function of beam position leads to a value of $(1.8 \pm 0.2) \times 10^{-7}$ Mμ for the 2-dimensional concentration, CL. If the sample were 40 μ deep, then the 3-dimensional concentration of diffusing molecules would be about 5×10^{-9} M. The concentration of base pairs is known to be 2×10^{-4} M, so there would be about 4×10^{4} base pairs per diffusing molecule. Each base pair weighs 670 daltons, on the average, so the weight of the diffusing molecule would be almost 3×10^{7} daltons. This is almost two orders of magnitude below the estimate from the diffusion coefficient.

The molecular weight inferred from $\langle i \rangle^2/G(0)$ is still an overestimate by roughly a factor of three. Part but not all of the difference could lie with the sample depth, which was observed optically to be approximately 20 μ deep where measurements were made, instead of 40 μ. If the sample depth were 20 μ instead of 40 μ, it would have the effect of reducing the estimate of the molecular weight by a factor of two. Another reason for an overestimate is correlation between DNA molecules. The DNA concentration is relatively high in these preparations, and are expected to be viscous. Thus, diffusion of neighboring molecules could be correlated, and the apparent molecular weight would be increased.

A third explanation for overestimates in the molecular weight in non-homogeneous samples is that G(0) is weighted in favor of heavy molecules which would bind more dye. They would contribute disproportionately, making it appear that larger molecules were in the beam. This effect is discussed in one of the following sections. It is not expected to be appreciable unless the distribution of molecular weights is skewed toward large molecules.

In view of these possibilities, and given the uncertainty in the expected molecular weight of calf thymus DNA, one can say that the observed figure differs only modestly from expectations. On the other hand, modest agreement may be the most that can be expected for non-homogeneous samples when the sample depth and viscosity are not accurately controlled.

Efficiency, $ma_1a_2a_3Q$. The overall conversion of incident light into detected photons can be compared to the number of counted diffusing molecules. The quantity $ma_1a_2a_3Q$ includes detector efficiency in the factors a_1, a_2, and a_3. The quantum efficiency for fluorescence is Q. The relative efficiency of light collection for the average diffusing molecule is represented by the factor m. In this experiment, $ma_1a_2a_3Q$ is measured to be 4×10^{-15} coul. This value is very high compared to Rhodamine 6G, for instance. For R6G, $a_1a_2a_3$ was found to be about 1.0×10^{-17} coul. The difference in $a_1a_2a_3$ for the two dyes can be predicted using observed transmission spectra of the optical filters and the spectral response of the photocathode as stated by the manufacturer. Such a prediction should be regarded as preliminary, but it can be useful on those terms. Based on that information, it is expected that $a_1a_2a_3$ would be about 1.6×10^{-17} coul. for EtBr fluorescence. The emission spectra of free and bound EtBr differ slightly. The values of $a_1a_2a_3$ for bound and free EtBr would be within a few percent of each other.

The quantum efficiency for fluorescence of EtBr bound to DNA is about 0.2. Thus $a_1a_2a_3Q$ should be around 3×10^{-18} coul. for bound EtBr. By way of comparison, $ma_1a_2a_3Q$ is measured in cell nuclei to be about 2.6×10^{-18} coul.

The point is, that the figure of 4×10^{-15} coul. for $ma_1a_2a_3Q$ in this experiment is relatively large. That is strong evidence that $G(\tau)$ was dominated by diffusion of DNA molecules, each carrying many chromophores. The apparent number of chromophores per diffusing molecule is m. Taking $a_1a_2a_3Q$ to be about 3×10^{-18} coul., and $ma_1a_2a_3Q$ to be 4×10^{-15} coul., we find m is around 1300.

Given the total DNA and dye concentrations, and the binding constant, K, the ratio of bound to free dye concentrations should be about 450; essentially all the dye is bound. The concentration of diffusers was determined to be about 5×10^{-9} M. The concentration of dye was 1×10^{-4} M, so the number of dye molecules per diffuser would be 2×10^4. This is to be compared with 1300, the figure computed for m. Now, m is not to be taken literally as the number of chromophores per diffuser. It is the apparent number of chromophores. Interactions between bound dye molecules will lower quantum efficiency for fluorescence. Thus, m is a lower bound on the actual number of chromophores per molecule. The effect of bleaching is also important. The prediction using binding properties ignores bleaching. The actual number of chromophores per diffuser will be reduced by bleaching. Again, the effect is to make m less than the predicted value.

The matter of the disagreement between m and the predicted value is not settled by these data. After reviewing other experiments it will be raised again. A complete resolution is unlikely, however, because the magnitude of bleaching is never directly measured. At best, qualitative comparisons or rough quantitative claims can be made.

Nevertheless, it is clear that m is much greater than one. That is to say, the data refer to the diffusion of DNA molecules, described by the $G_0(\tau)$ term. To that extent, the computation of $ma_1a_2a_3Q$ has been helpful.

References

1. E. Elson, and D. Magde, Biopolymers, 13, 1, 1974.

2. D. Magde, E. Elson, and W. Webb, Biopolymers, 13, 29, 1974.

3. Calf thymus DNA is widely used in research. Its popularity is attributed to several factors. Calf thymus is a rapidly proliferating tissue, having a relatively high DNA content. It is suggested by some people that it is not tasty as food, even to dogs, making it readily available for use in research.

Results for SV-40 DNA and EtBr

Certain viruses contain DNA that is closed and twisted tightly in coils. One such virus is SV-40. It infects monkeys, and the code SV stands for simian virus. Versions other than 40 exist. SV-40 DNA has been studied intensively. It is known to contain 5200 base pairs, and the base sequence is known. Since SV-40 DNA is closed and twisted, it is fairly compact. If one strand of DNA is cut or nicked, the molecule unwinds, becoming less compact. It remains closed. A double nick breaks the circle, making a linear molecule. SV-40 DNA with no nicks is called Form I. SV-40 DNA with single nicks is called Form II. Linear SV-40 DNA is Form III.

Preparation of the sample. Purified Form II SV-40 DNA in solution was obtained from Stephen Treon. EtBr was added, making final concentrations of 3×10^{-5} M EtBr and 47 μg/ml DNA. The mass concentration was determined from the absorption spectrum of the solution. A sample was prepared from 10 μl, and would have an average depth of 21 μ. Excitation was at 488 nm.

Diffusion time and 2-dimensional concentration. Results for several experiments involving SV-40 DNA are summarized in table II. Diffusion times for SV-40 DNA were similar to times measured for calf thymus DNA. The diffusion coefficient was inferred by measuring diffusion times for different relative positions of the beam focal spot and sample. The value found was $(1.5 \pm 0.7) \times 10^{-8}$ cm^2/sec. The uncertainty associated with the diffusion coefficient is considerable because the data were somewhat scattered. Corresponding to this diffusion coefficient is a hydrodynamic radius of about 0.15 μ, assuming a viscosity close to that of water. SV-40 DNA has a

circumference of about 1.5 μ, when laid out in a circle. In solution, of course, it is relaxed into a loose jumble. Thus the figure for the hydrodynamic radius of 0.15 μ is not unreasonable. Again, interpretation of such figures should take into account the fact that the viscosity of the medium has not been measured directly.

The measured value of $\langle i \rangle^2/G(0)$ can be combined with the mass concentration to make an estimate of the molecular weight. Making allowance for blurring of the focal spot, the computed molecular weight is 4.3×10^6 daltons.

SV-40 DNA has 5200 base pairs, each weighing 670 daltons, on the average. Thus, SV-40 DNA molecules weigh about 3.5×10^6 daltons. The discrepancy between the known and measured molecular weights is about 20%. The most significant sources of uncertainty in the measured value are sample depth, $\langle i \rangle^2/G(0)$, the measured mass density, and the beam waist radius. The estimated uncertainties of each of these is 10% or greater. Considering these factors, the agreement between computed and expected molecular weights is well within experimental error.

Different DNA molecules bind different numbers of EtBr molecules. The effect of this on G(0) should be made clear. SV-40 DNA molecules are all the same size, as opposed to calf thymus DNA molecules, which are widely distributed. The variability in the number of bound chromophores can be described in this case by Poisson statistics. The effect of such variations on G(0) can be computed, using a result stated earlier.

$$\frac{G(0)}{\langle i\rangle^2} = \frac{\sum_i (\varepsilon_i Q_i)^2 C_i}{\pi w^2 L \left(\sum_i \varepsilon_i Q_i C_i\right)^2} \qquad (1)$$

where the summation runs over the molecules of different optical properties, and C_i is the average concentration of molecules having decadic extinction coefficient ε_i and quantum efficiency for fluorescence of Q_i. We may suppose there are N binding sites on a molecule, and that n sites are occupied. If binding obeys Poisson statistics, then the probability of finding n occuppied sites is

$$P_\lambda(n) = \frac{e^{-\lambda} \lambda^n}{n!} \qquad (2)$$

On the average, λ sites are occuppied. In the present model, we may take C_n to be the average concentration of molecules bearing n chromophores. Then $C_n = C\, P_\lambda(n)$, where C is the total concentration of DNA molecules. Also, we may take $\varepsilon_n = n\varepsilon$, where ε is the decadic extinction coefficient of bound EtBr. $Q_n = Q$ for all molecules. Equation 1 becomes

$$\frac{G(0)}{\langle i\rangle^2} = \frac{\sum_n n^2 P_\lambda(n)}{\pi w^2 LC\left(\sum_n n P_\lambda(n)\right)^2} = \frac{\lambda + \lambda^2}{\lambda^2} \frac{1}{\pi w^2 LC} .$$

Thus, when $\lambda >> 1$, $\langle i\rangle^2/G(0)$ measures the number of large molecules. No numerical correction factor is present, due to variations in the number of bound chromophores. When $\lambda << 1$, $\langle i\rangle^2/G(0)$ measures only the fraction of large molecules that bear an EtBr molecule.

Efficiency $ma_1a_2a_3Q$. The computed value for $ma_1a_2a_3Q$ for the sample of SV-40 DNA and EtBr is 1.5×10^{-15} coul. If we again take 3×10^{-18} coul. as a rough figure for $a_1a_2a_2Q$, then the apparent number of chromophores per diffuser would be about 500. We can compute the

expected number of chromophores per SV-40 DNA molecule from the binding constant, and the known total dye and DNA concentrations.

In this case, there is an excess of dye, so all the available binding sites should be occuppied. The expected number of bound dye molecules would then be about 2100. This is about four times greater than m, the apparent number of bound chromophores calculated from $ma_1a_2a_3Q$. This is comparable to the situation observed for calf thymus DNA. The reasons for the two findings are probably the same. It is likely that bleaching alone could account for the observed underestimate of the number of bound chromophores.

Use of agarose gel to immobilze SV-40 DNA. Agarose gels are used to separate or purify DNA molecules in solution. The sample can be placed at one end of an agarose column and made to pass through the gel. The migration rates through the gel will depend on molecular size, pore size in the gel, and other factors. Agarose is dissolved in boiling water. Warm agarose solution can be poured into an appropriate mold. As the agarose cools, it gels. The transition occurs between 40°C and 45°C.

Samples were prepared for fluorescence fluctuation experiments by mixing an agarose solution containing EtBr with SV-40 DNA solution at 45°C on a hot plate. A small volume of the mixture was sandwiched between a warmed microscope slide and cover slip. Sample volumes were not measured because the mixture would gel, even in warmed pipettes. Sample homogeneity is also subject to some question. Lumps seemed to form in the mixture as the solutions were combined.

Final SV-40 DNA concentration was about 1.5×10^{-4} M DNA base pairs, or 3×10^{-8} M DNA molecules. Final dye concentration was

10^{-6} M, and final agarose concentration was 1% by weight. This agarose concentration is not high enough to completely immobilize DNA motion in a column, but it was felt that higher concentrations of agarose might make them too difficult to work with in very thin samples. Excitation was at 514.5 nm.

Diffusion times and number concentrations. Diffusion times were comparable to times measured for calf thymus and SV-40 DNA in solution. They correspond in these measurements to diffusion coefficients of the order of 10^{-8} cm^2/sec. Such diffusion times are interpreted in terms of EtBr molecules slowed by binding to DNA. Two preparations are discussed here, giving similar results. The diffusion coefficients are close to the one measured for SV-40 DNA in solution. Based on binding properties, EtBr molecules should have a diffusion coefficient of roughly 3 X 10^{-8} $cm^2/sec.$, in water, or lower in a more viscous medium.

Sample depths were inferred from strong reflections at the glass-water interfaces. Using the sample depths and values of $\langle i \rangle^2/G(0)$, the number concentration was computed to be about 4 X 10^{-7} M in both cases. The SV-40 DNA concentration is expected to be about 3 X 10^{-8} M. The bound EtBr concentration was expected to be 10^{-6} M. It would seem, then, that $G_+(\tau)$ was observed.

Efficiency, $ma_1a_2a_3Q$. Working from the known binding properties, and average concentrations of reactants, it is expected that about 75 EtBr molecules would bind to each DNA molecule in the sample. The values computed for m, the apparent number of bound chromophores, fall in the range of 2-4. Such values for m suggest that $G_+(\tau)$ was observed, rather than $G_0(\tau)$. It is possible, of course, that both

$G_+(\tau)$ and $G_0(\tau)$ contributed significantly to the overall autocorrelation function.

These data should be regarded as preliminary. The samples were probably not homogeneous, the viscosity was not measured, the nature of the gel was not well known, and the background light intensity was uncertain. Still, these data suggest that, with slightly greater skill in preparing samples, EtBr diffusion can be distinguished from DNA motion.

Results Nucleohistones and EtBr

Calf thymus DNA and histones from calf thymus chromatin are available in purified form from commercial sources. Under certain conditions, the histones can be made to recombine with DNA, making nucleohistone particles very similar to the original chromatin.

Calf thymus histones, not including H1, and calf thymus DNA, obtained from Cal Biochem were made to recombine, forming nucleohistone particles. This was done by decreasing the salt concentration slowly, thereby annealing the histones to the DNA. The concentration of DNA in the final solution was determined spectrophotometrically to be close to 7×10^{-5} M base pairs. EtBr was introduced into the solution making a final EtBr concentration of 10^{-5} M. Samples were prepared from 5 µl of the final solution, and would have an average depth of about 10 µ.

Diffusion times and concentrations. Results for nucleohistone particles are included in table II. Observations were made at several positions of the beam relative to the sample. Consequently, the beam waist radius was measured twice. It was found to be $(0.90 \pm 0.08)\mu$. The diffusion coefficient was about 3.5×10^{-8} $cm^2/sec.$ which is comparable to, but slightly larger than the measured diffusion coefficients for calf thymus DNA and SV-40 DNA.

The concentration of DNA measured spectrophotometrically corresponded to about half the DNA used as starting material. The concentration derived from $\langle i \rangle^2/G(0)$ corresponds to half the spectrophotometric figure, assuming DNA molecular weights averaging 10^7 daltons.

The observed concentration is not very far from expectations.

One reason for it being greater than expected by a factor of two is that the process of annealing the histones to the DNA involves considerable mixing of the solution. The DNA segments are delicate, and are known to break into fragments under such conditions. Again, another source of uncertainty is the sample depth, which may vary by several microns from place to place in the sample.

Efficiency, $ma_1a_2a_3aQ$. If the DNA were present without histones, one would expect essentially all of the EtBr to be bound, given the excess of DNA. Then there would be roughly 2000 bound chromophores per observed diffusing molecule. In fact, the apparent number of chromophores, inferred from $ma_1a_2a_3Q$, is roughly 130. In measurements involving DNA in the absence of histones, m underestimated the number of bound chromophores by a factor of 5-8. Chromatin is known to bind less dye than free DNA. The binding of dye to chromatin can be complex, as described above. Unfortunately, the uncertainties in measurements presented here are too large to justify careful quantitative comparisons. Still, the value of m obtained from these observations is consistent with the differences in binding expected between free DNA and chromatin.

Discussion of the Results for EtBr Binding to Calf Thymus and SV-40 DNA, and to Calf Thymus Nucleohistone Particles

The experiments involving EtBr and DNA were intended to give an idea of what the possibilities and limitations are of this type of experiment. The measurements themselves were not difficult. It is extremely important, however, that the samples be prepared carefully. One way of thinking about the samples is to notice that they have very large surface areas, given their volumes. It is important that surface effects be controlled. Also, very small sample volumes are used. If the samples are not homogeneous and carefully handled, then interpretation of the data will be much more difficult.

In another section, results from cell nuclei are discussed. The data collected in those experiments are relatively reproducible, and were collected relatively easily. This is evidence that some of the difficulties encountered in the experiments described here arise from sample preparation rather than from the measurement technique as applied to the problem of EtBr-DNA interactions.

It is also important to say that binding constants should not be measured in quite this way, especially if conventional alternatives are available. Neither the diffusion time, $\langle i \rangle^2/G(0)$, nor $ma_1a_2a_3Q$ gives a precise estimate of binding in these data. To construct a Scatchard plot, for instance, requires considerable accuracy.

There are important positive conclusions that can be drawn from these data, as well. First, the diffusion coefficients are similar, at 1.5 to 3.5 $X10^{-8}$ cm^2/sec. Secondly, estimates of molecular

weight show a surprisingly close correspondence to expectations. It has never been claimed that fluctuation correlation spectroscopy experiments of this type were suitable for precise molecular weight determinations. Still, the computed estimates fell within reasonable limits, given the experimental uncertainties. Often, the estimated number concentrations were somewhat less than the concentration in the bulk sample. Surface effects are the most likely explanation for the discrepancy. Sample depth should also be closely watched when attempting to make accurate determinations of number concentration.

The interpretation of $ma_1a_2a_3Q$ is becoming more definite. In every measurement, $ma_1a_2a_3Q$ is smaller than a priori expectations. This is not unreasonable, given the effects of photodegradation of the dye. In any event, the apparent number of chromophores per diffuser is much greater than one, in many of the measurements, indicating that the observed diffusion involves large DNA molecules, rather than individual EtBr molecules.

Results for Whole Cells

It was stated before that there have been reports fo EtBr being used to stain living cells. Dyes with the ability to do this are called vital stains. Many experiments were undertaken, that were intended to exploit this property. For the most part, they were only partially successful, yielding qualitative results, at best. In a few cases, more specific data could be obtained.

Preparation of samples. The cell line used for these observations is derived from human lung tissue. It is denoted IMR-90. These cells are said to age, in the sense that they can pass through only 40 or 50 population doublings. Beyond that point, they do not grow well in culture. Experiments were done with cells between passage 18 and 35. Cells were grown in culture dishes containing circular microscope cover slips. When the cells are introduced to the dish, they settle on the cover slips, and attach themselves to the glass. They were grown in a CO_2 rich atmosphere for several days, until they covered the dish in a monolayer. Once the cells became confluent, one of the cover slips was removed for study. It was washed in golden Eagles medium containing EtBr. This medium is faintly brown or yellow in appearance. It can be used to sustain cells for a short time in standard atmosphere.

The washed cover slip was inverted, and placed on a microscope slide. The slide has a small depression filled with medium containing EtBr. The cover slip spans the depression, so that the cells are suspended in medium. Excess medium is removed with a tissue held near the edge of the cover slip. Warm paraffin is then used to seal the cover slip to the microscope slide.

General observations. Several hundred cells were examined. In some populations, none of the cells took up dye. In other populations, most of the cells took up dye. In a few cases, EtBr was taken up by some but not all of the cells. At high dye concentrations, some cells were very strongly stained, and were visible even when illuminated indirectly, by scattered laser light. All stained cells concentrated dye in the nucleus, although some dye appeared to be present in the cytoplasm. Uptake took place quickly, after introduction of dye into the medium. Uptake was never observed visually.

At high dye concentrations (10^{-5} - 10^{-4} M), it was possible to observe areas in the nucleus where dye was destroyed by illumination. In such cases, the darkened region would remain dark for at least 10-15 minutes. This suggests that destroyed dye molecules remained in the binding sites and were not invovled in diffusion.

The bleaching process was not intensively studied. Measurements of fluorescence intensity suggest that at least 80% of the dye could be bleached in a few minutes, but that greater losses were very gradual. If the sample were left in the dark for a few minutes, then some recovery occured. When light and dark periods of a minute or two alternated, the greatest loss occured in the initial light period. Much of that loss never recovered. During subsequent light periods, fluorescence intensity would also drop, but recovery during dark periods was nearly complete.

The presence of EtBr in the nucleus is indicated by intense fluorescence, compared to other parts of the cell. Of the cells observed to contain dye, only a small fraction could be used to collect autocorrelation functions. In many cases, the only

correlations observed were those associated with the electronic filters. At least some of the dye must have been moving in and out of the beam. Stationary molecules would soon be destroyed, and fluorescence would disappear. The failure to detect correlations from diffusing molecules can be attributed to other possibilities. If the kinetic behavior of the dye were much faster or slower than the scale of observation, then the autocorrelation function would appear to be flat, as observed. If the number of fluorescent molecules in the beam were extremely large, say, more than 10^6, then the amplitude of the autocorrelation function would be so small as to make the signal undetectable. Similarly, if background light were significant, the desired signal would be obscured.

In a few experiments, autocorrelation functions typical of diffusion would be observed for a short time. These signals would gradually disappear over a period of 10-20 minutes, and never return. The specific cause of these problems was never determined.

Results. A small number of cells was found that were suitable for collecting data. In each case, EtBr concentration was 10^{-6} M. The results are summarized in table III. Diffusion times were measured that would correspond to a diffusion coefficient of 1-3 X 10^{-8} cm^2/sec. $\langle i \rangle^2/G(0)$ showed considerable variation, but was generally in the range corresponding to a concentration of 5-50 X 10^{-6} M. Background fluorescence was not taken into account in computing these values of $\langle i \rangle^2/G(0)$. The overall efficiency, $ma_1a_2a_3Q$ fell in the range from 1-10 X 10^{-18} coul.

One nucleus was observed for a considerable period of time. The data are shown in figures 18 and 19. All observations were made at

Table III.

PROPERTY	OBSERVED VALUE	SOURCE
Diffusion time	50 - 100 msec.	$G(\tau)$
Diffusion coefficient	1-3 X 10^{-8} cm^2/sec	τ_+ and w_o
$\langle i \rangle^2/G(0)$	10^4 - 10^5	$G(\tau)$
$ma_1a_2a_3Q$	1-10 X 10^{-18} coul	$\langle i \rangle^2/G(0)$ and instrumental settings
$(1 + K[A])n_n/n_w$	200 - 600	τ_+
K[A]	5 - 50	$\langle i \rangle^2/G(0)$ and free dye concentration

Figure 18. Apparent diffusion times, τ_+ as a function of beam position relative to the nucleus of a single IMR-90 cell. Dye concentration in the medium outside the cell was 10^{-6} M.

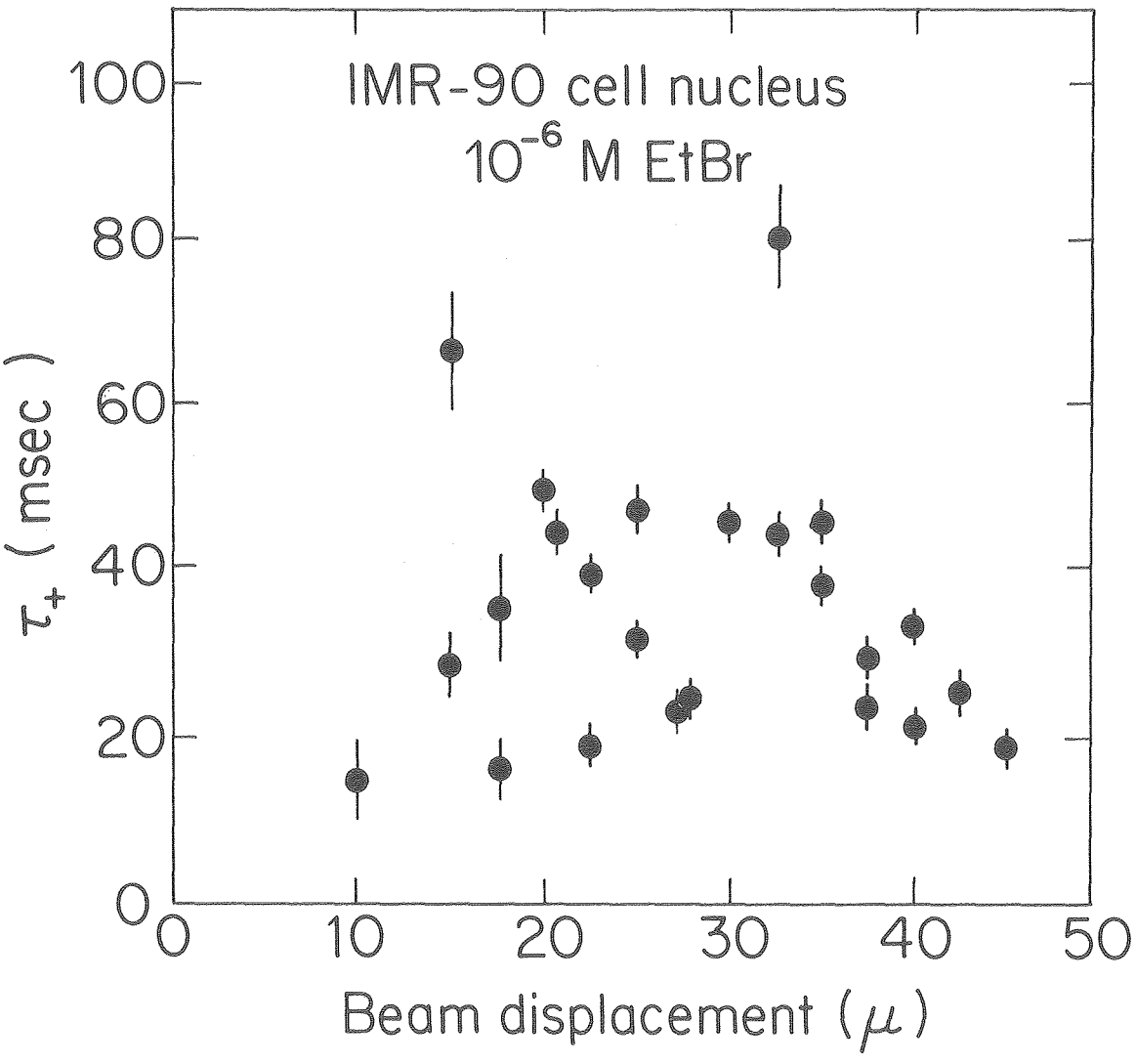

XBL 7812-13062

Figure 19. Values of $\langle i \rangle^2/G(0)$ are plotted as a function of beam position relative to the nucleus of a single IMR-90 cell. These values are derived from the same autocorrelation functions used to obtain the apparent diffusion times shown in figure 18.

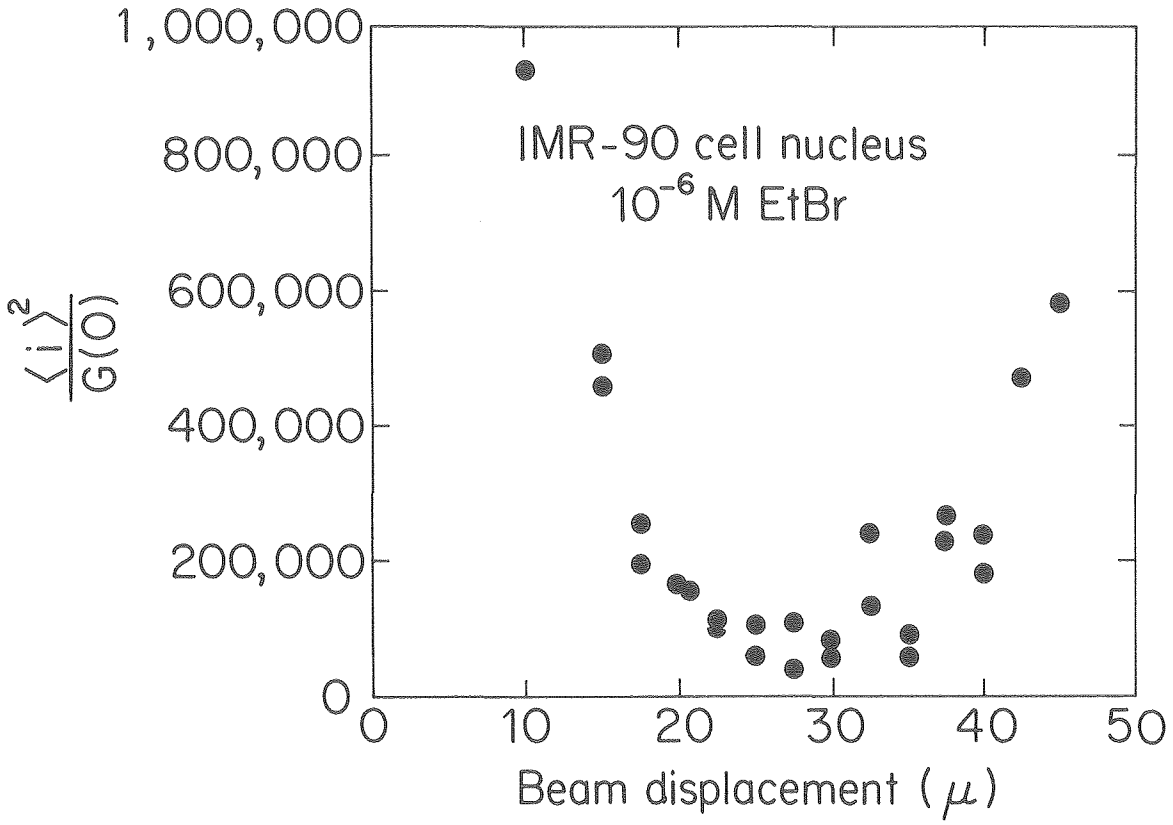

XBL 7812-13063

the same site in the nucleus. The measurements of $\langle i \rangle^2/G(0)$, shown in fig. 19, behave roughly as expected. The diffusion times, however, seem to become somewhat faster as the beam diameter is increased. It is clear that translational diffusion is not the only process involved, here. This phenomenon could not be pursued. It was fortuitous that it was observed at all, and attempts to duplicate the finding were unsuccessful.

The most likey explanation for the data in figures 18 and 19 is that a second kinetic process was involved that was independent of beam size. A possible candidate is rotational diffusion. Rotational correlation times do not depend on beam size. The autocorrelator was AC coupled in this experiment. That is, fluctuations much longer than 400 delay increments were filtered out electronically. The alleged rotational fluctuations are presumed to persist over approxiamtely 15 msec. When the beam is widened, the fast rotational fluctuations are superimposed on slow translational fluctuations. The resulting autocorrelation function appears to decay quickly. For narrow beams, the translational fluctuations contribute significantly in the time scale of the fast rotational fluctuations. The observed autocorrelation function decays more slowly, and the diffusion time is longer.

This model was used to evaluate the data, and was found to be consistent with the measurements. Other models can not be ruled out, of course, given the variability in the data. The point is, that circumstances exist under which the apparent diffusion time might behave as shown in fig. 18.

Discussion. The results of experiments involving whole cells are similar in a way to the glass of water that is half empty of half full. The measurements are not particularly precise or compelling. They strongly suggest that EtBr is not suitable as a vital stain to probe IMR-90 cells in this manner. In fact, many of the observations made in these experiments lead to the conclusion that EtBr is not readily taken up by healthy cells. This is critical in fluctuation experiments of this type because dye is constantly being lost in the beam. Fresh dye must get to the nucleus quickly from the external medium. Failure to do so may be responsible for the gradual loss of signal observed in some cases.

Another troubling aspect of these experiments is the question of why some cells take up EtBr, and others do not. It will be suggested that healthy cells exclude EtBr, while sick or damaged ones can't keep it out.

These questions call for major changes in the experimental procedure, which will be discussed in following sections.

The positive aspects of these experiments are the limited physical successes in the face of considerable biological difficulties. One particularly hopeful result is that the overall efficiency falls in the range one would expect for fluctuations arising from diffusion of EtBr molecules, slowed by binding. Finding $ma_1a_2a_3Q$ consistently in the expected range makes it possible to take more seriously the unexpected results for $\langle i\rangle^2/G(0)$ and the correlation times. We can rule out, for example, diffusion of segments of chromatin as sources of the fluctuations.

The observed correlation times and $\langle i\rangle^2/G(0)$ values can be

taken as rough estimates of τ_+ and the number of EtBr molecules. Even if other processes are involved, $G_+(\tau)$ will be a significant contributor to the computed values of τ_+ and $\langle i \rangle^2/G(0)$. Uncertainty in the values is such that only general conclusions are justified, in any event.

If we presume that the apparent diffusion constant is based on diffusion of EtBr, slowed by binding, then we may write

$$D_{app} = \frac{D_{free}}{(1 + K[A])} \frac{\eta_n}{\eta_w}$$

where D_{app} is the observed diffusion coefficient, D_{free} is the diffusion coefficient in water, η_n and η_w are the viscosities of the nucleus and water, respectively, and K[A] is the ratio of bound to free dye. Measurements of D_{app} were in the range 1-3 X 10^{-8} cm^2/sec. This corresponds to values of $(1 + K[A])\ \eta_n/\eta_w$ in the range 200-600.

A similar estimate can be made from $\langle i \rangle^2/G(0)$. The concentration of free dye should be less than or equal to 10^{-6} M. Bound dye concentration can be inferred from $\langle i \rangle^2/G(0)$ to be in the range 5-50 X 10^{-6} M. Combining these figures, K[A] is in the range 5-50.

The effect of bleaching should be to reduce the concentration of free dye. Thus, K[A] may be larger than indicated. Bleaching also reduces τ_+ and $\langle i \rangle^2/G(0)$ by comparable amounts. It would seem, then, that the viscosity of the nucleus is of the order of 10 times that of water, or less.

This claim is made tentatively, to be sure. It should be stressed that this viscosity is relevant to EtBr and not to macromolecules. Presumably, large molecules are involved in very

complex structural and hydrodynamic interactions. Consequently, one thinks of the nucleus as being very viscous. Nevertheless, in the same way small molecules can run through a gel, it may be possible for EtBr to move through the nucleus.

Results for Cell Nuclei

The limited success in collecting data from whole cells was attributed, in large part, to the inability of EtBr to pass freely through the cytoplasmic membrane. Other vital stains are known to be able to do this, but their biochemical specificity and optical properties make them less attractive than EtBr. It is possible to treat cells to make their membranes permeable to various agents. The intention of such efforts is to disrupt the cell as little as possible. A compromise of sorts was struck in the experiments described below. Cells were harvested from their dish, and the plasma membranes were totally or partially disrupted, allowing EtBr to enter the nucleus from the medium.

Nuclear membranes are very porous, compared to cytoplasmic membranes. The example is given that huge RNA molecules pass through the nuclear membrane. Actually, the nuclear membrane is not a completely ineffectual barrier. Still, experience has shown that the nuclear membrane does not prevent EtBr from passing into the nucleus.

Preparation of samples. The cell line used for these experiments is derived from green monkey kidney tissue. It is referred to as TC-7. TC-7 cells can be cultured indefinitely, as opposed to IMR-90 cells. They have relatively large nuclei, and can be infected with well characterized viruses, including SV-40. They also show a remarkable consistency in their staining of their DNA, as indicated by flow cytometry. Cells are prepared by transferring to culture dishes in fresh medium at low cell density. The cells settle to the bottom of the dish, attach themselves, and start to grow. High density cells cover the dish in a monolayer, and enter a resting state, where cell

division is greatly reduced. The cells were harvested at low density, in a state of active growth, or were allowed to grow for at least a week, when they could be harvested at high cell density. Low density is defined in these experiments as being one fourth the density of confluent cells, because confluent populations are split into quarters for transfer as low density cells. Transferred cells become synchronized, to some extent, and enter the active growth state together. Synchrony is lost after a few population doublings.

Nuclei were prepared in two ways. Washed nuclei were obtained by dissolving the cytoplasmic membranes with detergent. Using milder conditions, the nuclei could be left clinging to a microscope cover slip, with much of the cytoplasm and some of the cell membrane intact.

Washed nuclei were prepared by harvesting cells from one or two 100 mm. culture dishes with a rubber policeman or by incubating the cells for one minute at 37° C in trypsin. Trypsin digests the structures holding the cells to the dish. The cells were aspirated with TD buffer. This buffer is commonly used to suspend cells. It contains Tris and EDTA, and is similar to buffers described earlier. The cells were suspended, and agitated gently to break up clumps. A part of the suspension was taken for flow cytometry. The rest was centrifuged at 1000 rpm for 60 seconds in a JA-21 rotor. The supernatant was discarded. The pellet was resuspended in 0.2 ml. of 0.25% NP-40 detergent. The suspension was gently aspirated to prevent clumps from forming. Cell membranes dissolved immediately. The suspension was centrifuged at 1000 rpm for at least 60 seconds in a JA-21 rotor. The pellet was resuspended in 5 ml. of saline solution containing 3×10^{-8} M EtBr. The suspension was centrifuged again,

and all the saline solution was removed except approximately 0.2 ml. The nuclei were resuspended in the remaining saline solution. A 5 µl sample was placed on a microscope slide. A cover slip was placed over the drop, and sealed with warm paraffin, to retard evaporation.

In the second preparation method, six cover slips were placed in the culture dishes. Transferred cells settled on the cover slips and attached themselves after several hours. When harvested, five cover slips were treated with trypsin, and the cells were aspirated with TD buffer. They were used for flow cytometry. One cover slip was placed on a small copper screen. The screen with the cover slip was placed in a dish containing 0.1% Triton X-100, a commonly used detergent. Higher detergent concentrations were found to remove the cell membranes immediately. At 0.1% Triton X-100, the cell membranes would remain visible for a few minutes, and then would break up. Freshly transferred cells would break up in one or two minutes. Cells allowed to reach high density on the cover slip would require 2-3 minutes for the membranes to break away. The cells were viewed on the dish in a microscope. Once the membranes were disrupted, the nuclei would become clearly visible. At this point, the screen with the cover slip was removed from the detergent solution, and rinsed for 5 minutes in a dish containing saline and 3×10^{-8} M EtBr. The cover slip was then inverted, and placed on a microscope slide over a small depression containing the same saline-dye solution. Excess saline was removed with a tissue until the cover slip rested on the slide. The edges were sealed with warm paraffin.

Flow cytometry produces a histogram showing the number of cells

having particular DNA contents. The cells were fixed in 25% ethanol with 10 mM $MgCl_2$. This makes the cell membrane permeable to small molecules. It also kills the cells. The cells are treated with RNase to digest RNA. Excess propidium iodide is used to stain the DNA. It also binds to RNA. Propidium iodide fluorescence is excited, and measured from individual cells in a flow cytometer.

Observations. Isolated TC-7 nuclei appear either disc shaped or more prolate, like a rice grain. The long dimension may be 10-15 μ, and the shorter dimension may be 5-10 μ. They are never seen to move. Nucleoli, a few microns across, are sometimes present in the nucleus. They tend to fluoresce more strongly than surrounding areas. The enhanced fluorescence tends to fade after a minute or two, suggesting irreversible damage in strong binding sites. At dye concentrations of 3×10^{-8} M, fluorescence is limited to the region being illuminated directly. The beam itself occupies a small fraction of the nucleus.

In the process of isolating washed nuclei, there may be a substantial loss of material, making it difficult to locate nuclei. It is possible, therefore, that a biased selection of nuclei may have taken place. In some preparations, the optical contrast between the nucleus and the medium is very low. Finding nuclei in such preparations may be very tedious, if not impossible. Broken nuclei were never observed.

Triton washed nuclei on cover slips are seen embedded in a small mass of cytoplasm. Within the remaining cytoplasm are small bright spots that are probably points of attachment of the cell to the cover slip. The cytoplasm fluoresces strongly. This is believed

to be from RNA bound EtBr. It is not known to what extent the cytoplasm covers the side of the nucleus facing the medium. Nuclei from cells at low density have open spaces between them where background fluorescence is comparable to blank fluorescence. Nuclei from cells at high density are completely surrounded by cytoplasm, leaving few or no open spaces between them. Nuclei are never seen to move. Cytoplasm is never seen to become dislodged, and the preparation can remain suspended on the cover slip for days. Comparison of microphotographs of the cells before Triton washing with the isolated nuclei indicates that no more than a few percent of the nuclei may be lost in preparation.

Results. Histograms of data collected from nuclei are shown in figures 20, 21, 22, 23, and 24. Data in these figures and other information is summarized in table IV. Four classes of nuclei are indicated. Nuclei were prepared by lysing cells in suspension and by dissolving the outer membranes from cells attached to cover slips. The cells themselves were harvested at high cell density after growing for at least a week, (resting), or were harvested about 24 hours after transfer, at low cell density (stimulated to grow).

In the process of obtaining nuclei for fluctuation experiments, a part of each population of cells was examined in the flow cytometer. In figure 20, histograms are shown which are representative of cells corresponding to each class of nuclei examined in fluctuation experiments. Histogram a shows a distribution of DNA content per cell that is typical of cells in G_0 or G_1. The small peak corresponding to G_2 and M cells contains some counts from two cells, stuck together. The suspension of cells was filtered

Figure 20. Distributions of DNA content per cell are shown for four populations of cells. In each distribution, the peak contains 5000 counts. a) Confluent resting cells grown in culture dishes. b) Cells stimulated to grow on culture dishes by transfer in fresh medium with fetal calf serum. c) Confluent resting cells grown on cover slips. d) Cells stimulated to grow on cover slips by transfer in fresh medium with fetal calf serum. The stimulated cells in b) and d) were harvested 24 hours after transfer.

DNA Content

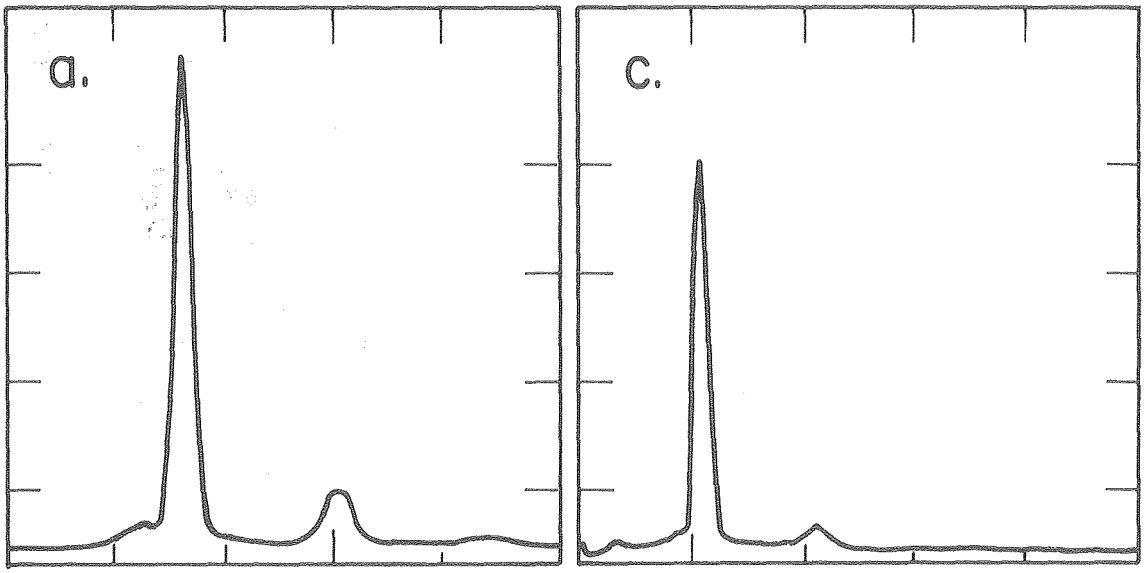

Resting cells grown on culture dish

Resting cells grown on cover slips

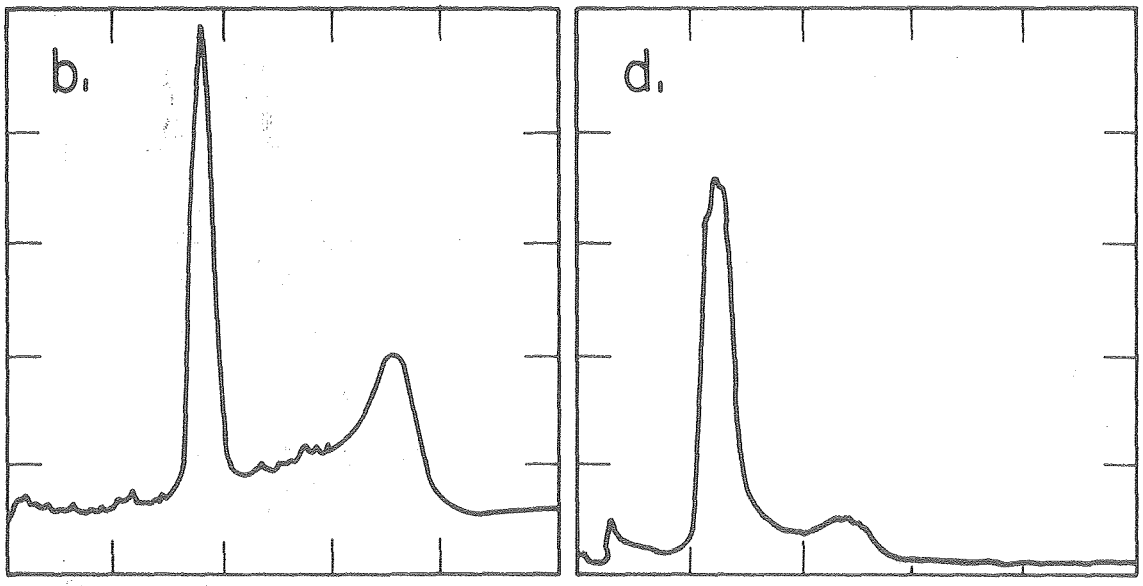

Cells on culture dish stimulated to grow

Cells on cover slips stimulated to grow

XBL 7910-5066

Figure 21. Distributions of diffusion times are plotted for the four populations of cells shown in figure 20. Each datum corresponds to one site in a nucleus. Four types of nuclei are shown. a) Washed nuclei from resting cells harvested from culture dishes. b) Washed nuclei from cells stimulated to grow, harvested from culture dishes 24 hours after transfer. c) Unwashed nuclei from resting cells grown on cover slips. d) Unwashed nuclei from cells stimulated to grow on cover slips, harvested 24 hours after transfer.

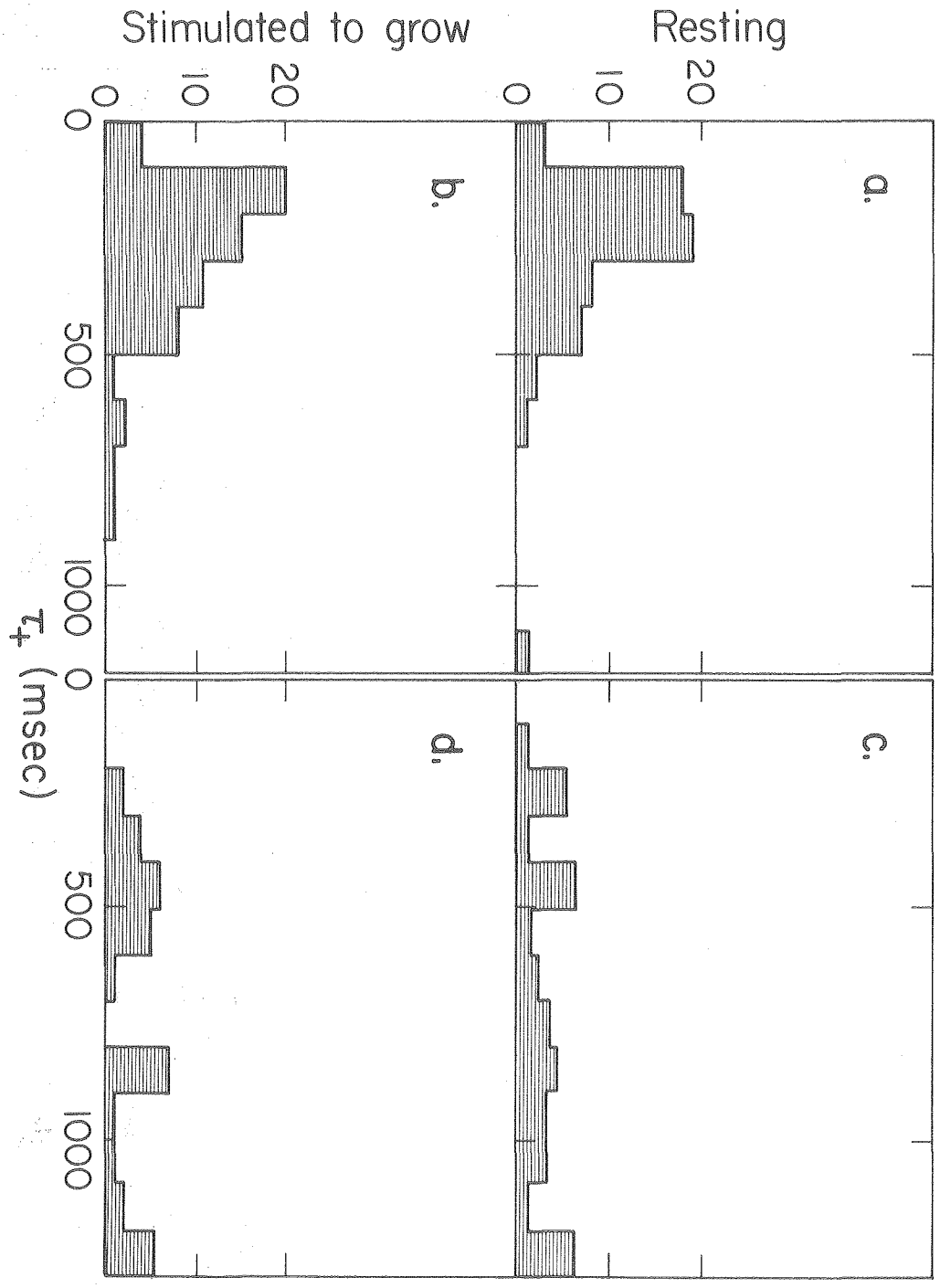

XBL 7910-5063

Figure 22. Distributions of $\langle i \rangle^2/G(0)$ measured in cell nuclei are plotted for the four populations of cells shown in figure 20. Data are obtained simultaneously with the diffusion times in figure 21. Thus, the four classes of nuclei involved are identical to the ones in figure 21.

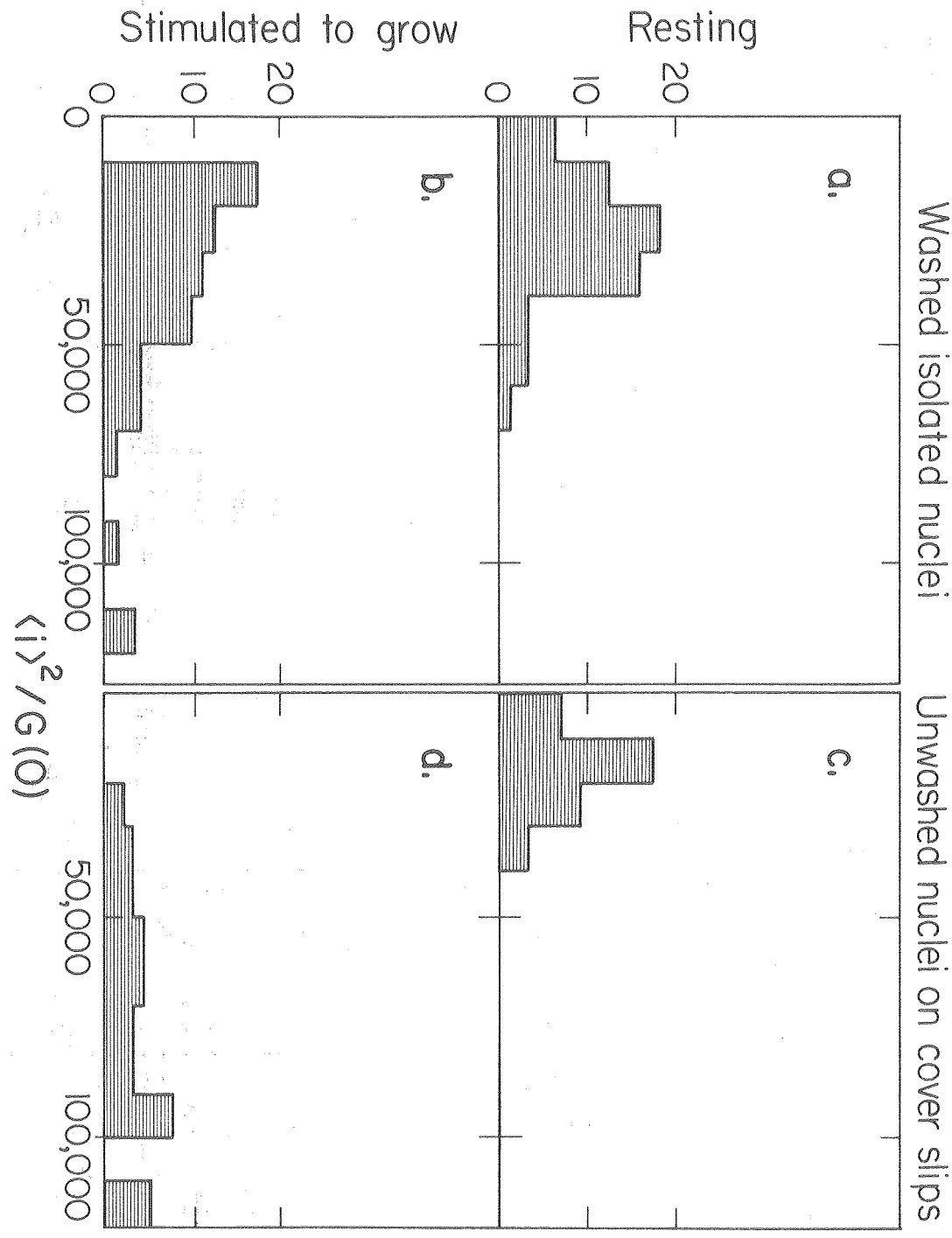

XBL 7910-5064

Figure 23. Distributions of the overall detection efficiency, $ma_1a_2a_3Q$, are plotted for nuclei from the populations of cells shown in figure 20. These data correspond to the nuclei from which the data in figures 21 and 22 were derived.

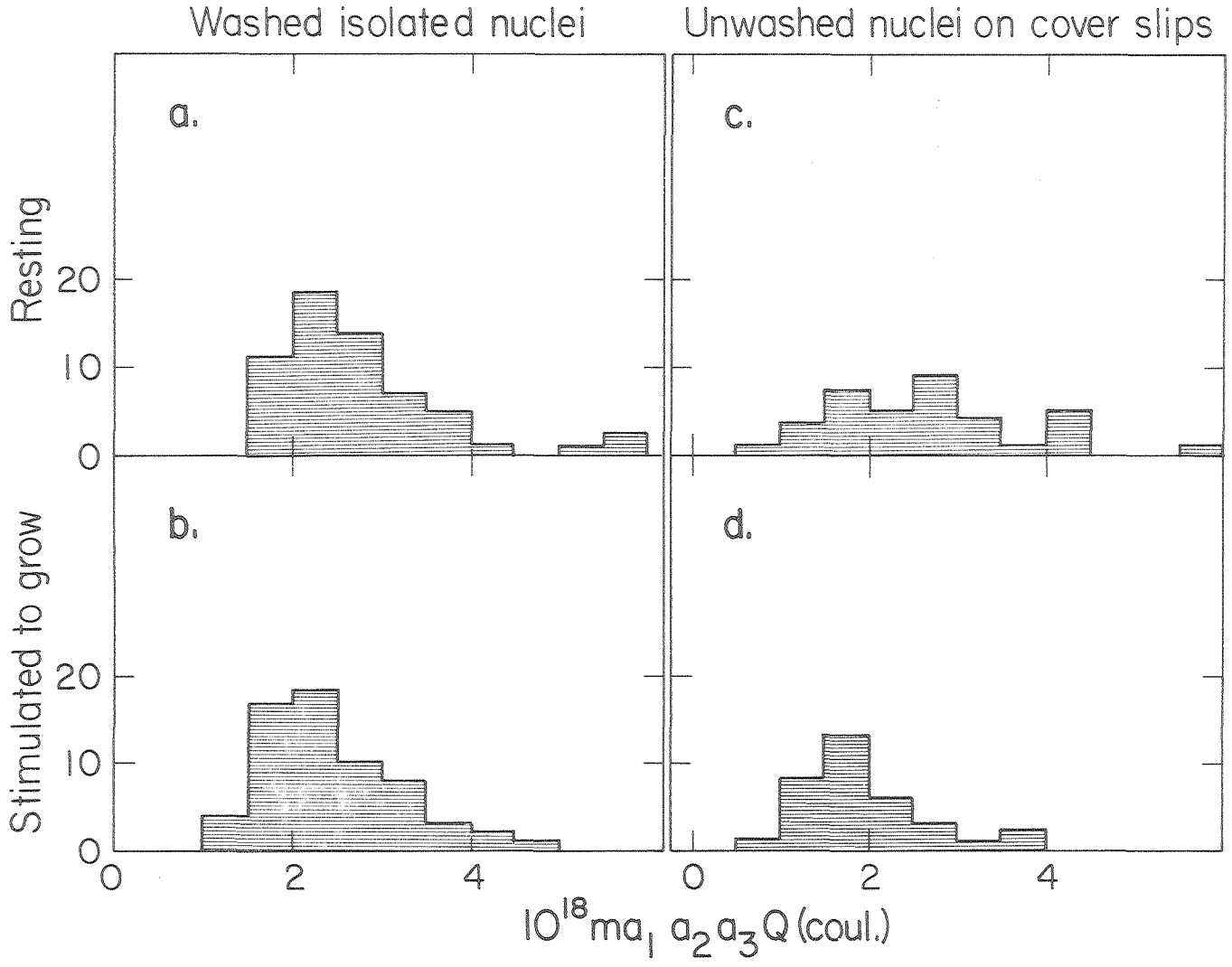

XBL 7910-5065

Figure 24. The viscosity of the nucleus relative to the viscosity of water can be inferred from the diffusion times, plotted in figure 21, and the values of $\langle i \rangle^2/G(0)$, shown in figure 22. This was done for each observed nuclear site. The results are plotted here for nuclei from the four populations of cells.

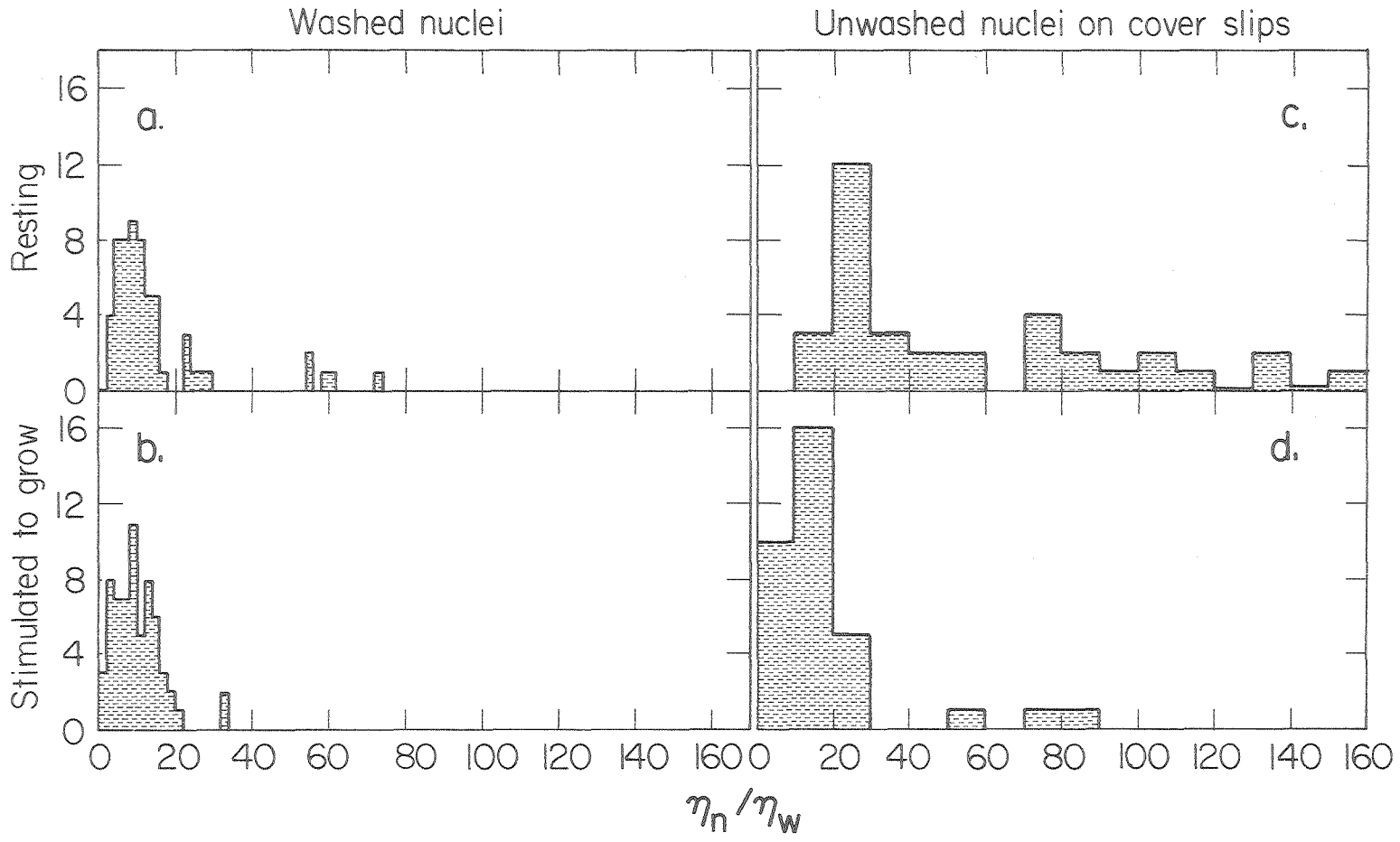

XBL 7910-5062

TABLE IV

PREPARATION OF NUCLEI	A[1] AVERAGE τ_+ (msec)	B[2] DIFFUSION COEFFICIENT X 10^9 (cm^2/sec)	C[3] $(1 + K[A])\frac{n_n}{n_w}$	D[1] $\langle i \rangle^2/G(0)$	E[4] K[A]	F[1] $\frac{n_n}{n_w}$
WASHED NUCLEI FROM RESTING CELLS	285 ± 25	6.8 ± 0.6	870 ± 75	27000 ± 2000	77 ± 6	15.1 ± 2.0
WASHED NUCLEI FROM STIMULATED CELLS	280 ± 20	6.9 ± 0.5	880 ± 65	38000 ± 3000	108 ± 9	10.0 ± 0.8
NUCLEI ON COVER SLIPS FROM RESTING CELLS	800 ± 75	2.4 ± 0.2	2500 ± 230	17000 ± 1300	48 ± 4	56.5 ± 6.8
NUCLEI ON COVER SLIPS FROM STIMULATED CELLS	700 ± 75	2.5 ± 0.2	2400 ± 230	60000 ± 7000	170 ± 20	18.2 ± 3.0

(1) Values are means ± standard error of the mean.

(2) Diffusion coefficient, assuming a beam radius of .88μ.

(3) Values are given by the observed diffusion coefficient divided by 6 X 10^{-6} cm^2/sec.

(4) $\langle i \rangle^2/G(0)$ measures the number of bound dye molecules in the volume $\pi w^2 L$. L is taken to be 8μ, w is taken as .88μ, and the free dye concentration is taken to be 3 X 10^{-8} M. Values in column E are the ratios of free to bound dye concentrations.

through a nylon screen to minimize this problem. In this histogram, a very small peak corresponding to triplets can also be seen. The peaks are relatively sharp. TC-7 cells are especially suitable for flow cytometry in this respect. Much of the remaining peak width is due to variability in the detection of fluorescence intensity.

In histogram b, many cells in S and G_2 + M are detected. Synchrony is not ideal, and the population is relatively heterogeneous. The distribution in histogram c is essentially identical to a. They both correspond to populations of resting cells. The distribution in d is different from the one in b. Most of the cells represented in d were apparently delayed in G_1, although some are well into S. The broadening of the G_1 peak is due to cells leaving G_1 and entering S. These cells had attached themselves to glass cover slips instead of the specially coated plastic culture dishes used for the cells in a and b. That probably accounts for the delay.

In fluctuation measurements, each nucleus was observed in two locations, on the average. Each site in a nucleus was treated as being independent in the histograms shown in figures 21, 22, 23, and 24. Thus, each nucleus contributes two data points, on the average, to each of the four histograms.

Figure 21, shows the distributions of diffusion times in the four classes of nuclei. Washed isolated nuclei from growing and resting cells have indistinguishable distributions. The diffusion times correspond to diffusion coefficients of 6.9 and 6.8 X 10^{-9} cm^2/sec. Assuming EtBr has a diffusion coefficient of 6 X 10^{-6} cm^2/sec. in water, then, by the reasoning outlined before, we may

write

$$(1 + K[A])\eta_n/\eta_w = 875 \pm 75$$

for washed isolated nuclei,

where K[A] is the ratio of bound to free EtBr, and η_n and η_w are the viscosities of the nucleus and water, respectively. Similarly, the distributions are indistinguishable for unwashed nuclei on cover slips derived from stimulated and resting cells. However, they are both very different from the distributions seen for washed nuclei isolated from stimulated and resting cells. The mean diffusion coefficients for nuclei on cover slips are 2.4 and 2.5 X 10^{-9} cm^2/sec, corresponding to

$$(1 + K[A])\eta_n/\eta_w = 2500 \pm 240$$

for unwashed nuclei on cover slips.

This is greater by a factor of three than the value seen for washed nuclei.

Similar information can be inferred from $\langle i \rangle^2/G(0)$. Histograms of measurements of $\langle i \rangle^2/G(0)$ are given in figure 22. Washed isolated nuclei from resting and stimulated cells have very similar distributions. Assuming that the concentration of free dye in the nucleus is 3 X 10^{-8} M, and that the nuclei are 8 μ deep, the means correspond to

$$K[A] = 75 \pm 6 \quad \text{for resting cell nuclei,}$$

$$\text{and} \quad K[A] = 110 \pm 9 \quad \text{for stimulated cell nuclei}$$

prepared by washing the isolated nuclei.

In the case of unwashed nuclei on cover slips, the results are

somewhat different. The distribution of $\langle i \rangle^2/G(0)$ for nuclei on cover slips from resting cells is shifted to lower values, relative to washed nuclei from resting cells. The values of $\langle i \rangle^2/G(0)$ for nuclei from stimulated cells are shifted considerably higher. The means of these distributions correspond to

$$K[A] = 48 \pm 4 \quad \text{for resting cell nuclei,}$$
$$K[A] = 220 \pm 20 \quad \text{for stimulated cell nuclei.}$$

Figure 23 shows histograms of the overall efficiency, $ma_1a_2a_3Q$, for the four classes of nuclei. The beam radius was not measured for most of the nuclei considered. The value of w was taken to be 1.0 μ in the computations of the efficiency. This allows for slight misfocussing of the microscope. The four distributions are very similar. The histograms for washed isolated nuclei, a and b, are indistinguishable. Histogram c is very similar if not identical to a and b. Histogram d appears to be different from the others.

Discussion. Interpretation of these data will require some care. It might be helpful to start with the data in figure 23. It was pointed out that histograms a, b, and c were very similar, but that d was different. Data in both a and b were each collected from 5 preparations of nuclei. Two preparations of each class of nuclei were used to obtain histograms c and d. Thus, there were 14 preparations involved. In thirteen, the values of $ma_1a_2a_3Q$ agreed with each other within the precision of the measurements. In the remaining case, values were consistently lower by roughly 50%. This case involved cells at low density on cover slips. One possible explanation for the low values is that background fluorescence was

not correctly accounted for. Fluorescence was measured in the cytoplasm associated with each nucleus. Presumably, cytoplasmic RNA, which can bind EtBr, was responsible for the observed fluorescence. Background was measured adjacent to the nucleus. The amount of fluorescence from cytoplasm adhering to the glass adjacent to the nucleus was assumed to be equivalent to the background fluorescence when observing the nucleus itself. With washed nuclei, this is not a problem, because no cytoplasm remains. For unwashed nuclei from high density cells, backgrounds were relatively high. Modest alterations of background fluorescence could account for the observed differences in values of $ma_1a_2a_3Q$. It is possible, then, that background fluorescence was underestimated in the case of one preparation of nuclei represented in histogram d. The corresponding values of $\langle i \rangle^2/G(0)$ were higher than comparable values, which is consistent with an underestimate of background fluorescence.

If we suppose that background corrections were responsible for the relatively small differences in values of $ma_1a_2a_3Q$, then we could conclude that $ma_1a_2a_3Q$ is approximately 2.6×10^{-18} coul. in all cases. It may be recalled that a priori estimates were made of $a_1a_2a_3Q$, based on observed pass bands of optical filters and manufacturers specifications for the photocathode quantum efficiency. That estimate was 3×10^{-18} coul. There is strong evidence, then, that the observed autocorrelation functions arise from diffusion of individual EtBr molecules.

We may now look more closely at figures 21 and 22. Diffusion times and $\langle i \rangle^2/G(0)$ should both increase as binding increases. Comparing nuclei from cells stimulated to grow, it is found that both

diffusion times and $\langle i \rangle^2/G(0)$ increase by roughly 2 or 3 times. If allowance is made for background fluorescence, as suggested above, then $\langle i \rangle^2/G(0)$ increases in unwashed nuclei compared to washed nuclei by about 60%. In the case of nuclei from resting cells, $\langle i \rangle^2/G(0)$ decreases while diffusion times increase, when going from washed to unwashed nuclei.

A word of caution is called for. These data are averaged over all observed nuclei in the population. They should not be interpreted literally as applying to "cells stimulated to grow." They apply to the population of cells stimulated to grow, some of which may be found in any of the states of the cell cycle. No attempt is made to correlate real or imagined peaks in histograms to subgroups of the populations of growing cells.

With these qualifications, we may take these data at face value. The viscosity of the nucleus might account for some of the observed changes by effecting both $\langle i \rangle^2/G(0)$ and the diffusion times. The binding equilibrium might shift to smaller amounts of bound material in a diffusion controlled reaction, when the viscosity increases. Of course, diffusion times would increase with viscosity.

Pursuing this line of thought, viscosities can be estimated from data for diffusion times, and two dimensional concentrations. This procedure was described when discussing the results for whole cells. Such computations were made for observations at different sites in observed nuclei. It was assumed that the average nuclear depth was 8 μ, the concentration of free dye was 3×10^{-8} M, and that the diffusion coefficient of EtBr in water is 6×10^{-6} cm^2/sec. The distributions of viscosities inferred in this way are shown in figure

24 for the four classes of nuclei. The means of the distributions of relative viscosities and ratios of bound to free dye for each population are stated in columns E and F of table IV.

Several observations may be made. First, is the very close agreement of the inferred viscosities with the tentative estimates made from in vivo observations of IMR-90 cells. Specific conclusions may also be proposed. The inferred viscosity of nuclei from cells stimulated to grow is less than the inferred viscosity of corresponding nuclei from resting cells. The inferred viscosity in unwashed nuclei is greater than the inferred viscosity in washed nuclei. Unwashed nuclei from resting cells would have the highest viscosity. The amount of bound dye in nuclei from stimulated cells is greater than the amount in nuclei from resting cells. Unwashed nuclei from resting cells bind less dye than washed nuclei from resting cells, while unwashed nuclei from stimulated cells bind more dye than washed nuclei stimulated cells.

There is support in the literature for some of these conclusions. In discussing the known binding properties of EtBr with chromatin, reports were described of increased EtBr binding by chromatin isolated from growing cells. The magnitude of the increase varied from one report to the next, but fell in the range of 30-200%. The increase in binding from inferred from experiments described here is about 40% for washed nuclei. For unwashed nuclei, the increase is about 3-4 times if allowance is made for background corrections, or 4-5 times if no allowance is made. Reports were also described claiming that chromatin becomes more condensed in early S phase in intact HeLa cells. This would have the effect of increasing K[A] in nuclei from

cells stimulated to grow over values for nuclei from resting cells.

It is also true, of course, that the stimulated cells are synthesizing chromatin. Consequently, the concentration of DNA binding sites might be expected to increase. This would increase K[A] in stimulated cells compared to resting cells.

Morphological changes might also effect values listed in column E. Column E is presented, assuming an average nuclear depth, L, of 8 μ. If nuclear depth changes were to account for changes listed in column E, then L would have to be smaller in stimulated cells than in resting cells. There is no reason to expect such a thing to happen. It is mentioned below, that attempts to measure distributions of nuclear sizes using a Coulter counter were unsuccessful. When such data become available, this question can be reconsidered, critically.

The results in table IV can be interpreted in biochemical terms. As the cells are stimulated to grow, transcription and replication mechanisms become activated. These and related activities might be associated with decreases in viscosity. Also, unwashed nuclei are subjected to extremely mild conditions compared to washed nuclei. Thus, the lower viscosities of washed nuclei could be attributed to the loss of nuclear material, or the breakdown of certain nuclear structures in the washing process.

Several matters deserve comment. One is a computation of the expected value of K[A] in these experiments. Such an effort will require an estimate of the binding site concentration, [A]. The number of DNA base pairs in the nucleus is known to be about 5×10^9. Fluoresence intensity was observed to be more or less independent of position in the nucleus, suggesting a uniform

chromatin concentration. Knowing the volume, then, we could estimate [A]. The volumes of TC-7 nuclei vary considerably. Attempts were made to measure the distribution of nuclear volumes using a Coulter counter. That device uses the displacement of an electrolyte solution by small particles to infer particle volume. Comparison with standard particles calibrates the observed values. The distribution of volumes can be obtained using a multichannel analyzer. Unfortunately, TC-7 nuclei are not suitable particles for such measurements. The obtained distributions corresponded to extremely small volumes, and had to be presumed subject to artifacts.

Microphotographs of nuclei can be made and nuclear dimensions can be compared to standards. As mentioned earlier, nuclei can appear to be circular or elliptical. The longer dimension is about 10-15 μ. The shorter dimension may be 5-10 μ. A typical volume, then, would be about 400 μ^3. Considerable variations could be expected. The corresponding base pair concentration would be of the order of 20 mM. If *in situ* binding of EtBr to chromatin is similar to *in vitro* binding, then two binding sites would exist. The strong one would have a binding constant of the order of 10^7 M^{-1}. The weaker one would have a binding constant of about 10^5 M^{-1}. Taking 10% of the base pairs to be involved in strong binding, the ratio of bound to free dye would be of the order of 10^4. Neglecting bleaching, the data in table IV suggest a ratio of bound to free dye two orders of magnitude smaller. Bleaching alone could not account for the difference. It would appear then, that the product of the binding constant with the concentration of free sites in the nucleus is less than the corresponding *in vitro* value. The viscosity being greater

than that of water might account for part of the difference, by lowering the binding constant. Of course, real differences in the binding properties are also possible explanations.

A related matter is the extent to which available binding sites are filled. If [B] is the concentration of free dye, then K[B] is the ratio of filled to empty binding sites. Since [B] is less than or equal to 3×10^{-8} M, we may conclude that K[B] is much less than one. A reasonable estimate is that $K[B] < 0.01$. Thus, well over 90% of the binding sites are unoccupied.

Another point of interest is the question of dye binding in the nucleolus. It is possible to translate the nucleus across the beam axis, so that the beam passes through the nucleolus. Initially, fluorescence intensity from the nucleolus is very strong. Within minutes, the signal decays to levels found elsewhere in the nucleus. Rapid recovery is not observed. Values of τ_+, $\langle i \rangle^2/G(0)$ and $ma_1a_2a_3Q$ measured in the nucleolus are not significantly different from values measured elsewhere in the nucleus. These observations suggest that EtBr is bound preferentially in the nucleolus, but that the binding sites become damaged, or they become blocked by damaged dye molecules. In any event, the binding that is particular to the nucleolus is not observed in the fluctuation measurements.

It may be asked whether measurements from different sites in the nucleus are statistically different from each other. This question was not considered in detail. However, certain general observations were made. When repeated measurements were made at the same point in the nucleus, the variability among measurements was about 10%. Similarly, average variations among measurements from different sites

in the same nucleus were approximately 20%. Measurements from different nuclei, including nuclei prepared on different days could vary by 50% or more. No attempt was made to correlate variations to morphological features.

The important results may be reviewed.

1) The overall internal consistency of the data indicates that measurements were made as intended.

2) Correlated fluctuations were detected from individual EtBr molecules in the cell nucleus, corresponding to the $G_+(\tau)$ term.

3) The overall efficiency, $ma_1a_2a_3Q$ was established as a useful quantity.

4) The nuclear viscosity in vivo and in situ is roughly 10 times that of water. Nuclear viscosity depends to some extent on the growth state of the cells used to provide nuclei for in situ experiments. Resting cells' nuclei are more viscous than nuclei from stimulated cells, on the average. Unwashed nuclei are more viscous than washed nuclei, on the average.

5) Binding strength, defined as the ratio of bound to free dye, can be measured in situ. Nuclei from stimulated cells bind more dye than nuclei from resting cells, on the average. Comparisons of binding strength averages in washed and unwashed nuclei are complex.

6) Variations in binding and hydrodynamic properties can be measured as a function of position in the nucleus. Wide variations are not expected.

7) Chromatin motion is not detected.

8) Binding in nucleoli is stronger than in the rest of the nucleus.

However, the binding process in the nucleolus is not suitable for measurements of this kind.

CONCLUSIONS

The basic goal of the research described above is to establish fluorescence correlation spectroscopy as a suitable technique for probing the cell nucleus. It has been accomplished. Measurements have been made consistently and reproducibly on weel defined and easily prepared cell nuclei. Many questions of biological interest can now be considered in this manner. In addition, there is reason to believe that vital stains can be used, instead of EtBr, that could extend fluorescence correlation spectroscopy to individual living cells as they pass through the cell cycle.

To be sure, there are difficulties, and many situations can be handled more naturally with other experimental procedures. But in matters involving cell nuclei and relatively few molecules, it is now reasonable to consider fluorescence correlation spectroscopy as one of only a few workable probes.

Hydrodynamic properties and information about binding are emphasized in the experiments described above. By choosing appropriate conditions, $G_0(\tau)$ can be selected, which gives primarily hydrodynamic data. Other circumstances favor $G_+(\tau)$, which gives information about binding properties, as well. To help distinguish among sources of the correlated fluctuations, a quantity was introduced that measures the amount of fluorescence per diffusing particle. It has proved to be useful, and has behaved as expected.

In fact, the internal consistency of the results presented above is remarkably high, considering the low signal level, and the natural variability in the systems being studied. Hopefully,

extensions of this work will answer many important questions about the biology of the cell nucleus.